Atmospheric Heterogeneous Reactions of N_2O_5 and NO_3 Radicals with Mineral Dust Particles

Dissertation zur des Grades

„Doktor der Naturwissenschaften“

am Fachbereich Chemie, Pharmazie und Geowissenschaften

der Johannes Gutenberg-Universität Mainz

vorgelegt von

Mingjin TANG

geboren in Jiangxi, CHINA

Mainz, 2011

Dekan: [redacted]

1. Berichterstatter: [redacted]

2. Berichterstatter: [redacted]

Tag der mündlichen Prüfung: 20.12.2011

Abstract

The heterogeneous reactions of mineral dust particles with N_2O_5 and NO_3 radicals have been investigated at atmospheric pressure, room temperature, and different relative humidities. These studies are important for evaluating the role of these reactions in the removal of NOx in the atmosphere and the chemical aging of dust particles during transport.

The uptake coefficient of N_2O_5, $\gamma(N_2O_5)$, was determined to be 0.020±0.002 (1 σ) on dispersed Saharan dust particles, independent of relative humidities (0-67%) and initial N_2O_5 concentration (5×10^{11}-3×10^{13} molecules cm^{-3}). Gas-phase and particulate products analysis suggests that N_2O_5 undergoes heterogeneous hydrolysis on the dust surface, leading to the formation of particulate nitrate with a yield of about 2. The independence of $\gamma(N_2O_5)$ on relative humidity is due to the large amount of internal water (up to >10% of the dust mass) contained by dust particles. The independence of $\gamma(N_2O_5)$ on initial N_2O_5 concentration can be explained by availability of a large internal surface for dust particles. Nevertheless, the dust particles can be deactivated if the particulate nitrate reaches high levels resulting from exposure to HNO_3(g). In addition, the uptake of N_2O_5 on Illite and Arizona Test dust was studied, and $\gamma(N_2O_5)$ at RH=0% was determined to be 0.084±0.019 (1 σ) on Illite and 0.010±0.001 (1 σ) for Arizona Test Dust, respectively.

Using a novel relative rate method, the uptake coefficient ratio of NO_3 to N_2O_5, $\gamma(NO_3)/\gamma(N_2O_5)$, was measured to be 0.9±0.4 (1 σ) on Saharan dust particles. This result was independent of relative humidity (0-70%), NO_3 and N_2O_5 concentration, and reaction time, though surface deactivation was observed for both species. The uptake of NO_3 radicals on mineral dust particles is proposed to proceed via the reaction of adsorbed NO_3 with internal water contained by dust particles, leading to the formation of nitrate.

Zusammenfassung

Die heterogenen Reaktionen von N_2O_5 bzw. NO_3 auf mineralischen Staubpartikeln wurden untersucht, um deren Einfluss auf den Abbau atmosphärischer Stickoxide (NOx) sowie auf die chemische Veränderung der Staubpartikel während ihres Transportes durch die Atmosphäre besser verstehen zu können. Die experimentellen Studien wurden bei Atmosphärendruck, Raumtemperatur und unterschiedlichen relativen Luftfeuchten durchgeführt. Der Aufnahmekoeffizient $\gamma(N_2O_5)$ von N_2O_5 auf dispergiertem Staub aus der Sahara wurde zu 0,020 ± 0,002 (1σ) bestimmt, unabhängig von der relativen Feuchte (0 - 67 %) sowie der N_2O_5-Konzentration ($5x10^{11}$ - $3x10^{13}$ Moleküle cm^{-3}).

Die Analyse der Reaktionsprodukte in der Gasphase sowie auf der Partikeloberfläche führt zu der Annahme, dass N_2O_5 auf der Staubpartikeloberfläche zu Nitrat hydrolysiert wird. Es konnte kein Einfluss der relativen Feuchte auf den Aufnahmekoeffizienten ermittelt werden, was durch das vorhandene interlamellare Wasser, welches bis zu 10 % der Partikelmasse betragen kann, erklärbar ist. Der gemessene Wert des Aufnahmekoeffizienten ist unabhängig von der Eingangs-N_2O_5-Konzentration, was sich über die sehr große innere Oberfläche der Partikel erklären lässt. Dennoch ließ sich durch eine vorherige Konditionierung der Partikel mit gasförmigem HNO_3, was eine Nitratanreicherung an der Oberfläche bewirkt, die Effizienz der N_2O_5-Aufnahme auf die Staubpartikel reduzieren. Zusätzliche Studien befassten sich mit der Bestimmung des Aufnahmekoeffizienten von N_2O_5 auf Illit-Partikeln und auf Teststaub aus Arizona. Bei einer relativen Luftfeuchte von 0 % wurden für $\gamma(N_2O_5)$ Werte von 0,084 ± 0,019 (1σ) für Illit und von 0,010 ± 0,001 (1σ) für Arizona Teststaub ermittelt.

Unter Anwendung einer neuartigen Messmethode, die auf der zeitgleichen Messung der Konzentrationsabnahme von NO_3 und N_2O_5 relativ zueinander beruht, wurde das Verhältnis $\gamma(NO_3)/\gamma(N_2O_5)$ der Aufnahmekoeffizienten von NO_3 und N_2O_5 auf Saharastaub zu 0,9 ± 0,4 (1σ) bestimmt. Dieser Wert war unabhängig von der relativen Feuchte, den NO_3- und N_2O_5-Konzentrationen sowie der Reaktionszeit, obwohl eine Oberflächendeaktivierung für beide Spurenstoffe beobachtet wurde.

Acknowledgement

This work was carried out under the supervision of [redacted]. [redacted] accepted me as a PhD candidate in his group and provided me the opportunity to combine laboratory studies with field measurement during my work: this combination was challenging and exciting, and also greatly extended my overview in atmospheric chemistry. [redacted] keeps on offering me scientific ideas and also teaching me experimental skills. He is always ready with great patience to discuss with me about questions and problems I have in the research, and have spent so much time on reading my papers and thesis. I really enjoy the research work in his group.

[redacted] recommended me to join John's group as a PhD candidate. I also appreciate very much the suggestions that he never hesitates to offer whenever I need during the past three or four years. [redacted] is appreciated for accepting me as one of his PhD students in the university, and showing considerable interest in my research.

[redacted] is especially acknowledged for his excellent technical support. He has designed many apparatus and developed lots of programs, which made the experimental work possible and also much easier. I also would like to thank [redacted], for his numerous help both in the laboratory studies and in field work, [redacted] for his help in nitric acid measurement, [redacted] for analyzing nitrate in the dust particles by ion chromatography, [redacted] for helping the APS measurement, and [redacted] for helping me develop FACSMILE programs.

My scholarship for the PhD study was offered by [redacted]. [redacted] and [redacted], [redacted], are warmly acknowledged for their help in varieties of bureaucratic business.

During the past several years I have been enjoying the collaboration and friendship with so many excellent colleagues. Though the number of people is so large that I cannot mention all of them here, I do want to thank [redacted].

Contents

Abstract I

Zusammenfassung II

Acknowledgement III

1 Introduction ..... - 1 -

1.1 The atmosphere ..... - 1 -

1.2 Tropospheric photochemistry and ozone formation ..... - 2 -

1.3 Tropospheric nocturnal chemistry ..... - 5 -

1.3.1 Tropospheric nighttime chemistry of NO_3 ..... - 6 -

1.3.2 Tropospheric chemistry of N_2O_5 ..... - 8 -

1.3.3 Observation of NO_3 and N_2O_5 in the troposphere ..... - 9 -

1.3.4 Impacts of NO_3 and N_2O_5 chemistry in the troposphere ..... - 10 -

1.4 Mineral dust aerosols in the troposphere ..... - 13 -

1.4.1 Emission, transport, and mineralogy of mineral dust aerosols ..... - 13 -

1.4.2 Tropospheric chemistry of mineral dust aerosols ..... - 14 -

1.5 Atmospheric heterogeneous reactions ..... - 17 -

2 Experimental procedures and setups ..... - 23 -

2.1 Relative rate method apparatus ..... - 23 -

2.1.1 NO_3 and N_2O_5 generation ..... - 24 -

2.1.2 Aerosol sample generation and preparation ..... - 24 -

2.2 Aerosol flow tubes ..... - 25 -

2.2.1 The old aerosol flow tube for N_2O_5 ..... - 26 -

2.2.2 The new aerosol flow tube for N_2O_5 ..... - 30 -

2.2.3 The aerosol flow tube for HNO_3 ..... - 34 -

2.2.4 Aerosol measurement ..... - 35 -

2.3 NO_3, N_2O_5, and HNO_3 detection ..... - 35 -
2.3.1 Cavity Ring-Down spectroscopy ..... - 36 -
2.3.2 Chemical Ionization Mass Spectrometry ..... - 42 -
2.4 Product measurements ..... - 43 -
2.4.1 Gas phase NO_2 detection ..... - 43 -
2.4.2 Particulate nitrate detection ..... - 45 -
3 Heterogeneous uptake of NO_3 and N_2O_5: a relative rate study ..... - 47 -
3.1 Introduction ..... - 47 -
3.2 Data analysis ..... - 47 -
3.3 Results and discussion ..... - 49 -
3.3.1 Saharan dust ..... - 49 -
3.3.2 Ambient Urban aerosols ..... - 54 -
3.3.3 Soot ..... - 55 -
3.4 Summary ..... - 57 -
4 Kinetics of heterogeneous uptake of N_2O_5 on mineral dusts: aerosol flow tube studies .. - 59 -
4.1 Introduction ..... - 59 -
4.2 Data analysis ..... - 59 -
4.3 Uptake of N_2O_5 on Saharan dust ..... - 66 -
4.3.1 Influence of relative humidity ..... - 67 -
4.3.2 Influence of initial N_2O_5 concentration ..... - 68 -
4.3.3 Influence of O_3 and NO_2 ..... - 69 -
4.3.4 Possible interference in measuring uptake coefficients ..... - 71 -
4.4 Uptake of N_2O_5 on other dust particles ..... - 74 -
4.4.1 Uptake of N_2O_5 on ATD ..... - 74 -

4.4.2 Uptake of N_2O_5 on Illite ..... - 76 -
4.5 Comparison with previous results ..... - 77 -
4.5.1 Uptake onto bulk dust samples ..... - 77 -
4.5.2 Uptake onto dispersed dust particles ..... - 79 -
4.6 Summary ..... - 81 -
5 Mechanisms of heterogeneous reaction of N_2O_5 and NO_3 radicals with mineral dust particles ..... - 83 -
5.1 Introduction ..... - 83 -
5.1.1 Reactions of N_2O_5 and NO_3 with aqueous particles ..... - 83 -
5.1.2 Reaction of N_2O_5 and NO_3 with mineral dust particles ..... - 85 -
5.3 Effects of particulate nitrate on the N_2O_5 uptake ..... - 87 -
5.3.1 Nitrate formed in the aerosol flow tubes ..... - 87 -
5.3.2 Effects of nitrate coating on the N_2O_5 uptake ..... - 90 -
5.4 Products of the heterogeneous reaction of N_2O_5 with dust particles ..... - 93 -
5.4.1 Cavity Ring-Down spectroscopy detection of NO_2 and N_2O_5 ..... - 94 -
5.4.2 Ion chromatography analysis of particulate nitrate ..... - 97 -
5.5 Mechanism ..... - 97 -
5.6 Summary ..... - 99 -
6 Atmospheric implication and outlook ..... - 101 -
6.1 Summary ..... - 101 -
6.2 Atmospheric implications ..... - 102 -
6.3 Future work ..... - 104 -
7 References ..... - 107 -
Appendices ..... - 131 -
A1. Uptake of HNO_3(g) on Saharan dust ..... - 131 -

A2. Estimation of nitrate formed in the mixing volume ..... - 134 -

A3. Chemicals and materials used in this work ..... - 136 -

A4. Codes of FACSIMILE simulations used in this work ..... - 137 -

A4.1 Oxidation of NO_2 by O_3 in the photochemical reactor ..... - 137 -

A4.2 Effects on $\gamma(N_2O_5)$ of the reformation of N_2O_5 and heterogeneous removal of NO_3 in the aerosol flow tube ..... - 140 -

A4.3 Simulating the response of N_2O_5 to the introduction of dust aerosol ..... - 143 -

A5. Chemical formulae and structures of main minerals contained by dust particles ..... - 146 -

A6. Publications and projects/campaigns during the PhD study ..... - 149 -

A6.1 Publications ..... - 149 -

A6.2 Projects/campaigns ..... - 150 -

1 Introduction

1.1 The atmosphere

Our atmosphere, retained by Earth's gravity, is a layer of gas (and cloud and aerosol particles) surrounding the planet. The Earth's atmosphere mainly consists of (by volume) N_2 (78%), O_2 (21%), and Ar (1%), the concentrations of which have remained quite stable over time. Water vapor concentrations are highly variable, reaching as high as 3%. The remaining gaseous components, often referred to as trace gases, including carbon dioxide, methane, sulfur dioxide, nitrogen dioxide, and ozone etc., comprise less than 1% of the atmosphere. The atmosphere is a dynamic system in which its constituents are continuously exchanged with soil, ocean, and biosphere. It is a rather efficient oxidizing medium. Once present in atmosphere, trace gases are converted at different rates to substances which are usually at higher chemical oxidation states than their parent species. The lifetimes of traces gases in the atmosphere are highly variable, ranging from less than 1 second (for example, OH radicals) to many years (for example, CH_4).

The Earth's atmosphere is characterized by variations of temperature and pressure with height. According to the average temperature profile with altitude, the atmosphere is divided into several layers. The troposphere is the lowest layer of the atmosphere, which extends from the Earth's surface to the tropopause, which is at about 10-15 km altitude. The stratosphere is the layer between the tropopause and the stratopause (about 45-55 km altitude). The troposphere and stratosphere together are called the lower atmosphere, while the upper atmosphere extends from the stratopause, including mesosphere, thermosphere, and exosphere.

The troposphere contains about 80% of the mass of the atmosphere, though it only accounts for a small fraction of its height. In the troposphere, temperature decreases with altitude due to the increasing distance from the sun-warmed Earth's surface, and this thermal structure leads to rapid vertical mixing in the troposphere. In contrast, temperature increases with altitude in the stratosphere, as a result of the absorption of ultraviolet radiation of ozone in the stratosphere. In the stratosphere, O_2 is slowly

dissociated by solar ultraviolet of wavelength less than 242 nm to atomic oxygen (R1-1), which reacts rapidly with O_2 to form ozone (R1-2):

$$O_2 + h\nu\ (\lambda < 242\ \text{nm}) \rightarrow O + O \quad \text{(R1-1)}$$

$$O + O_2 + M \rightarrow O_3 + M \quad \text{(R1-2)}$$

where M is the third molecule (e.g. N_2, O_2) that absorbs the excess vibrational energy and stabilizes the formed O_3. Most of the atmospheric ozone (about 90%) is present in the stratosphere, and the peak ozone concentration occurs in the region of 20-30 km, which is called the stratospheric ozone layer. Stratospheric ozone absorbs all the solar ultraviolet radiations of the wavelengths in the range of 240-290 nm, which is harmful to the unicellular organizations and the surface cells of higher plants and animals. While stratospheric ozone protects the Earth's surface from being exposed to harmful solar ultraviolet radiation, ozone at the ground level, at elevated concentrations, is detrimental to the health of both plants and animals. In addition, ozone in the upper troposphere is an important greenhouse gas, which absorbs the long wavelength radiation emitted by the Earth's surface and warms the atmosphere.

In addition to gases, liquid and solid particles, the sizes of which are in the range of a few nanometers to hundreds of micrometers, are also present in the atmosphere. Particles are directly emitted into the atmosphere (for example, mineral dust and sea salt) or formed in the atmosphere by gas-to-particle conversion processes (for example, non-sea-salt sulfate and secondary organic aerosols). Particles also undergo dynamic change in the atmosphere and are mainly removed by deposition at the Earth's surface and incorporation into cloud droplets during cloud formation. Residence times of particles in the troposphere vary from a few hours to a few weeks.

1.2 Tropospheric photochemistry and ozone formation

Apart from the transport across the tropopause from the stratosphere, tropospheric ozone (O_3) is produced during the photolysis of NO_2 at wavelengths < 424 nm (R1-3):

$$NO_2 + h\nu\ (\lambda < 424\ \text{nm}) \rightarrow NO + O \quad \text{(R1-3)}$$

$$O + O_2 + M \rightarrow O_3 + M \quad \text{(R1-4)}$$

(R1-4) is the only significant chemical source of O_3 in the troposphere. Once formed, O_3 can react with NO to regenerate NO_2:

$$NO + O_3 \rightarrow NO_2 + O_2 \quad \text{(R1-5)}$$

Nitrogen oxides (NOx), NO and NO_2, are emitted into the atmosphere with an annual flux of more than 50 Tg (N) yr^{-1} [*IPCC*, 1995]. The major sources of NOx include fossil-fuel combustion, soil release, biomass burning, and lightning. According to (R1-3), (R1-4), and (R1-5), the steady-state O_3 concentration is given by

$$[O_3]_{ss} = \frac{k_3[NO_2]}{k_5[NO]} \quad \text{(E1-1)}$$

where [NO] and $[NO_2]$ are the concentration of NO and NO_2, respectively, and k_3 and k_5 are the rate constants of (R1-3) and R(1-5). The steady-state O_3 concentration is proportional to the $[NO_2]$/[NO] ratio. Most of the NOx is emitted in the form of NO rather than NO_2, and O_3 concentrations in the troposphere are usually found to be higher than the values calculated from the simple steady-state analysis [*Seinfeld and Pandis*, 1997], indicating the occurrence of some other reactions in the troposphere which convert NO to NO_2 without the consumption of O_3.

As shown in Figure 1-1, these reactions are fueled by carbon-containing species, such as CO and volatile organic compounds (VOCs), and are initiated by the oxidation of these species by OH radicals, the major source of which is the photolysis of O_3:

$$O_3 + h\nu\ (\lambda < 1180\ \text{nm}) \rightarrow O_2 + O(^3P) \quad \text{(R1-6)}$$

$$O_3 + h\nu\ (\lambda < 319\ \text{nm}) \rightarrow O_2 + O(^1D) \quad \text{(R1-7)}$$

$O(^3P)$ atoms combines rapidly with O_2 to reform O_3 (R1-4), whilst $O(^1D)$ is quenched to the ground state ($O(^3P)$) by collision with N_2 and O_2:

$$O(^1D) + M \rightarrow O + M \quad \text{(R1-8)}$$

$O(^1D)$ also reacts with H_2O(g) and consequently two OH radicals are formed:

$$O(^1D) + H_2O \rightarrow OH + OH \quad \text{(R1-9)}$$

In the lower troposphere, as much as 10% of the $O(^1D)$ produced in (R1-7) reacts with H_2O to generate OH radicals. OH can also be formed from other sources, e.g. the photolysis of H_2O_2 and HONO:

$H_2O_2 + h\nu\ (\lambda < 400\ nm) \rightarrow OH + OH$ (R1-10)

$HONO + h\nu\ (\lambda < 370\ nm) \rightarrow NO + OH$ (R1-11)

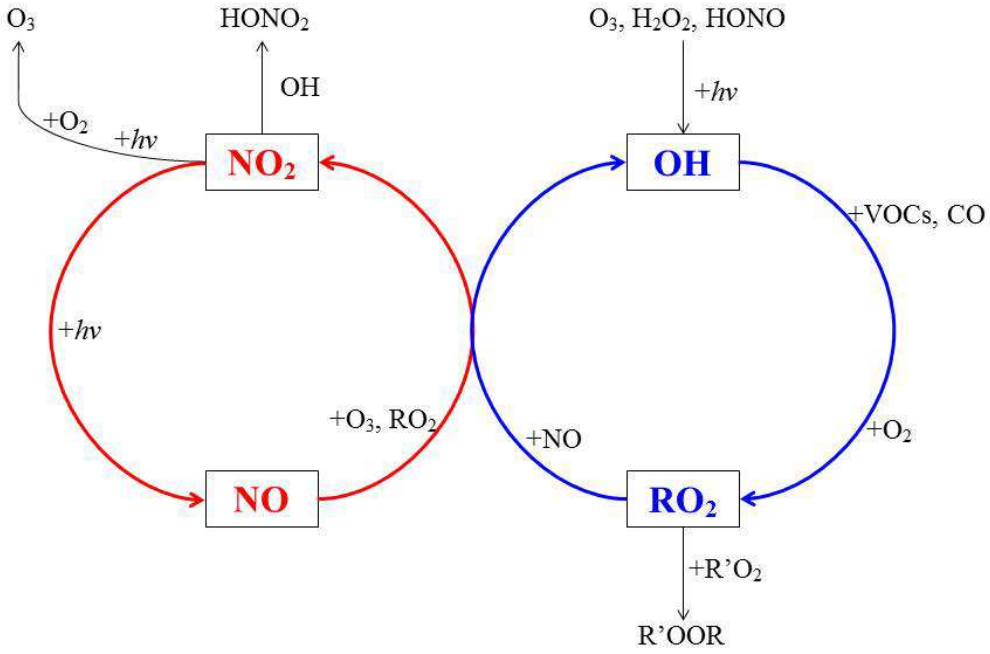

Figure 1-1. A simplified schematic of tropospheric photochemistry

During the daytime the OH concentration is on the order of 10^6 molecules cm^{-3} in the troposphere. OH reacts with CO to form HO_2 radicals (R1-12), and reacts with VOCs to form RO_2 radicals (R1-13):

$CO + OH + O_2 \rightarrow CO_2 + HO_2$ (R1-12)

$RH + OH + O_2 \rightarrow H_2O + RO_2$ (R1-13)

HO_2 and RO_2 radicals convert NO to NO_2 without the consumption of O_3, and OH and RO radicals are formed, respectively:

$HO_2 + NO \rightarrow OH + NO_2$ (R1-14)

$RO_2 + NO \rightarrow RO + NO_2$ (R1-15)

RO radicals react with O_2 to produce HO_2, which is then converted to OH radicals by the reaction with NO (R1-14).

$RO + O_2 \rightarrow R'CHO + HO_2$ (R1-16)

The net effects of reactions from (R1-12) to (R1-16) are that CO and VOCs are oxidized and O_3 is produced, while OH and HO_2 act as catalysts. The key termination reactions of the NOx-VOCs photochemistry include

$$OH + NO_2 + M \rightarrow HNO_3 + M \quad \text{(R1-17)}$$

$$HO_2 + HO_2 \rightarrow H_2O_2 + O_2 \quad \text{(R1-18)}$$

$$RO_2 + HO_2 \rightarrow ROOH + O_2 \quad \text{(R1-19)}$$

$$RO_2 + NO + M \rightarrow RONO_2 + M \quad \text{(R1-20)}$$

and the reversible formations of PANs:

$$RC(O)OO + NO_2 + M \leftrightarrow RC(O)OONO_2 + M \quad \text{(R1-21)}$$

1.3 Tropospheric nocturnal chemistry

In the daytime, the oxidation of NO_2 by OH to form HNO_3 (R1-17) is frequently the dominant process to remove NOx from the troposphere [*Seinfeld and Pandis*, 1997]. During the nighttime, OH production from O_3 photolysis stops and its concentration is estimated to be below 2×10^5 molecules cm^{-3}. NO_2 is now removed via oxidation by O_3 to form NO_3 radicals (R1-22), which react further with NO_2 to produce N_2O_5 (R1-23a). N_2O_5 decomposes back to NO_2 and NO_3 (R1-23b) to establish a dynamic equilibrium between NO_2, NO_3, and N_2O_5, as shown in Figure 1-2.

$$NO_2 + O_3 \rightarrow NO_3 + O_2 \quad \text{(R1-22)}$$

$$NO_2 + NO_3 + M \rightarrow N_2O_5 + M \quad \text{(R1-23a)}$$

$$N_2O_5 + M \rightarrow NO_2 + NO_3 + M \quad \text{(R1-23b)}$$

The rate constants for NO_3 photolysis are estimated to be 0.17-0.19 s^{-1} for (R1-24a) and 0.016-0.020 s^{-1} for (R-24b) at the earth's surface in the absence of clouds when the solar zenith angle is 0° [*Johnston et al.*, 1996; *Orlando et al.*, 1993].

$$NO_3 + h\nu\ (\lambda<700\ \text{nm}) \rightarrow NO + O_2 \quad \text{(R1-24a)}$$

$$NO_3 + h\nu\ (\lambda<580\ \text{nm}) \rightarrow NO_2 + O \quad \text{(R1-24b)}$$

NO_3 radicals absorb sunlight strongly and result in lifetimes of a few second, preventing build up significant NO_3 (and thus N_2O_5) during the daytime in the atmosphere. In

addition, NO_3 radicals also react with NO (R1-25) with a rate constant of 2.6×10^{-11} cm^3 $molecule^{-1}$ s^{-1} at 298 K [*Atkinson et al.*, 2004], leading to a loss rate of 0.65 s^{-1} in the presence of 1 ppbv NO.

$$NO + NO_3 \rightarrow NO_2 + NO_2 \qquad \text{(R1-25)}$$

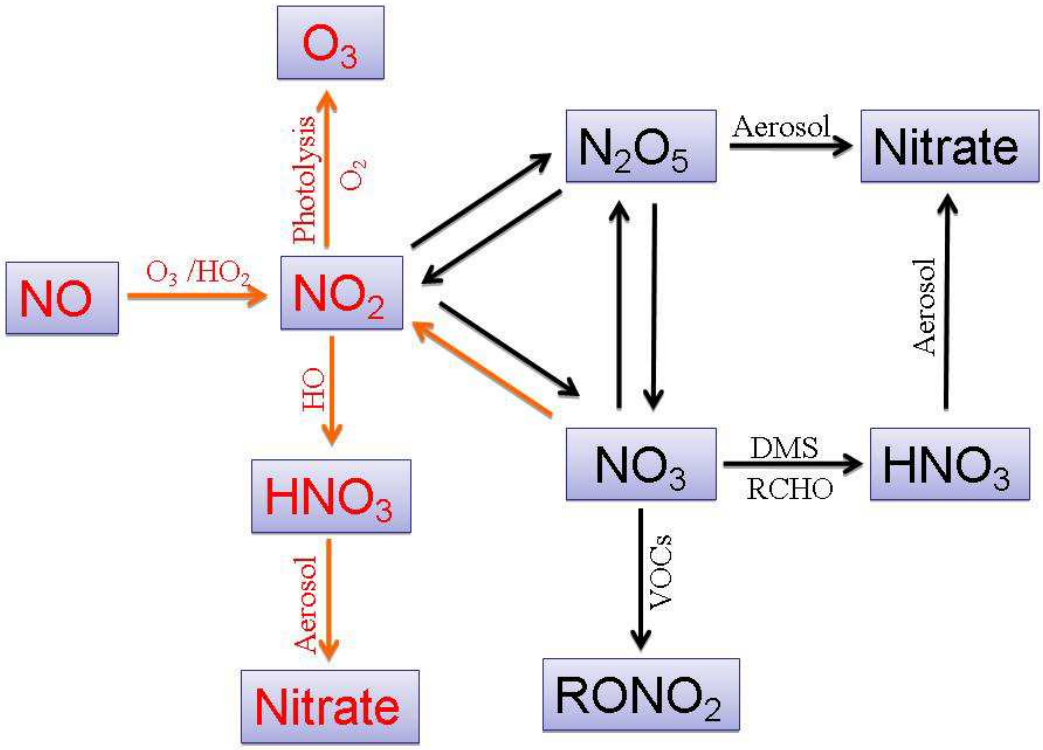

Figure 1-2. A simple schematic of the daytime and nighttime chemistry of NOy in the troposphere

1.3.1 Tropospheric nighttime chemistry of NO_3

At nighttime when its photolysis ceases and NO is removed from the troposphere by (R1-5), NO_3 mixing ratios can build up to hundreds of pptv. Reactions with NO_3 radicals are important nocturnal oxidation processes for many organic traces gases. NO_3 radicals react with alkanes and DMS by H abstraction and with alkenes by the addition of NO_3 to the C=C bond, e.g.

$$CH_3CH_2CH_2CH_3 + NO_3 \rightarrow CH_3CH_2CH\cdot CH_3 + HNO_3 \qquad \text{(R1-26)}$$

$$CH_3SCH_3 + NO_3 \rightarrow CH_3SCH_2\cdot + HNO_3 \qquad \text{(R1-27)}$$

$CH_3CH=CHCH_3 + NO_3 \rightarrow CH_3CH(ONO_2)CH\cdot CH_3$ (R1-28)

The second-order rate constants and the corresponding lifetimes of some VOCs in the atmosphere with respect to the oxidation by OH, NO_3, and O_3, are listed in Table 1-1, assuming that OH, NO_3 and O_3 concentrations are 2.5×10^6, 2.5×10^8, and 1.25×10^{12} molecules cm^{-3}, respectively.

Table 1-1 Second order rate constants and the corresponding lifetimes of some organic compounds in the atmosphere with respect to the reaction with OH, NO_3, and O_3 [a]

Species	k(X+OH) [b]	k(X+NO_3) [b]	k(X+O_3) [b]	τ(X+OH) [c]	**τ(X+NO_3) [c]**	τ(X+O_3) [c]
cis-2-butene	5.60E-11	3.50E-13	1.25E-16	1.98 h	**3.17 h**	1.78 h
isoprene	1.00E-10	7.00E-13	1.27E-17	1.11 h	**1.59 h**	17.5 h
α-pinene	5.30E-11	6.20E-12	9.00E-17	2.10 h	**0.18 h**	2.47 h
DMS	4.80E-12	1.10E-12	2.00E-19	23.2 h	**1.01 h**	46.3 d
methane	6.40E-15	1.00E-18		1.98 yr	**126 yr**	
n-butane	2.35E-12	4.60E-17		47.3 h	**2.76 yr**	
benzene	1.20E-12	3.00E-17	1.00E-21	92.6 h	**4.23 yr**	25.4 yr
methyl-benzene	5.60E-12	7.80E-17	1.00E-21	19.8 h	**1.63 yr**	25.4 yr
ethanol	2.30E-12	2.00E-15		48.3 h	**23.2 d**	
acetaldehyde	1.50E-11	2.70E-15		7.41 h	**17.2 d**	
acetone	1.80E-13	2.00E-17		25.7 d	**6.34 yr**	

[a] It is assumed that OH, NO_3 and O_3 concentrations are 2.5×10^6, 2.5×10^8, and 1.25×10^{12} molecules cm^{-3}. [b] Second order rate constants (cm^3 $molecule^{-1}$ s^{-1}) with respect to the reactions with OH, NO_3, and O_3. All the kinetics data are adopted from the recommendation of the IUPAC Subcommittee for Gas Kinetic Data Evaluation [*Atkinson et al.*, 2004; 2006]. Some of the reactions are so slow that only the upper limits of the second order rate constants are recommended. [c] Lifetimes of VOCs and DMS with respect to the reactions with OH, NO_3, and O_3 (h = hour, d = day, and yr = year).

As shown in Table 1-1, the reactions with NO_3 contribute significantly or even dominantly to the degradation of alkenes and DMS (see Section 1.3.4), and are especially important for the oxidation of biogenically emitted terpenes (e.g. α-pinene). For other types of VOCs, e.g. alkanes, aromatic hydrocarbons, alcohols, aldehyde, and ketones, the

oxidation by NO_3 and O_3 are too slow to be important, when compared to the reactions with OH radicals.

Although the losses are dominated by gas phase reactions, NO_3 radicals can also heterogeneously interact with particles. The heterogeneous uptake coefficient (defined as the probability that a molecule which collides with the surface is uptaken by the surface; see Section 1.5 for details) of NO_3 on pure water and ionic solutions (Cl^-, Br^-, NO_2^-, HSO_3^-, SO_3^{2-}, $HCOO^-$, CH_3COO^-, and OH^-) is between 1.5×10^{-4} and 6×10^{-3}, depending on the type of salts and the salt concentration in the solution [*Imamura et al.*, 1997; *Rudich et al.*, 1996a; *Rudich et al.*, 1996b]. The Henry's law coefficient for NO_3 is low, with reported values of 0.6±0.3 M atm^{-1} (1 σ) [*Rudich et al.*, 1996a] or 1.8±3 M atm^{-1} (2 σ) [*Thomas et al.*, 1998]. The uptake coefficient of NO_3 was determined to be $(4.9\pm3)\times10^{-2}$ on solid NaCl salt and 0.16±0.08 on solid NaBr salt [*Seisel et al.*, 1997]. The uptake coefficients of NO_3 on dry NaCl, NaBr, NaI, and $MgCl_2\cdot6H_2O$ were also reported to be in the range of 1×10^{-4}-1×10^{-2} [*Gershenzon et al.*, 1999; *Zelenov et al.*, 2008]. The interaction of NO_3 with ice and sulfuric acid solution at the temperature of 170 K< T <200 K was found to be relatively slow, with the upper limit for the uptake coefficient of $\gamma < 10^{-3}$ [*Fenter and Rossi*, 1997].

The uptake coefficients of NO_3 on organic surface vary with organic compositions [*Gross and Bertram*, 2008; 2009; *Gross et al.*, 2009; *Iannone et al.*, 2011], and generally the reactivity of NO_3 with the organic surfaces correlates with the known gas-phase reactivity of NO_3 [*Moise et al.*, 2002].

1.3.2 Tropospheric chemistry of N_2O_5

In contrast to NO_3, N_2O_5 possesses no gas-phase reactivity [*Atkinson et al.*, 2004] and its loss in the atmosphere is dominated by heterogeneous reaction on the surface of atmospheric particles. The uptake of N_2O_5 on sulfate [*Griffiths and Cox*, 2009; *Hallquist et al.*, 2000; *Hallquist et al.*, 2003; *Hu and Abbatt*, 1997; *Mozurkewich and Calvert*, 1988; *Stewart et al.*, 2004], nitrate [*Bertram and Thornton*, 2009; *Wahner et al.*, 1998], sea salts [*Behnke et al.*, 1997; *George et al.*, 1994; *Schweitzer et al.*, 1998; *Thornton and Abbatt*, 2005], and organic particles [*Badger et al.*, 2006; *Escorcia et al.*, 1998; *Escoreia et al.*, 2010; *Thornton et al.*, 2003] has been extensively investigated. For example, the uptake

coefficients of N_2O_5 on Cl^-/Br^- solution surface currently recommended by the IUPAC Subcommittee for Gas Kinetic Data Evaluation [*IUPAC*, 2009] are given by:

$$\gamma = 2.5 \times 10^{-5} e^{1800/T} \quad \text{(E1-2)}$$

where T is the temperature in K, and this equation is valid in the temperature range of 260-300 K. The uptake coefficients of N_2O_5 (and the temperature dependence if data are available) on other liquid surface, e.g. H_2O, H_2SO_4, NH_4HSO_4, $(NH_4)_2SO_4$, $NaNO_3$, NH_4NO_3, and organic particles, are also reviewed and evaluated by this committee [*IUPAC*, 2009]. However, uptake coefficients of N_2O_5 on ambient aerosols [*Bertram et al.*, 2009a; *Bertram et al.*, 2009b; *Brown et al.*, 2006; *Brown et al.*, 2009a], are often a factor of 10 or more lower than the values used in the current large-scale model parameterizations, which are based on the laboratory measurements. The difference in the uptake coefficients determined by laboratory studies and field measurements is related to the multi-component nature of atmospheric aerosols, which can impact the heterogeneous hydrolysis of N_2O_5. The mechanism of heterogeneous reactions of N_2O_5 with atmospheric particles is discussed in detail in Section 5.1.1.

1.3.3 Observation of NO_3 and N_2O_5 in the troposphere

Ambient NO_3 radicals were detected for the first time in 1980 by using long path Differential Optical Absorption Spectroscopy (DOAS) [*Platt et al.*, 1980]. Long path DOAS provides the average concentration over a long distance (usually several kilometers), and it is difficult to be deployed on mobile research platforms like ships and aircrafts. Recently several new techniques, including Cavity Ring-Down spectroscopy (CRD) and Cavity Enhanced Absorption Spectroscopy (CEAS) [*Bitter et al.*, 2005; *S S Brown et al.*, 2002; *King et al.*, 2000; *Schuster et al.*, 2009], and Laser Induced Fluorescence (LIF) [*Matsumoto et al.*, 2005; *Wood et al.*, 2003], have been developed to measure atmospheric NO_3. NO_3 radicals could also be sampled and trapped by a cold finger at 77 K, and then analyzed by Matrix Isolation Electron Spin Resonance (MIESR) [*Mihelcic et al.*, 1993].

Recently, atmospheric N_2O_5 has also been detected after being thermally dissociated to NO_3, using CRD [*Bitter et al.*, 2005; *Brown et al.*, 2002; *Schuster et al.*, 2009; *Simpson*, 2003], Laser Induced Fluorescence (LIF) [*Matsumoto et al.*, 2005; *Wood et al.*, 2003],

and Chemical Ionization Mass Spectrometry (CIMS) [*Slusher et al.*, 2004], and also directly measured by CIMS [*Kercher et al.*, 2009].

The mixing ratios of NO_3 (and thus N_2O_5) vary with the concentrations of precursors (i.e. NO_2 and O_3) and sinks (alkenes, DMS, aerosols), as well as the temperature. The highest NO_3 mixing ratio reported up to date is more than 800 pptv in an arid and polluted environment [*Asaf et al.*, 2009]. The N_2O_5 mixing ratio can reach more than 10 ppbv [*Brown et al.*, 2003b]. In the atmosphere NO_2, NO_3, and N_2O_5 are in equilibrium most of the time [*Brown et al.*, 2003a]. The lifetimes of NO_3 and N_2O_5 also vary a lot with the strength of sinks, with NO_3 lifetimes ranging from about 10 s to more than 5000 s in the troposphere [*Ayers and Simpson*, 2006; *Crowley et al.*, 2010a; *Geyer et al.*, 2001; *Heintz et al.*, 1996; *Martinez et al.*, 2000].

Most of the NO_3 and N_2O_5 measurements have been performed at ground level, while NO_3 profiles can also be derived from passive DOAS during sunrise [*von Friedeburg et al.*, 2002] or long path DOAS by installing several reflection mirrors at different heights [*Stutz et al.*, 2004]. The development of new instruments, e.g. CRD and CIMS, makes the direct measurements of NO_3 and N_2O_5 vertical profiles possible by deploying them on mobile research platforms (e.g. aircrafts). In general NO_3 and N_2O_5 concentrations and their lifetimes were found to increase greatly with height above the ground [*Brown et al.*, 2007a; *Brown et al.*, 2007b; *Stutz et al.*, 2004].

1.3.4 Impacts of NO_3 and N_2O_5 chemistry in the troposphere

1.3.4.1 NOx loss and photochemical O_3 production

The nocturnal losses of NOx, mainly through the reactions of NO_3 with VOCs and heterogeneous uptake of N_2O_5, impact the NOx budget directly and thus influence the photochemical production rate of O_3 (and OH) [*Dentener and Crutzen*, 1993; *Evans and Jacob*, 2005], as shown in Figure 1-1. The contribution of the nocturnal NOx loss to the diurnal loss depends largely on the seasons and the locations. The relative contribution of the reactions of NO_3 with VOCs versus the heterogeneous reactions of N_2O_5 also varies, depending on the concentrations of biogenic alkenes and DMS, the aerosol surface concentration, relative humidity, and temperature [*Geyer et al.*, 2001]. For example, in a rural site in the Baltic Sea, the nocturnal removal of NOx was dominated by the

heterogeneous losses of N_2O_5 [*Heintz et al.*, 1996], whereas in a polluted marine environment, the contribution of the reactions of NO_3 with VOCs to the nocturnal NOx loss are approximately equal to that of the heterogeneous reaction of N_2O_5 [*Aldener et al.*, 2006]. In a rural mountain-site in south-western Germany, the nocturnal NOx losses were dominated by the reactions of NO_3 radicals with VOCs [*Crowley et al.*, 2010a]. Other nocturnal NOx loss processes, including the dry deposition of NO_3 and N_2O_5, gas-phase reaction with of N_2O_5 with H_2O, and the heterogeneous removal of NO_3 on aerosol surface, are generally of no real importance [*Geyer et al.*, 2001].

1.3.4.2 Degradation of organic species

The reactions with NO_3 are important degradation processes for biogenic alkenes and DMS, and sometimes even dominate over the contribution of the oxidation by OH radicals. For example, the reaction with NO_3 was found to be responsible for ~70% of the oxidation of total VOCs and ~75% of the olefinic VOCs in the summer of Jerusalem, about twice of the oxidation potential of the OH radicals [*Asaf et al.*, 2009]. In the anthropogenically-influenced eastern Mediterranean, depending on the season, NO_3 is estimated to be 2.7-8.5 times as effective as OH in DMS oxidation [*Vrekoussis et al.*, 2006]. In a coastal region with influence from both biogenic and anthropogenic emissions, the VOCs emitted by the natural sources were oxidized by NO_3 to a significant fraction, while anthropogenic VOCs and oxygenated VOCs mainly reacted with OH [*Warneke et al.*, 2004]. In the same campaign, the average DMS lifetime with respect to oxidation by OH at noon was 13.5±3.4 (1 σ) h, while at night DMS lifetimes with respect to NO_3 oxidation varied with sampling regions from 11 min to 28 h [*Osthoff et al.*, 2009].

1.3.4.3 Particulate nitrate formation

The heterogeneous loss of N_2O_5 on aerosol surface impacts the photochemical O_3 production via removal of NO_2. From the aerosol point of view, the heterogeneous reaction of N_2O_5 on aerosol surface and the reaction of NO_3 with DMS to from HNO_3 by H abstraction (R1-28), can also contribute significantly to the formation of particulate nitrate. In the anthropogenically-influenced eastern Mediterranean, the reaction of DMS with NO_3 and the heterogeneous reaction of N_2O_5 together account for ~50-65% of the total nitrate production [*Vrekoussis et al.*, 2006]. The total nitrate formation through the

heterogeneous N_2O_5 hydrolysis is estimated to be a factor of nine larger than the daytime total nitrate in the winter at the San Francisco Bay [*Wood et al.*, 2005].

1.3.4.4 Chlorine activation

The heterogeneous reaction of N_2O_5 with chloride in particles produces $ClNO_2$ [*Behnke et al.*, 1997; *Finlayson-Pitts*, 2003; *Finlayson-Pitts et al.*, 1989; *Frenzel et al.*, 1998; *Roberts et al.*, 2008; *Roberts et al.*, 2009], which will accumulate at night and be photolyzed after sunrise to produce Cl atoms, which can increase the oxidation rate of hydrocarbons in the troposphere and influence photochemical cycles that catalytically destroy or produce tropospheric ozone [*Knipping and Dabdub*, 2003]. Levels of $ClNO_2$ up to hundreds of pptv have been observed in both the marine [*Osthoff et al.*, 2008] and continental boundary layer [*Thornton et al.*, 2010].

1.3.4.5 Organic nitrate and organic aerosol formation

The oxidation of biogenic VOCs (e.g. isoprene and α-pinene) by NO_3 radicals, can also contribute to the formation of organic nitrates and secondary organic aerosols (SOA) [*Bonn and Moortgat*, 2002; *Fry et al.*, 2011; *Ng et al.*, 2008; *Perring et al.*, 2009]. For example, the organic nitrate yield from the reaction of isoprene with NO_3 radicals is found to be 65±12 %, of which the majority was nitrooxy carbonyls [*Perring et al.*, 2009]. The organic nitrate yield from the reaction of NO_3 with limonene was measured to be approximate 30%, while the SOA mass yield was observed to be 25-40% [*Fry et al.*, 2011]. The SOA yield from the reaction of NO_3 with isoprene (defined as the ratio of the mass of organic aerosol formed to the mass of parent hydrocarbon reacted) in a smog chamber study ranges from 4.3% to 23.8%, and ~2 to 3 Tg yr^{-1} of SOA is estimated to result from the reaction of isoprene with NO_3 radicals, using a uniform SOA yield of 10% [*Ng et al.*, 2008]. The contribution of nocturnal oxidation of isoprene to SOA was determined in the range of 1-17% in the summer of Northeast US, and the isoprene SOA mass derived from oxidation by NO_3 was calculated to exceed that due to OH by approximately 50% [*Brown et al.*, 2009b].

1.3.4.5 Aging of organic aerosols

The heterogeneous oxidation of organic particles by NO_3 radicals might be an important process for the aging of organic aerosols in the atmosphere [*Docherty and*

Ziemann, 2006; *George and Abbatt*, 2010; *Gross and Bertram*, 2009; *Knopf et al.*, 2006]. The heterogeneous interaction with NO_3 and N_2O_5 might also contribute to the nitration of particulate polycyclic aromatic hydrocarbons and proteins, probably making these particles more harmful to human health [*Franze et al.*, 2005; *Schauer et al.*, 2004].

1.4 Mineral dust aerosols in the troposphere

1.4.1 Emission, transport, and mineralogy of mineral dust aerosols

Mineral dust aerosols consist of soil particles that are lifted into the atmosphere when winds of high speeds occur over erodible surfaces [*Mahowald et al.*, 2005]. The average modeled emission fluxes of the total aerosols, sea salt, mineral dust, sulfate, organic aerosol, and black carbon are 18800, 16600, 1840, 179, 96.6, and 11.9 Tg yr^{-1}, respectively, making mineral dust the second largest source of atmospheric aerosols globally [*Textor et al.*, 2006]. The average atmospheric burden is 19.2 Tg for mineral dust, 7.52 Tg for sea salt, 1.99 Tg for non-sea-salt sulfate, 1.70 Tg for organic particles, and 0.24 Tg for soot [*Textor et al.*, 2006].

Mineral dust aerosol is mainly emitted from arid and semiarid areas, and the main sources are distributed across a band of arid regions in the Northern Hemisphere that extends from the west coast of North Africa, across the Middle East, and into central Asia [*Prospero*, 1999]. After being emitted into the atmosphere, mineral dust particles with a mass mean diameter <10 μm can be transported over thousands of kilometers [*Prospero*, 1999]. For example, African dust aerosol can be transported across the Atlantic to southeastern US [*Prospero*, 1999], the Caribbean [*Prospero and Lamb*, 2003], and Europe [*Ansmann et al.*, 2003; *Querol et al.*, 2009]. Dust aerosol emitted in central Asia has been found to be transported to Japan [*Shimizu et al.*, 2004], Korea [*Chun et al.*, 2001], and even western US across the Pacific [*Fairlie et al.*, 2007].

The mineralogical composition of dust has been estimated on a global scale [*Claquin et al.*, 1999]: illite, kaolinite, and smectite were found to be the major minerals in the clay fraction (<2 μm), while calcite, quartz, feldspar, hematite, and gypsum are the major minerals in the silt fraction (2-50 μm). Mineralogical classification of Asian dust particles shows that the most common single particles are clay aggregates (48%) that are often mixed with nano-sized calcite, followed by particles of quartz (22%), plagioclase (11%),

coarse calcite (6%), and K-feldspar (5%); the average mineral composition of the bulk dust samples was quartz (28%), interstratified illite-smectite (22%), plagioclase (11%), illite (19%), K-feldspar (8%), calcite (8%), chlorite (2%), smectite (1%), and kaolinite (1%) [*Jeong*, 2008]. For the Saharan dust transported to northeastern Spain, the minerals identified in the dust by X ray diffraction are as follows (by order of abundance): illite > quartz > smectite > palygorskite > kaolinite > calcite > dolomite > feldspar, and differences in mineralogy between source regions are significant for smectite, kaolinite, quartz, and dolomite [*Avila et al.*, 1997]. The chemical formulae and structures of main minerals contained by dust particles are listed in Appendices A5.

1.4.2 Tropospheric chemistry of mineral dust aerosols

The deposition of mineral dust into the ocean during transport, estimated to be 1500-1800 Tg yr^{-1} [*Mahowald et al.*, 2005], is the major input of soluble iron into many open-ocean regions, where the primary productivity is limited by the availability of iron [*Martin*, 1990]. Therefore, the deposition of mineral dust influences the oceanic biogeochemistry and the oceanic uptake and/or emission of a group of trace gases which are important to atmospheric chemistry and climate change, including CO_2, DMS, N_2O, CH_4, halocarbons, CO, and isoprene et al. [*Jickells et al.*, 2005].

Mineral dust aerosols can scatter and absorb solar and terrestrial radiation and thus influence radiative forcing directly. The maximum optical depth due to mineral dust aerosols is estimated to be 0.4-0.5 on the global scale [*Tegen and Fung*, 1994]. African mineral dust was found to be the dominant light-scattering aerosol throughout the tropical and subtropical North Atlantic region, with the net scattering about four times higher than that due to non-sea-salt sulfate [*X Li et al.*, 1996]. The dust aerosol radiative forcing is estimated to range from -0.47 to -0.24 W m^{-2} at the top of atmosphere and range from -0.81 to -1.13 W m^{-2} at the surface, after the mineralogy compositions and the corresponding mineral dust aerosol refractive indices are taken into account [*Balkanski et al.*, 2007].

Mineral dust particles can also act as ice nuclei (IN) and perhaps cloud condensation nuclei (CCN) and therefore influence radiative forcing indirectly. Many components (e.g., illite, kaolinite, calcite, and quartz) and surrogates (e.g. Arizona Test Dust) of mineral

dust particles are found to be effective ice nuclei in laboratory studies [*Archuleta et al.*, 2005; *Eastwood et al.*, 2008; *Knopf and Koop*, 2006; *Salam et al.*, 2006; *Zimmermann et al.*, 2008]. Asian dust particles were observed to affect the formation and phase of clouds, and hence their radiative properties as far away as in the US [*Sassen*, 2002]. When Saharan dust layers were present, the measured IN concentration in Florida (>1 cm^{-3}) exceeded typical values by at least a factor of 20-100 in the heterogeneous ice nucleation regime [*DeMott et al.*, 2003]. Saharan dust particles were also suggested to be a main constituent of ice nucleating aerosols in central Europe [*Klein et al.*, 2010]. The hygroscopic growth of mineral dust particles under subsaturated conditions is found to be quite small [*Gustafsson et al.*, 2005; *Navea et al.*, 2010; *Vlasenko et al.*, 2005]; however, they can also be activated as cloud droplets at supersaturation lower than required for insoluble particles [*Koehler et al.*, 2009; *Sullivan et al.*, 2009a], probably due to the soluble components in the particles [*Kelly et al.*, 2007]. It has also been demonstrated that Saharan dust particles do commonly act as cloud condensation nuclei (CCN) in the eastern North Atlantic [*Twohy et al.*, 2009].

Laboratory studies demonstrate the heterogeneous reactions of mineral dust particles with some atmospherically important traces gases, including (but not limited to) HNO_3 [*Goodman et al.*, 2000; *Hanisch and Crowley*, 2001a; *Vlasenko et al.*, 2006], N_2O_5 [*Seisel et al.*, 2005; *Wagner et al.*, 2008], NO_3 [*Karagulian and Rossi*, 2005], H_2O_2 [*Pradhan et al.*, 2010a; *Pradhan et al.*, 2010b], and NO_2 [*Ndour et al.*, 2009; *Ndour et al.*, 2008], thus directly or indirectly impacting the atmospheric burdens of NOx, O_3, and OH. For example, Asian dust was estimated to reduce NOx levels by up to 50%, HO_2 concentration by 20-80%, and ozone production rates by up to 25% in Eastern Asia [*Zhang et al.*, 1994]. A global modeling study suggested that the heterogeneous reactions with mineral dust can impact the oxidation of SO_2, the scavenging of HNO_3(g), and the formation of ozone [*Dentener et al.*, 1996]. In the MINATROC campaign the daytime mixing ratios of O_3, NOx, and H_2O_2 were observed to drop by 33%, 35%, and 48% during a Saharan dust event, respectively, while the mid-day ROx mixing ratios were reduced by 47% compared to dust-poor days [*de Reus et al.*, 2005]. During an Asian dust storm, O_3, SO_2, NO_2, and HNO_3 in the near-surface layer were modeled to be reduced by up to 20%, 55%, 20%, and 95%, respectively, due to the heterogeneous reactions with

mineral dust particles [*Tang et al.*, 2004]. The introduction of heterogeneous reactions with mineral dust can decrease modeled Ox and NOx concentrations in a megacity, Beijing, by 44-55% and 8-9%, respectively [*Zhu et al.*, 2009].

Heterogeneous processing of mineral dust can change its change chemical compositions. For example, laboratory studies suggest that nitrate is formed on the dust particles due to the heterogeneous reactions with HNO_3 [*Goodman et al.*, 2000] and N_2O_5 [*Seisel et al.*, 2005], and that sulfate is formed due to the heterogeneous oxidation of SO_2 on the dust surface [*L Li et al.*, 2006; *Usher et al.*, 2002].

Field measurements confirm that mineral dust particles undergo substantial chemical aging during transport and become internally mixed with nitrate and sulfate due to heterogeneous reactions. For example, during the transport of Asian dust, particulate nitrate was found to be nearly ten times lager in Japan than that near the source, and sulfate concentration was also increased, while the relative concentrations of crustal elements were almost constant [*Mori et al.*, 2003]. During ACE-Asia campaign in April 2001, measurements of individual dust particles show that significant fractions of the dust were internally mixed with secondary acids and ammonium, with nitrate and chloride enriched in supermicron dust while sulfate and ammonium enriched in the submicron mode [*Sullivan et al.*, 2007]. About 5-30% of the $CaCO_3$ in the Asian dust was converted to $CaSO_4$ or $Ca(NO_3)_2$ with an additional ~4% consumed through the reaction with HCl during the transport across the North Pacific, while in the boundary layer of Mexico city rich in NOx, 30% of the $CaCO_3$ was converted to $Ca(NO_3)_2$ and another 8% reacted with HCl [*McNaughton et al.*, 2009].

Modeling studies further highlight the importance of heterogeneous reactions in the aging of mineral dust aerosols. For example, dust is found to be an important surface for particulate nitrate formation [*Zhang et al.*, 1994]. During the ACE-Asia campaign, heterogeneous reactions led to >20% of the sulfate and >70% of the nitrate being associated with the coarse fraction of dust particles [*Tang et al.*, 2004]. The fraction of aerosol nitrate on dust in the model was estimated to increase from ~30% in fresh Asian outflow to 80-90% over the Northeast Pacific [*Fairlie et al.*, 2010].

The change of composition of mineral dust due to heterogeneous reactions further modifies its physicochemical properties (e.g. hygroscopic growth) and thus its efficiency to act as cloud condensation nuclei (CCN). Soluble Ca-containing chemicals, e.g. $Ca(NO_3)_2$ and $CaCl_2$, are very hygroscopic and can be activated as CCN similar to sulfate, and insoluble Ca-containing species, e.g. $CaCO_3$ and $CaSO_4$, are much less hygroscopic and have poor CCN activation ability, while calcium oxalate lies in between [*Sullivan et al.*, 2009a]. Solid $CaCO_3$ particles can also become internally mixed with $Ca(NO_3)_2$ and be converted to aqueous droplets due to the heterogeneous interaction with HNO_3(g) [*Krueger et al.*, 2003] or NO_2 [*Liu et al.*, 2008]. Nitrate-containing Asian dust particles are found to appear in the aqueous phase even at relative humidity (RH) as low as 15%, while dust particles containing no nitrate (even when sulfate is contained) do not change their crystalline morphology even when RH increases to 90% [*Shi et al.*, 2008].

The aging of dust particles can also change their efficiency of acting as ice nuclei (IN). Sulfate (H_2SO_4 or $(NH_4)_2SO_4$) coating can cause permanent chemical and/or physical modification of the ice active surface sites on the dust particles and thus reduce the ice nucleation ability of mineral dust particles [*Chernoff and Bertram*, 2010; *Cziczo et al.*, 2009; *Eastwood et al.*, 2009; *Niedermeier et al.*, 2010; *Sullivan et al.*, 2010b]. The effect of nitrate coating on the ice nucleation of dust particles is quite complex: exposing Arizona Test Dust particles to HNO_3(s) is found to impair subsequent deposition ice nucleation below water-saturation, but promote condensation/immersion freezing on approach to water saturation, and have no apparent impact on freezing of activated droplets above water saturation [*Sullivan et al.*, 2010a].

1.5 Atmospheric heterogeneous reactions

Heterogeneous reactions are chemical reactions in which the reactants are components of two or more phases or in which one or more reactants undergo chemical change at an interface. In atmospheric chemistry community, heterogeneous reactions usually mean reactions between gaseous species and the liquid or solid phase and/or its surface. The most widely used approach to describe the kinetics of heterogeneous processes is to use the uptake coefficient, γ, which is the net probability that a molecule X which undergoes a collision with a surface is actually taken up at the surface [*IUPAC*,

2009]. This approach links the processes at the interface and beyond with the pseudo-first-order loss of X in the gas phase:

$$\frac{d[X]}{dt} = -k[X] = -\gamma \cdot \frac{\bar{c}}{4} \cdot A \cdot [X] \quad \text{(E1-3)}$$

where [X] is the concentration of X in the gas phase (molecules cm^{-3}), t is the reaction time (s), k is the pseudo-first-order loss rate constant of X (s^{-1}), A is the surface concentration of the condensed phase ($cm^2\ cm^{-3}$), and $\bar{c}$ is the average molecular speed of X ($cm\ s^{-1}$):

$$\bar{c} = \sqrt{\frac{8RT}{\pi M}} \quad \text{(E1-4)}$$

where R is the gas constant, T is the temperature in K, and M is the mole mass of X. For a specific heterogeneous reaction, γ might depend on the reaction time, the gas phase concentration of X, temperature, relative humidity, and the coexistence of other gases.

If the uptake of X on the surface is fast, molecules of X near the surface will be significantly depleted and the uptake process might be limited by gas phase diffusion of X to the surface, resulting in a measured uptake coefficient, γ_{mea}, which is smaller than the true uptake coefficient, γ. In this case, a correction factor is usually applied so that (E1-3) can still be used to relate the net flux of X onto the surface with the overall loss of X in the gas phase. Under approximate steady-state assumptions, the effect of gas phase diffusion can be corrected by using approximate formulas which can be written as a resistance equation that decouples gas phase diffusion and heterogeneous processes:

$$\frac{1}{\gamma_{mea}} = \frac{1}{\gamma} + \frac{1}{\Gamma_{diff}} \quad \text{(E1-5)}$$

The parameter Γ_{diff} takes into account the effect of gas phase diffusion. There are several different approaches to calculate Γ_{diff} [*Davidovits et al.*, 1995; *Davidovits et al.*, 2006; *Fuchs and Sutugin*, 1970; *Kolb et al.*, 2002; *Kolb et al.*, 1995; *Poschl et al.*, 2007]. In this study the Fuchs-Sutugin formulation [*Fuchs and Sutugin*, 1970] is used:

$$\frac{1}{\Gamma_{diff}} = \frac{0.75+0.283Kn}{Kn(1+Kn)} \quad \text{(E1-6)}$$

where Kn is the Knudsen number, defined as

$$Kn = 2\lambda/d \quad \text{(E1-7)}$$

where d is the diameter of the particle, and λ is gas phase mean free path of X and can be expressed as

$$\lambda = 3D_g/\bar{c} \quad \text{(E1-8)}$$

where D_g is the gas phase diffusion coefficient of X, which can be measured or estimated [*Reid et al.*, 1987].

For the heterogeneous interaction of a trace gas, X, with liquid particles, the overall uptake process further consists of several fundamental steps, including the mass accommodation onto the surface, the solvation, diffusion, and reaction in the liquid phase [*Ammann et al.*, 2003; *Davidovits et al.*, 1995; *Davidovits et al.*, 2006; *Davidovits et al.*, 1991; *Poschl et al.*, 2007]. In addition, reactions can occur directly on the surface without being accommodated [*Hanson*, 1997; *Shi et al.*, 1999]. Under proper steady-state assumption, all the processes can be deconvoluted and expressed as a resistance equation [*Davidovits et al.*, 2006].

This study investigated the heterogeneous reactions with mineral dust particles, for which the diffusion and solubility of a trace gas, X, are usually mall or negligible. Heterogeneous reactions with solid particles are often characterized by adsorption of X on the surface, followed by the competition between reaction of the surface and desorption of X from the surface. There are generally two different mechanisms of surface reactions:

The first type is Langmuir-Hinshelwood mechanism, which involves the adsorption of the trace gas (in this case, X) and the following reaction of the adsorbed X with a surface adsorbed species, Y. The uptake coefficient of X, γ, can be parameterized as [*Crowley et al.*, 2010b]

$$\frac{1}{\gamma} = \frac{1}{\alpha_s} + \frac{1}{\Gamma_s} \quad \text{(E1-9)}$$

where α_s is the accommodation coefficient of X on the surface, and $1/\Gamma_s$ can be considered as the resistance for the surface reaction, which is given by

$$\frac{1}{\Gamma_s} = \frac{1+K_{LangC}(X)[X]_g}{k_s[Y]_s\alpha_s\tau_{des}} \quad \text{(E1-10)}$$

where $[X]_g$ is the concentration of X in the gas phase (molecules cm^{-3}), k_s is the surface reaction rate coefficient (cm^2 $molecule^{-1}$ s^{-1}), $[Y]_s$ is the surface concentration of Y (molecules cm^{-3}), and τ_{des} is the lifetime of adsorbed X with respect to the desorption (s^{-1}). (E1-9) and (E1-10) imply that the uptake coefficient depends negatively on the gas phase concentration of X, if $K_{LangC}(X)[X]_g$ is similar or larger than 1 (i.e. at high surface coverage). This is very important to interpret the uptake coefficients measured by laboratory experiments to values at ambient conditions, because the concentrations of X used in the laboratory studies are sometimes orders of magnitude higher than ambient levels, leading to a significantly higher surface coverage. This mechanism has been successfully used to parameterize the uptake coefficient of HNO_3(g) on Arizona Test Dust [*Vlasenko et al.*, 2009; *Vlasenko et al.*, 2006].

The second type is Eley-Rideal mechanism, which involves the direct reaction of X with a surface adsorbed species, Y. In this case, the uptake coefficient of X, γ, can be parameterized by [*Crowley et al.*, 2010b]

$$\gamma = \gamma_{gs}(X) \cdot \theta(Y) \qquad \text{(E1-11)}$$

where $\gamma_{gs}(X)$ is the elementary reaction probability that a gas molecule X which collides with Y adsorbed on the surface reacts with it, and $\theta(Y)$ is the surface coverage of Y. (E1-11) suggests that in the Eley-Rideal mechanism, the uptake coefficient of X does not depend on the gas phase concentration of X.

Two extreme types of reaction are: 1) catalytic and 2) surface poisoning. In the first case, the surface reactive sites are not consumed and the reaction continues with the same rate, independent of exposure time (upper panel of Figure 1-3). In the second case, the heterogeneous reaction can completely deactivate the surface, i.e. the surface reactivity is consumed and it cannot uptake any more X molecules after some exposure time (lower panel of Figure 1-3). An intermediate case is when some process can replenish the surface on the time-scale of the deactivation, or if diffusion into the bulk plays an important role. In this case, the uptake becomes slower with time but does not stop (middle panel of Figure 1-3).

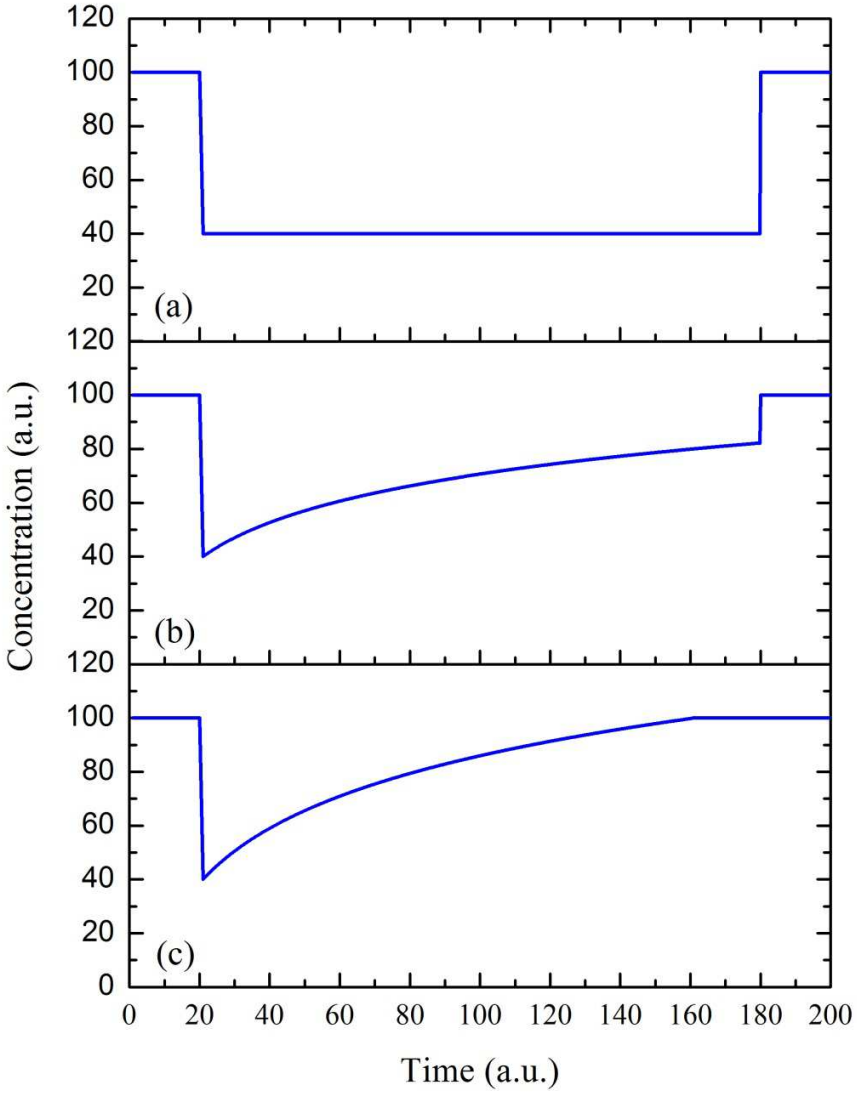

Figure 1-3. Synthetic data of the decay of the trace gas, X, due to the heterogeneous uptake when the particles sample is exposed to the gas from 20 to 180 a.u. (a.u. = arbitrary unit). Upper panel: no surface deactivation. Middle panel: partial surface deactivation. Lower panel: complete surface deactivation.

2 Experimental procedures and setups

In the course of this work, four different experimental setups were used to investigate the heterogeneous reactions of NO_3 and N_2O_5 with mineral dust particles: (1) a novel relative rate method was developed to study the heterogeneous uptake of NO_3 and N_2O_5 on atmospherically-relevant particles; (2-3) two atmospheric-pressure aerosol flow tubes were employed to investigate the heterogeneous interaction of N_2O_5 (and HNO_3) with airborne mineral dust particles; (4) the fraction of NO_2 produced from the heterogeneous reaction of N_2O_5 with Saharan dust was measured by Thermal Dissociation-Cavity Ring Down spectroscopy. All the chemicals and materials used in this work are listed in Appendices A3.

2.1 Relative rate method apparatus

The apparatus for relative uptake measurements, as shown in Figure 2-1, consists of three main parts: NO_3 and N_2O_5 generation (red), trace gases-particle samples interaction (blue), and NO_3/N_2O_5 detection (green).

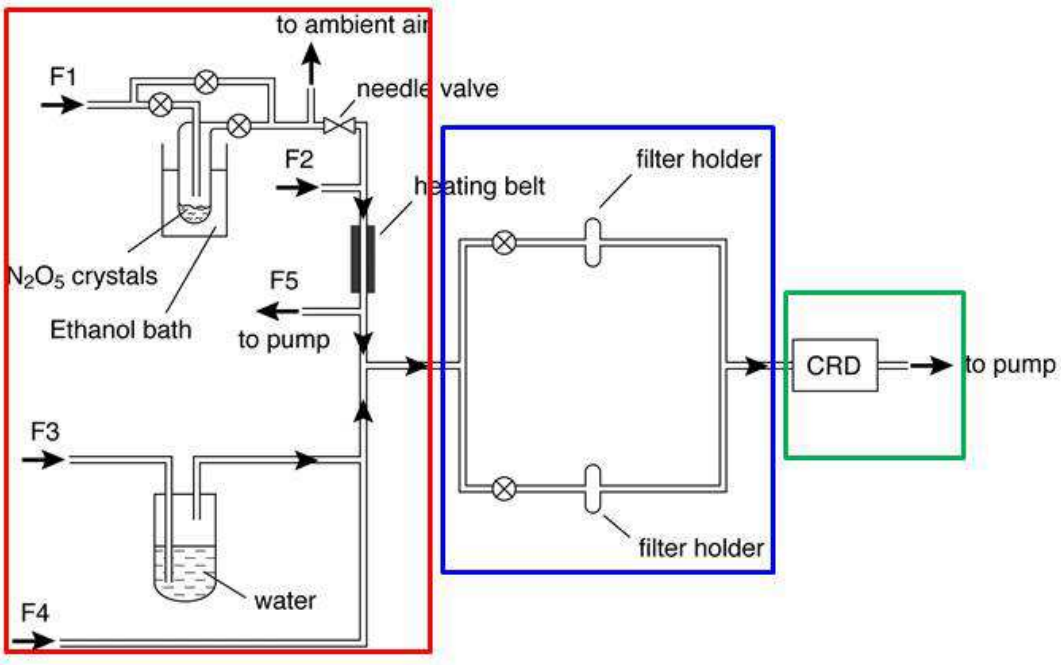

Figure 2-1. Schematic diagram of the relative rate method apparatus. F1, F2, F3, F4, and F5 are mass flow controllers. The heater was operated at 60–65 °C. The ethanol bath was kept at –60 °C.

2.1.1 NO_3 and N_2O_5 generation

N_2O_5 crystalline was prepared by mixing dried flows of pure NO_2 (99.5%) and O_3 in O_2 at room temperature (R2-1 and R2-2a) in a glass reactor and trapping the product in a cold finger held in ethanol-dry ice bath [*Fahey et al.*, 1985]:

$$NO_2 + O_3 \rightarrow NO_3 + O_2 \quad \text{(R2-1)}$$

$$NO_2 + NO_3 + M \rightarrow N_2O_5 + M \quad \text{(R2-2a)}$$

A large excess of O_3 concentrations ensured that all NO_2 was oxidized. This was checked by visually inspecting the complete disappearance of the brown color of NO_2 gas within a few seconds of mixing.

Gaseous N_2O_5 was eluted from a crystalline sample held at ~213 K in a 200 sccm (standard cubic centimeter per minute) flow of N_2 (F1) and then diluted dynamically to generate a flow (~500 sccm) containing several hundred pptv of N_2O_5, after being diluted to 10 SLM (standard liter per minute). The flow was then passed through a section of PFA tubing heated to 60–65 °C to convert some (usually ~50%) of the N_2O_5 to NO_3. The flow containing NO_3 and N_2O_5 was subsequently diluted further (F3+F4) by synthetic air to 10 SLM, the relative humidity (RH) of which could be adjusted by changing the ratio of flows through F3 (humidified flow) and F4. The concentration of NO_3 and N_2O_5 could be changed by adjusting F5.

The mixed NO_3 and N_2O_5 sample generated in this manner should contain a similar amount of NO_2. Previous work [*IUPAC*, 2009] has shown that NO_2 interacts only weakly with mineral dust with an uptake coefficient of less than 10^{-6}, so it does not significantly affect the measurements.

2.1.2 Aerosol sample generation and preparation

The total 10 SLM flow was directed through a clean 2-μm pore Teflon (PTFE) membrane filter (Pal Teflon R2PJ047) held in a PFA filter-holder (referred to as the "blank" path) or through a particles-loaded filter (referred to as the "sample" path). The gas-flow could be alternately directed through each path via PFA valves and the two paths were identical in terms of tubing materials and residence time, the only difference being the state of the filter.

Saharan dust particles were dispersed by a commercial rotating brush generator and then collected on the filters. The Saharan dust particles generated in this way have an average aerodynamic diameter of ~2 μm (see Chapter 4 for more details).

Ambient aerosols were sampled directly outside of our lab in the second floor of the MPI Chemistry main building. A sample flow rate of 1 m^3 h^{-1} was used over a typical sampling time of 48 h, and the mass of ambient particles collected on the filters was between ~0.4 and 0.8 mg. After the sampling, the filters were sealed and stored at 4 °C before use. As the building is close to busy roads and several large motorways, the aerosol is expected to be mainly transport-generated carbonaceous components. No aerosol characterization was carried out, though visual inspection confirmed the discoloration of the filter by black carbon particles.

Freshly-generated soot particles were sampled from the flame of a burning candle onto clean microscope glass slides before being transferred onto the PTFE filters using a clean knife edge. The soot did not adhere well to the filters and thus weight of the samples was not determined. The composition of soot generated using a candle flame is expected to depend on the burning mode of the candle and on chemical additives to the wax and the wick [*Pagels et al.*, 2009], hence the mass fractions of elemental carbon, inorganic and organic matter in our soot samples were unknown.

After exiting the filters the gas-mixture was directed into the two cavities of a Cavity Ring-Down spectrometer (CRD). 4 SLM was passed into the NO_3 channel and the other 6 SLM was passed into the NO_3+N_2O_5 channel. The CRD instrument is described in Section 2.3.

2.2 Aerosol flow tubes

Two different aerosol flow tubes (AFT, denoted here as “old” and “new”) were developed to study the heterogeneous interaction of mineral dust aerosols with N_2O_5, at concentrations ranging from 5×10^{11} to 3×10^{13} molecules cm^{-3}. The new AFT was also employed to investigate the heterogeneous uptake of HNO_3 on Saharan dust aerosols.

2.2.1 The old aerosol flow tube for N_2O_5

The old aerosol flow tube deployed in this study is similar to that used by Wagner at al. (2008), except the method used to sample gas from the flow tube. Experiments were all conducted at or close to atmospheric pressure (~750 Torr) and room temperature (296±2 K). The flow reactor, with the schematic shown in Figure 2-2 and the photo shown in Figure 2-3, is a vertically mounted Pyrex tube with the length of 120 cm and the inner diameter of 4.1 cm. N_2 was used for all the flows unless otherwise stated.

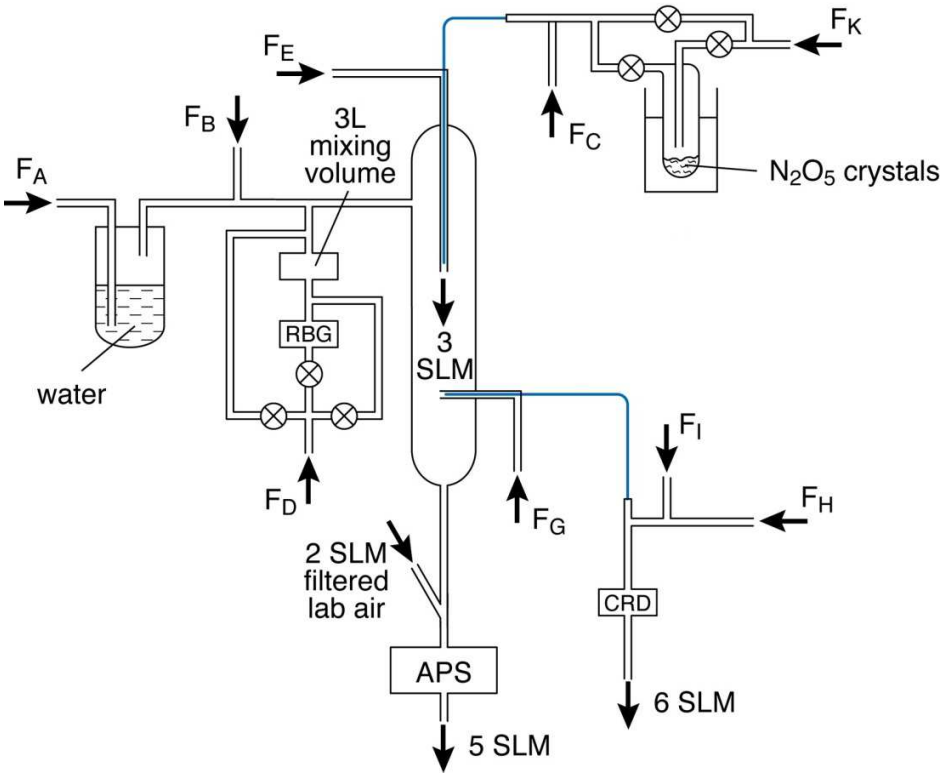

Figure 2-2. The schematic diagram of the old aerosol flow tube apparatus. RBG=Rotating Brush Generator, APS=Aerodynamic Particle Sizer, CRD=Cavity Ring-Down spectroscopy. The typical total flow in the AFT was 3010 sccm, with FA+FB=2000 sccm, FC+FK=200 sccm, FD=800 sccm, FE=10 sccm. The total flow in the CRD was 6000 sccm, with FH+FI=5600 sccm, a purge gas flow of 200 sccm, and the flow sampled from the AFT. FG, with a flow of 200 sccm, was used to prevent particles from entering the 1/8'' sample tube. The ethanol bath was usually kept at -50 °C.

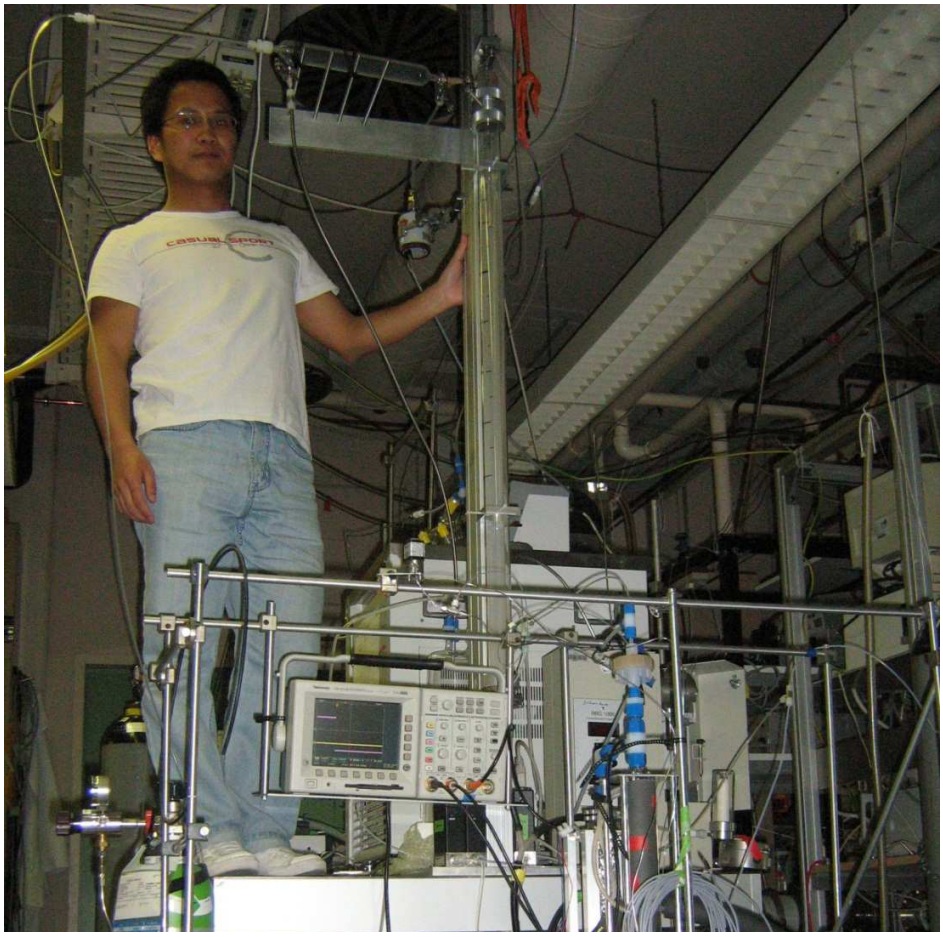

Figure 2-3. The photo of the old aerosol flow tube apparatus.

The typical total flow in the AFT was 3010 sccm, resulting in a Reynolds number of 112, an entrance length of ~26 cm to develop laminar flow, and a mixing length of ~42 cm. The Reynolds number, *Re*, is calculated by [*Keyser*, 1984]

$$Re = \frac{2 \cdot r \cdot v \cdot \rho}{\eta} \quad \text{(E2-1)}$$

where r is the radius of the flow tube (2.05 cm), v is the linear speed of the flow (4.19 cm s^{-1}, calculated from the total flow in the AFT and the radius of the AFT), ρ is the gas density (1.17×10^{-3} g cm^{-3} at 750 Torr and 25℃), and η is the gas viscosity ($1.791.17\times10^{-4}$ g cm^{-1} s^{-1}). The entrance length, *Le*, is then given by [*Keyser*, 1984]

$$Le = 0.012 \cdot r \cdot Re \quad \text{(E2-2)}$$

And the mixing length, *Lmix*, is given by [*Keyser*, 1984]

$$Lmix = \frac{v \cdot r^2}{5 \cdot Dg} \quad \text{(E2-3)}$$

where D_g is the diffusion coefficient of N_2O_5 (0.085 cm^2 s^{-1}, [*Wagner et al.*, 2008])

Bulk dust samples were dispersed and entrained into the 800 sccm flow (FD) using a commercially available rotating brush generator (RBG, for Saharan dust and illite) or a self-made dust aerosol generator (for ATD). The aerosol flow was then mixed with the 2000 sccm carrier gas flow (FA+FB), transported through the 1/4'' metal tube, and introduced into the top of the AFT via a side arm. The carrier gas flow could be humidified before mixing with the aerosol flow, enabling the RH in the AFT to be adjusted up to 67%. In some experiments, the aerosol flow after the dust generator was immediately mixed with the carrier gas; while in others, the aerosol flow was transported through a glass mixing volume (~5 L) before mixing with the carrier gas. The residence time in the mixing volume was about 6 min, and the purpose of using this mixing volume was to smooth spikes in the aerosol number concentration. The results of the two different sets of experiments are discussed in Chapter 4.

A small N_2 flow (10-40 sccm, FK) was used to elute the N_2O_5 crystalline held at 223 K, diluted by FC to 200 sccm, and transported through the 1/8'' PFA tube (i.d. ~1.5 mm) into the lower 10 cm of the injector (i.d. 5 mm, coated with FEP) and then into the flow tube. Another small flow (FE, 10 sccm) was used to purge the injector. The position of the movable injector defines the interaction time of N_2O_5 with mineral dust aerosols.

The wall of the AFT was kept dusty and thus highly reactive towards N_2O_5. In this case the loss of N_2O_5 on the wall was close to being gas-phase diffusion limited and thus remained constant during an experiment no matter how many dust particles were present in the AFT. The diffusion-limited wall loss rate in this cylindrical tube is calculated to be 0.075 s^{-1}, according to

$$k_w^{diff} = \frac{3.66 \cdot Dg}{r^2} \quad \text{(E2-4)}$$

where r is the radius of the flow tube (2.05 cm) and D_g is the diffusion coefficient of N_2O_5 (0.085 cm^2 s^{-1}, [*Wagner et al.*, 2008]). The wall loss rate was routinely determined by measuring the N_2O_5 concentration at different injector positions. A typical result of the wall loss rate measurement is shown in Figure 2-4, giving a measured wall loss rate of

0.048 ± 0.002 s^{-1} (1 σ), which confirms the assumption that the N_2O_5 wall loss is largely limited by gas phase diffusion.

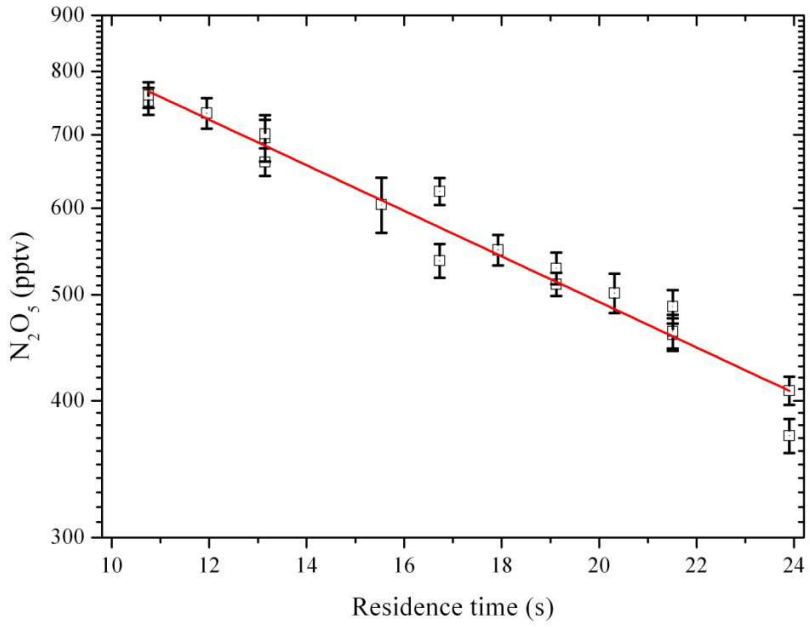

Figure 2-4. Exponential dependence of measured N_2O_5 concentration on residence time in the aerosol flow tube. The red curve is the weighed least squares error exponential fit, and the slope of the fit (0.048 ± 0.002 s^{-1}, 1 σ) is the measured wall loss rate.

2.2.1.1 Gas-particle separation

The Cavity Ring-Down spectroscopy (CRD) used to measure N_2O_5 is described in detail in section 2.3. This instrument has a very low detection limit (a few pptv) for NO_3 and N_2O_5, but is also very sensitive to the scattering of aerosols. As shown in Figure 2-2, the total flow in the CRD was 6000 sccm, consisting of the 200 sccm purge gas flow, the 5600 sccm dilution flow (FH+FI), and the flow sampled from the AFT through the 1/8'' PFA tube (200 sccm). High concentration aerosols in the AFT might deposit on the wall of the sampling tube and/or on the filter used to stop the particles entering into the CRD, and thus lead to additional loss of N_2O_5. Therefore, a counter flow of 200 sccm (FG, and the flow rate was optimized) was used to prevent the aerosols from being sampled. In addition, a Teflon filter was always placed before the CRD apparatus to protect the cavities.

The usage of the counter flow enabled particles-free air (<1 particles cm^{-3}, measured by a TSI 3010 Condensation Particle Counter) to be sampled from the flow tube, though it also resulted in additional dilution of N_2O_5. In order to calculate the dilution factor, 200 sccm NO_2 flow (about 2100 ppmv, measured optically) was introduced into the AFT through the injector and the final concentration in the CRD was measured by the absorption at 662 nm.

The total dilution factor, defined as the ratio of the concentration in the AFT to that measured in the CRD, was experimentally determined to be 645. With this dilution factor, the initial N_2O_5 concentration in the AFT could be calculated from the N_2O_5 concentration measured by CRD, after taking into account the loss on the wall of the AFT, the loss on the filter, and the loss in the CRD's cavity.

2.2.2 The new aerosol flow tube for N_2O_5

The new aerosol flow tube was designed and developed as part of this work. Experiments in the new AFT were all performed at close to atmospheric pressure (~750 Torr) and room temperature (296±2 K). The flow tube, as shown in Figure 2-5, is a vertically mounted Pyrex tube with the length of 125 cm (length between the side arm and the bottom end) and the inner diameter of 4.1 cm. The typical total flow in the AFT was 2200 sccm, resulting in a Reynolds number of 75 (E2-1), an entrance length of about 28 cm to develop the laminar flow (E2-2), and a mixing length of ~17 cm (E2-3). N_2 was used for all the flows unless otherwise stated.

Bulk Saharan dust samples were dispersed and entrained into the 800 sccm flow (FD) using the rotating brush generator. The aerosol flow was then delivered into a 5 L glass mixing volume. After exiting the mixing volume, the aerosol flow was diluted by the 1200 sccm carrier gas flow (FA+FB), transported through the 1/4'' metal tube, and introduced into the top of the AFT via a side arm. The carrier gas flow could be humidified before mixing with the aerosol flow, enabling the RH in the AFT to be adjusted up to 55%.

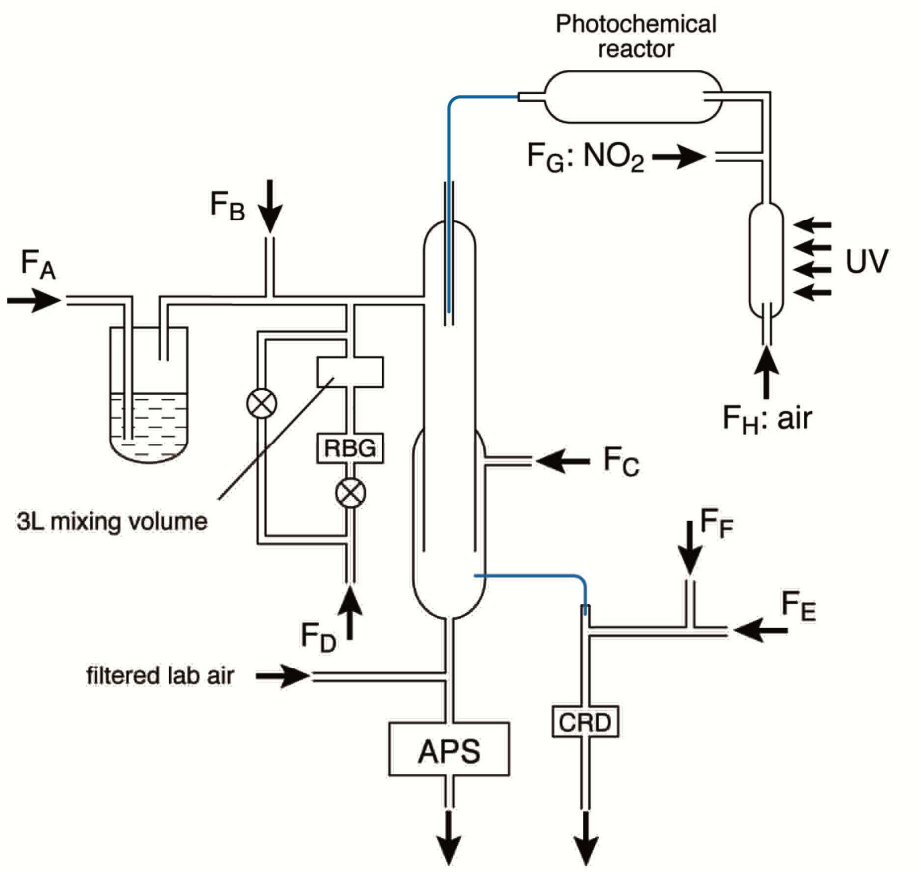

Figure 2-5. The schematic diagram of the new aerosol flow tube apparatus. RBG=Rotating Brush Generator, APS=Aerodynamic Particle Sizer, CRD=Cavity Ring-Down spectroscopy. The typical total flow in the AFT was 2200 sccm, with FA+FB=1200 sccm, FD=800 sccm, FG=180 sccm, FH=20 sccm, FC=200 sccm, and FE+FF=5500 sccm. The total flow sampled by CRD was 6000 sccm.

Similar to the old AFT, the wall of the new AFT was also coated with dust particles and kept highly reactive towards N_2O_5. The diffusion limited N_2O_5 wall loss rate was calculated to be 0.075 s^{-1} (E2-4), and the measured wall loss rate was determined to be ~0.08 s^{-1}, independent of relative humidity (shown in Figure 2-6). Therefore, the loss of N_2O_5 on the wall was limited by gas-phase diffusion and stayed constant no matter how many dust particles were introduced into the flow tube during the experiments.

2.2.2.1 Gas-particle separation

The lower 35 cm of the AFT was inserted coaxially into another vertically mounted, 60 cm long and 56 mm inner diameter Pyrex tube. The end of the AFT exhibits a sharp edge to avoid turbulences at the point of mixing. A N_2 sheath flow (FC) was fed into the

annular space between the two coaxial tubes, adjusted to 2000 sccm so that the average linear gas velocities matched at the point of mixing.

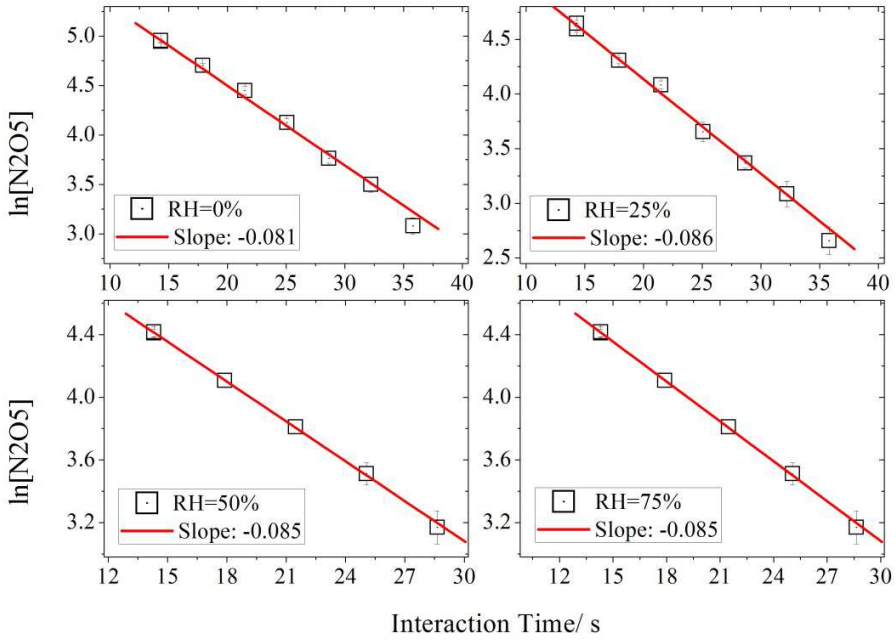

Figure 2-6. Experimentally-measured wall loss rate of N_2O_5 at different relative humidity. The red curves are the weighed least squares error exponential fits.

The principle of the gas-particle separation is that under laminar conditions, gas (in this case, N_2O_5) exchange occurs by diffusion (the diffusion coefficient is 0.085 cm^2 s^{-1}, [*Wagner et al.*, 2008]) between the inner and outer flows of the tube (I.D. 56 mm), while particles remain in the center due to their low diffusivity (10^{-7}-10^{-6} cm^2 s^{-1} for 1 μm particles with unit density [*Hinds*, 1996]).

At the bottom of the 56 mm inner diameter tube (about 25 cm from the end of the AFT), particle-free air was sampled into two identical 1/8'' PFA tubes, diluted by 5500 sccm carrier gas (FE+FF), and then delivered into the CRD, which measured the N_2O_5 concentration. The two 1/8'' tubes were just inserted 2-3 mm into the 56 mm inner diameter tube to avoid sampling the dust particles in the center. The total flow delivered into the CRD was set to 6000 sccm (controlled by MFCs), and the carrier gas was set to 5500 sccm (FE+FF), so approximately 500 sccm air (which was optimized by compromising the gas-particle separation efficiency and the dilution factor) was sampled from the flow tube, i.e. ~250 sccm in each 1/8'' tube. For some experiments, in order to

reach higher N_2O_5 concentration in the AFT, FE+FF was set to 5700 sccm or 5800 sccm, so only 300 sccm or 200 sccm air was sampled from the flow tube, respectively. The two 1/8'' PFA tubes were diametrically-distributed, so the disturbance of the flow condition in the 56 mm inner diameter tube could be minimized to avoid sampling particles.

The sampled flow by the two 1/8'' tubes was checked by a condensation particle counter (CPC, TSI 3010) and it remained particle-free (< 1 particles cm^{-3}) even when the aerosol reached 20,000 particle cm^{-3} in the AFT. The total dilution factor, defined as the ratio of the N_2O_5 concentration in the AFT to the N_2O_5 concentration measured by the CRD, was determined by the following method: 50 sccm NO_2 flow (1124 ppmv, measured optically) was delivered into the AFT through the 1/8'' PFA tube in the injector while all the other flows were kept the same as normal, and the NO_2 concentration in the CRD was measured by its absorption at 662 nm. The total dilution factor was measured to be 30, which is a factor of ~20 less than that for the old aerosol flow tube in which the counter flow was used for gas-particle separation.

2.2.2.2 Gaseous N_2O_5 generation

In some experiments, N_2O_5 was photochemically generated from the reaction of O_3 with NO_2 (R2-1) and the subsequent reaction of the formed NO_3 radicals with NO_2 (R2-2a). O_3 was generated by photolysis of synthetic air or oxygen (FH, 20 sccm) by a low pressure Hg lamp. The O_3 flow was mixed with 180 sccm NO_2 flow (FG, 1 ppmv in N_2) in an FEP-coated glass reactor (ID 5.6 cm, length 60 cm, volume 6 L). The O_3 concentration in the 20 sccm flow, measured by its absorption at 662 nm, was about 1000 ppmv (corresponding to about 10 ppmv O_3 in the AFT) when O_2 was used and 400 ppmv (corresponding to about 4 ppmv O_3 in the AFT) when synthetic air was used. Due to the large excess of O_3, the N_2O_5 concentration in the AFT was controlled by the amount of NO_2 and did not depend on the O_3 concentration. Simulation of the chemistry in the photochemical reactor confirms that less than 0.002 of the initial NO_2 was left after exiting the photochemical reactor, while the loss of O_3 was negligible. The simulation was carried out using FACSIMILE [*Curtis and Sweetenham*, 1987], and the code is given in Appendices A4.1.

In some experiments, 10 sccm N_2 was used to elute N_2O_5 crystalline kept at -50 °C in a cold bath and then diluted by another 200 sccm N_2 flow. After the dilution, most of the flow was directly pumped to the exhaust line and the remaining flow was diluted again by a 200 sccm N_2 and then transported through the 1/8'' PFA tube in the injector into the flow tube. This method generated gaseous N_2O_5 free of O_3 and NO_2 (though some amount of NO_2 might be formed due to the decomposition of N_2O_5, (R2-2b)), and the concentration of the generated N_2O_5 could be adjusted over a broad range.

$$N_2O_5 + M \rightarrow NO_2 + NO_3 + M \qquad \text{(R2-2b)}$$

In two experiments to test the influence of O_3 on the heterogeneous interaction of N_2O_5 with dust particles, O_3 was generated by the photolysis of a 20 sccm O_2 flow by a low pressure Hg lamp. After that, the O_3 flow was combined with the N_2O_5 flow, and delivered into the AFT through the 1/8'' PFA tube in the injector. The O_3 concentration in the AFT used in the two experiments were determined to be 6.8 ppmv and 14 ppmv, respectively.

2.2.3 The aerosol flow tube for HNO_3

The aerosol flow tube for HNO_3 uptake measurement is almost the same as the new AFT for N_2O_5. Gaseous HNO_3(g) was generated by eluting nitric acid solution with 200 sccm N_2 and then transported into the flow tube through the 1/8'' PFA tube inside the injector. After exiting the aerosol flow tube, the aerosol flow came into the 56 mm inner diameter tube (which was coaxial with the AFT) and was joined with the sheath flow of the same linear velocity. HNO_3(g) (its diffusion coefficient is 0.12 $cm^2\ s^{-1}$ [*Braman et al.*, 1982]) diffuses into the outer part of the 56 mm inner diameter tube but particles remains in the center due to the larger diffusion coefficient (10^{-7}-10^{-6} $cm^2\ s^{-1}$ for 1 μm particles with unit density [*Hinds*, 1996]). At the point which was about 25 cm lower than the bottom of the aerosol flow tube, 500 sccm particles-free air was sampled by a 1/4'' PFA tube, diluted to 3 SLM, and then measured by Chemical Ionization Mass Spectrometry (CIMS). The CIMS instrument is described in detail in Section 2.3.2. All the sampling tubes were kept at 60 °C to reduce the adsorption of nitric acid on the inner wall.

2.2.4 Aerosol measurement

After exiting the flow tubes, the aerosol flow was combined with filtered lab air to 5 liter per min, diluted by a factor of 20 by an aerosol dilutor (TSI 3302A), and then measured by an Aerodynamic Particle Sizer (APS, TSI 3321). The APS provides both the time-averaged (1-2 hours) size distribution and an analogue output proportional to the aerosol number concentration. No significant change in the particle size distribution, measured and averaged every 5-10 min, was observed over the course of an experiment (~ 1 h). Validation on the APS size distribution measurement using certificated Latex (spherical) and Quartz (un-spherical) particles was described previously [*Wagner et al.*, 2008].

In principle, the APS measures the time of flight of a particle over a fixed distance to derive the equivalent aerodynamic diameter (*Da*), defined as the diameter of the spherical particle of unity density with the identical aerodynamic properties. It can be converted to the equivalent Stokes diameter (*Ds*):

$$Ds = Da/\sqrt{\rho} \qquad \text{(E2-5)}$$

where ρ is the density of the particle [*Hinds*, 1996]. The mineral dust particles used in this study are not spherical; and for sedimenting particles, the aerodynamic shape factors, β, may be applied to derive the real Stokes diameter:

$$Ds = Da/\sqrt{\rho\beta} \qquad \text{(E2-6)}$$

For Saharan dust, a factor of 1.6 was used previously in our laboratory to correct the surface area [*Wagner et al.*, 2008], and this factor is also used to correct the surface area of Saharan dust particles in this study. For the other types of dust particles, the surface area are calculated based on the *Ds* given by (E2-5), i.e. ignoring the possible shape effects.

2.3 NO_3, N_2O_5, and HNO_3 detection

In this work NO_3 and N_2O_5 were measured by Cavity Ring-Down spectroscopy (CRD), and HNO_3 was detected by a Chemical Ionization Mass Spectrometry (CIMS).

2.3.1 Cavity Ring-Down spectroscopy

The schematic of the two-channel CRD is shown in Figure 2-7. It has been developed in our group chiefly as a field instrument. Instrumental details, including optical configuration, gas flows, and data acquisition, were described previously [*Crowley et al.*, 2010a; *Schuster et al.*, 2009] and thus only a brief description is given here.

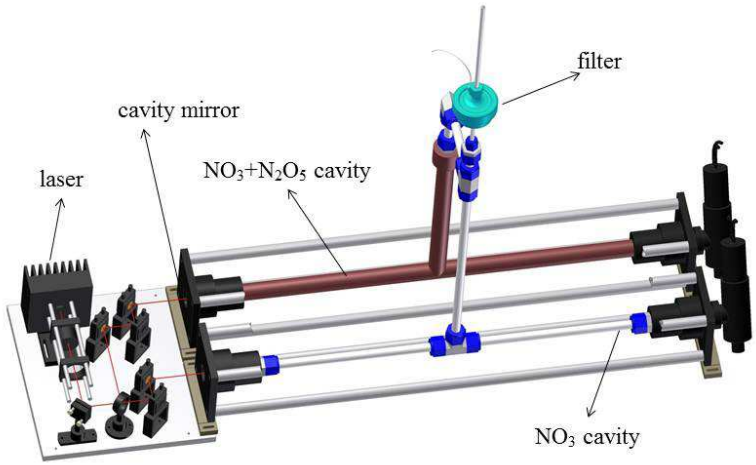

Figure 2-7. The schematic of two-channel Cavity Ring-Down spectroscopy at 662 nm. Gas was sampled through the filter and then split into the two channels. In the front channel held at room temperature, NO_3 was measured; in the back channel held at 90°C, the sum of NO_3 and N_2O_5 was measured.

The instrument makes use of the well-characterized, strong absorption band of NO_3 at around 662 nm (black line in Figure 2-8) by using a laser-diode modulated at 100 Hz. It relies on the measurement of the rate of decay of light exiting a high-finesse optical cavity to derive the ring-down constant (k_{rd}), which depends on scattering and absorption losses in the cavity [*Brown et al.*, 2002; *Okeefe and Deacon*, 1988]. The use of high-reflectivity mirrors results in the optical absorption length of ~40 km in both channels. The change in ring-down constants (Δk_{rd}) in the presence and absence of NO_3 is used to calculate the NO_3 concentration:

$$[NO_3] = \frac{\Delta k_{rd} \cdot L}{\sigma(NO_3) \cdot c \cdot d} \qquad \text{(E2-7)}$$

where [NO_3] is the concentration of NO_3 (molecules cm^{-3}), Δk_{rd} is the difference in the ring-down decay constants (s^{-1}) with and without NO_3 in the cavity, L is the distance between the two mirrors (70 cm), d is the length of the cavity which is filled with the absorber (NO_3), and c is the speed of light.

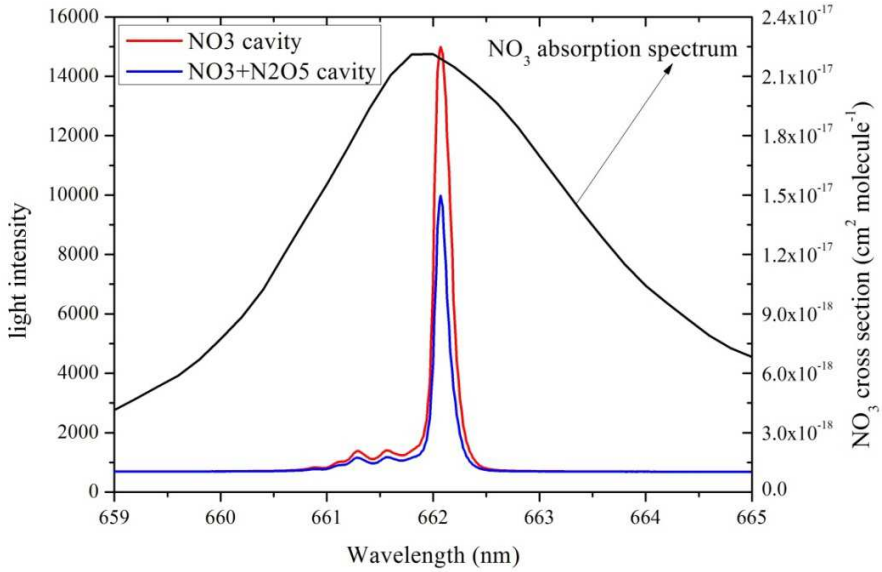

Figure 2-8. The wavelength dependent cavity-emission intensity in the two channels (blue and red lines, left y-axis) of the CRD spectroscopy. The NO_3 absorption (black line, right y-axis) between 659 and 665 nm at 298 K [*Yokelson et al.*, 1994] is also shown for comparison.

The chemical 'zero' (in the absence of NO_3) is achieved by adding 8 sccm NO (100 ppmv in N_2) to the sampled flow to titrate the NO_3 before splitting the flow to the two channels:

$$NO + NO_3 \rightarrow NO_2 + NO_2 \qquad \text{(R2-3)}$$

The rate constant of (R2-3) is 2.6×10^{-11} molecules cm^{-3} at 25 °C [*Atkinson et al.*, 2004], leading to a lifetime of 0.035 s for NO_3 when the total flow is 18 SLM (for comparison the typical residence time in the cavities is 0.5-1 s). In the other channel, the inlet and the cavity are both held at 90 °C so that N_2O_5 is thermally decomposed to NO_3:

$$N_2O_5 + M \rightarrow NO_2 + NO_3 + M \qquad \text{(R2-2b)}$$

The rate constant of (R2-2b) is about 23.5 s^{-1} at 90 °C and 750 Torr [*Atkinson et al.*, 2004], implying that only 9.5% and 0.9% N_2O_5 is left after 0.1 and 0.2 s, respectively.

Therefore, in the vertical inlet of this cavity all the N_2O_5 is thermally decomposed to NO_3 and the sum of NO_3 and N_2O_5 concentration is measured. The difference in the concentrations measured by the two cavities (after correction for transmission efficiencies, etc. see Section 2.3.1.1 for details) is the measured N_2O_5 concentration.

The wavelength dependent cavity-emission intensity in both channels of the CRD were measured independently and shown in Figure 2-8. The measured laser spectra, together with the reported cross sections of NO_3 [*Yokelson et al.*, 1994], were used to calculate the effective cross section of NO_3 in both channels. The effective cross section of NO_3 at 298 K, was determined to be 2.107×10^{-17} cm^2 $molecule^{-1}$ in the NO_3 channel and 2.099×10^{-17} cm^2 $molecule^{-1}$ in the NO_3+N_2O_5 channel. These values are used in (E2-7) to calculate the NO_3 (and thus N_2O_5) concentration.

2.3.1.1 Data corrections

The use of an extractive approach to measure NO_3 and N_2O_5 requires the knowledge of the transmission efficiencies of both species through the cavities. The use of purge gas to protect the mirrors of the cavities makes *d* smaller than *L*, and the ratio of *L* to *d* was also measured.

L/D ratio: In the laboratory study, typically the total flow was 4 SLM in the NO_3 channel and 6 SLM in the NO_3+N_2O_5 channel, and a purge gas flow of 200 sccm was used in each cavity to keep the mirrors clean. The *L/d* value is equal to ratio of measured NO_3 concentration without and with the purge gas. Due to its stability, NO_2, instead of NO_3, was used as the absorber in these experiments. The measured NO_2 concentration at different purge gas flows in both channels, normalized to the concentration measured when the purge gas was 200 sccm, is displayed in Figure 2-9. The *L/d* values, when the purge gas flow was 200 sccm in both channels, were experimentally determined to be 1.01±0.01 for the NO_3 channel (total flow: 4 SLM) and 1.02±0.01 for the NO_3+N_2O_5 channel (total flow: 6 SLM).

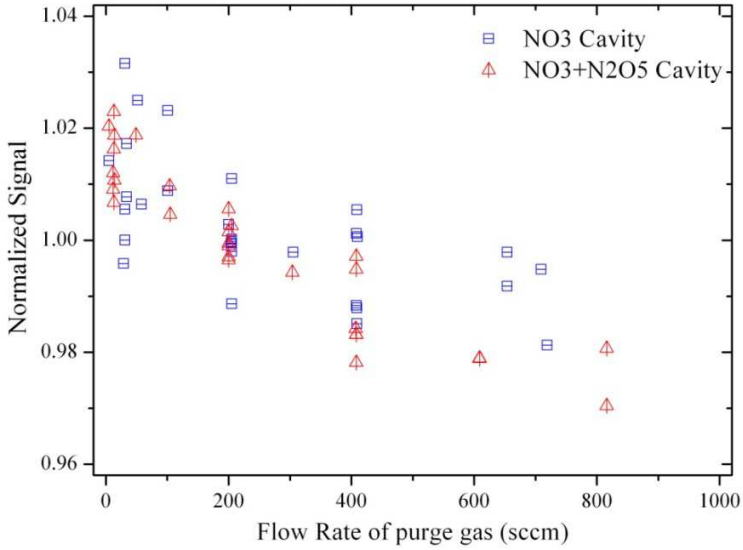

Figure 2-9. Measured concentration of absorbers in both channels of the CRD at different purge gas flows, normalized to the measured concentration when the purge gas flow was 200 sccm.

Transmission efficiency in the cavities: Sampling gas into the cavities leads to the loss of NO_3 (and thus N_2O_5) on the wall of the cavities, and the transmission efficiencies of NO_3 in both cavities should be determined in order to correct the measured concentrations. The apparatus used to measure the cavity transmission efficiencies in both channels is displayed in Figure 2-10.

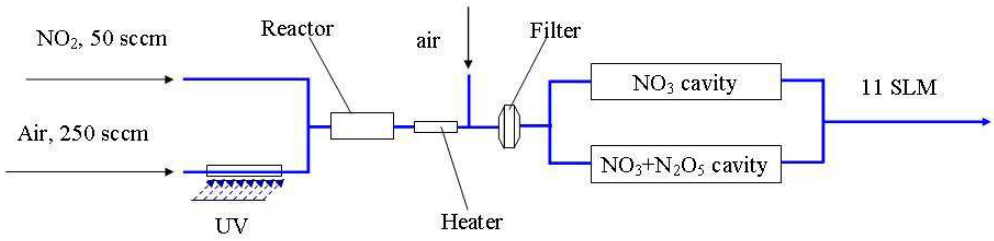

Figure 2-10. The schematic diagram of cavity transmission efficiencies measurement apparatus

N_2O_5 was generated by mixing NO_2 and O_3/air in an FEP-coated glass reactor (described in detail in Section 2.2.2.2), and all the N_2O_5 could be converted to NO_3 if the heater was set to 90 °C. After the heater, the gas was diluted by synthetic air to 11 SLM, passed through the filter and then into the CRD instrument. Before the splitting point, [NO_3] and [N_2O_5] both were stable during the experiments, and keeping the total flow

(the sum of the flows in two cavities) constant while changing the individual flows in the two channels led to the change of residence time in both channels. The change of residence time leads to the change in transmission efficiencies in the two channels and thus the change in the measured NO_3/N_2O_5 concentrations.

A typical dataset of the measured NO_3/N_2O_5 mixing ratios as the function of the residence time in the cavities is displayed in Figure 2-11; the loss of NO_3/N_2O_5 on the wall was pseudo-first-order process in both cavities. The inner diameters are 12.4 mm and 18.7 mm for the NO_3 cavity (volume: 79 cm^3) and the N_2O_5 cavity (volume, 180 cm^3), respectively. The average wall loss rates were measured to be 0.245±0.010 s^{-1} (1σ) for the NO_3 cavity and 0.181±0.010 s^{-1} (1σ) for the NO_3+N_2O_5 cavity.

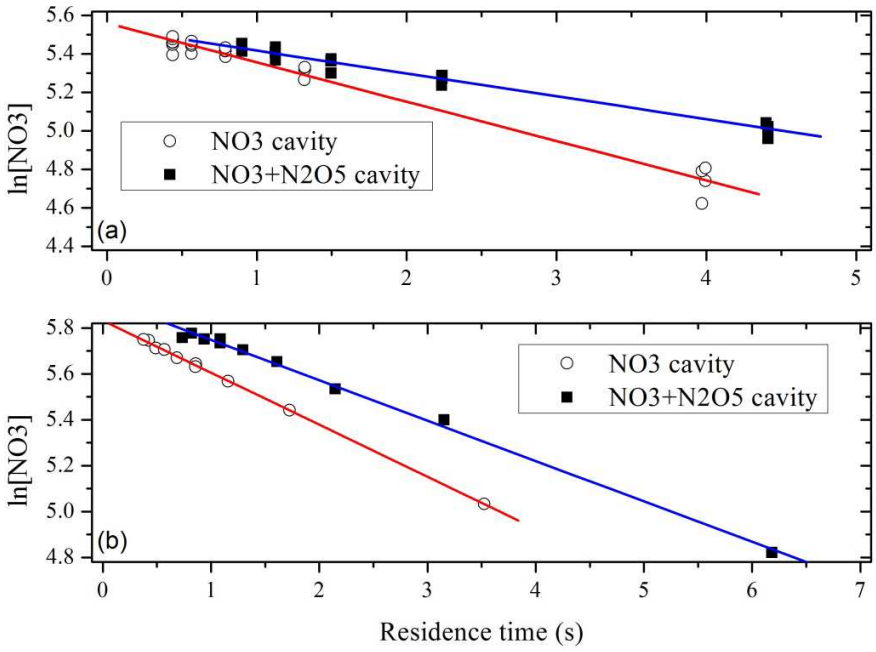

Figure 2-11. Typical results of the cavities' wall loss rates measurement. Upper panel: Photochemical source of NO_3 and N_2O_5 was used; lower panel: N_2O_5 crystals were used as the source of NO_3 and N_2O_5.

The uptake coefficients of NO_3 radicals on the wall, γ, can be calculated by

$$\gamma = \frac{2rk_{obs}}{\bar{c}} \qquad \text{(E2-8)}$$

where r is the radius of the tube (cm), k_{obs} is the measured wall loss rate (s^{-1}), and $\bar{c}$ is the average molecule speed (31900 cm s^{-1} at 298 K for NO_3), given by

$$\bar{c} = \sqrt{8RT/(\pi M)} \quad \text{(E2-9)}$$

where R is the gas constant, T is the temperature in K, and M is the molar mass of the molecule (in this case, NO_3). The measured loss rates corresponded to effective uptake coefficients of 9.5×10^{-6} in the NO_3 cavity and 1.1×10^{-5} in the NO_3+N_2O_5 cavity.

Transmission efficiencies through the filter: A 2-μm pore Teflon (PTFE) membrane filter held in a PFA filter-holder was used to prevent aerosol entering into the cavities. Transmission efficiencies of NO_3 and N_2O_5 were determined by measuring the NO_3 and N_2O_5 concentrations with and without the filter. The result is displayed in Figure 2-12, and the transmission efficiency was determined to be 86.1%±3.5% (1 σ) for NO_3 and 100.5%±1.3% (1 σ) for N_2O_5.

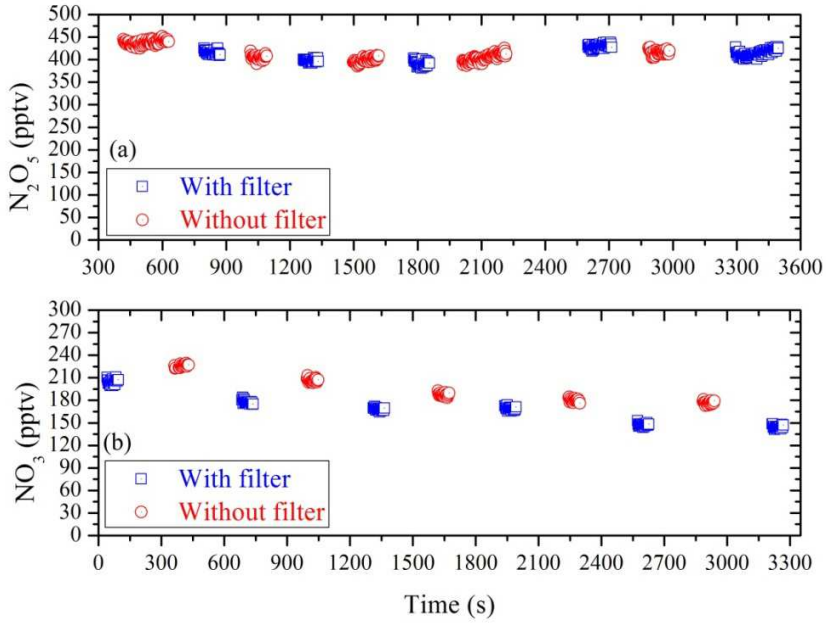

Figure 2-12. Mixing ratios of N_2O_5 (upper panel) and NO_3 (lower) when there was a PTFE filter or no filter present in the filter holder.

Taking all the errors into consideration, the detection limits for NO_3 and N_2O_5 are estimated to be several pptv in ~3 s signal acquisition time in the cavity, corresponding to the concentrations in the flow tubes of factors of ~600 (the old AFT) or ~30 (the new AFT) larger. However, in the kinetics studies, essentially only the relative change in NO_3 and/or N_2O_5 concentrations needs to be known. Therefore, the uncertainty in the absolute

concentration is not very important, and the accuracy of kinetics measurements is more dependent on the fluctuations of initial NO_3 and N_2O_5 concentrations.

2.3.2 Chemical Ionization Mass Spectrometry

Chemical Ionization Mass Spectrometry (CIMS) was used to detect HNO_3(g) in this study. Dr. Nicolas Pouvesle is acknowledged for helping me perform the HNO_3(g) measurement. Of the total 3 SLM flow sampled by the CIMS, 1 SLM was drawn into the ion-molecular reactor (IMR) where chemical ionization takes place at a total pressure of 21 Torr. The remaining flow was drawn into the exhaust line by a diaphragm pump.

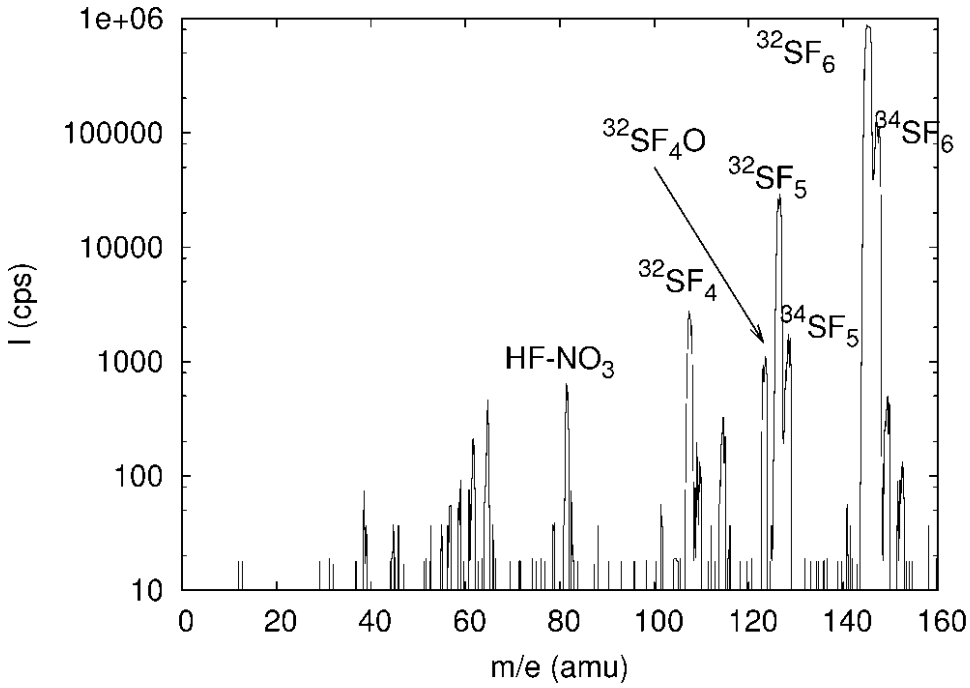

Figure 2-13. A reference mass spectrum of HNO_3 measured by CIMS using SF_6 as the primary ion source.

The IMR is a 12 cm long cylindrical reactor where the sampled flow comes from the front of the reactor, and the primary ions flow perpendicularly into the reactor at about 1 cm after the front inlet. The total flow in the IMR was maintained at 2 SLM by a scroll pump. A small SF_6 flow (about 2000 ppmv in N_2) was diluted by N_2 to 1 SLM and then passed through a 6 cm long tube containing a sealed Polonium-210 source. Alpha radiation emitted by Po-210 resulted in ionization and produced SF_6^- and also SF_5^- as the

primary ions. In the IMR, primary ions reacted with HNO_3(g) to form $HF{\cdot}NO_3^-$ which was mass selected by a quadrupole and detected by a chameltron.

$$SF_6^- + HNO_3 \rightarrow SF_5 + HF{\cdot}NO_3^- \quad \text{(R2-5)}$$

$$SF_5^- + HNO_3 \rightarrow SF_4 + HF{\cdot}NO_3^- \quad \text{(R2-6)}$$

A reference mass spectrum of HNO_3(g) measured by CIMS using SF_6 as the primary ion source is shown in Figure 2-13 and $HF{\cdot}NO_3^-$ (m/e=82) is used to qualify the HNO_3 concentration.

The instrument background was determined by passing the sampled flow through a scrubber filled with Na_2CO_3-doped charcoal to remove HNO_3(g). The instrument was calibrated by measuring a known amount of HNO_3(g) produced from a permeation source, and the detection limit was ~50 pptv for HNO_3(g).

2.4 Product measurements

2.4.1 Gas phase NO_2 detection

The experimental setup used to determine the fraction of NO_2 produced from the heterogeneous reaction of N_2O_5 with Saharan dust particles is similar to the relative rate method apparatus described in Section 2.1. NO_2 and N_2O_5 concentrations were simultaneously measured by Thermal Dissociation Cavity Ring-Down spectroscopy (TD-CRD, similar to the instrument developed in NOAA [*Osthoff et al.*, 2006]. This apparatus was developed in our group chiefly as a field instrument [Thieser et al, in preparation]. In principle, NO_2 is detected at its strong absorption band of 405 nm ($\sigma = 5.768\times10^{-19}$ cm^2 $molecule^{-1}$, [*Atkinson et al.*, 2004]) by using a laser diode. This instrument is very selective to NO_2 and free from the interference of any other NOy species (e.g. N_2O_5, PAN, etc.), and has a detection limit of ~50 pptv in 5 s.

Gaseous N_2O_5 was eluted from a crystalline sample at 223 K in a 10 sccm N_2 flow. Subsequently, the flow was diluted to a total flow of 4000 sccm by a two-stage dynamic dilution system. The total 4000 sccm flow was directed through a clean, 2-μm pore PTFE membrane filter (Pal Teflon R2PJ047) held in a PFA filter-holder (referred to as the "blank" path) or through a TPFE filter loaded with dust particles (referred to as the "sample" path). The gas-flow could be alternately directed through each path via PFA

valves and the two paths were the same in terms of tubing material and residence time, the only difference being the state of the filter.

After exiting the filters, the gas-mixture was split into two identical flows (2000 sccm for each). One flow was directly sampled into one cavity (held at room temperature) of the TD-CRD to measure the NO_2 concentration. The other flow was introduced into a quartz reactor (heated to 90℃). 100 sccm NO (2 ppmv) was also added to the flow before the glass rector, leading to about 0.1 ppmv NO in the reactor. Inside the reactor, N_2O_5 dissociated into NO_2 and NO_3 (R2-7). At 90℃ and atmospheric pressure, the rate constant of (R2-7) 23.5 s^{-1} and the lifetime is less than 0.05 s [*Atkinson et al.*, 2004]. The NO_3 produced from the thermal dissociation reacts rapidly with NO (R2-8):

$$N_2O_5 + M \rightarrow NO_2 + NO_3 + M \quad \text{(R2-7)}$$

$$NO + NO_3 \rightarrow NO_2 + NO_2 \quad \text{(R2-8)}$$

The rate constant of (R2-8) is 2.6×10^{-11} molecules cm^{-3} at 25 °C [*Atkinson et al.*, 2004], leading to a lifetime of less than 0.02 s of NO_3 with respect to (R2-8) in the presence of 0.1 ppmv NO. After exiting the reactor, the flow was sampled into the other cavity (held at 40 °C) of the TD-CRD and the total NO_2 concentration was measured. As indicated in (R2-7) and (R2-8), every N_2O_5 molecule in the flow leads to formation of three NO_2 molecules. The N_2O_5 concentration could be calculated from the difference of the measured NO_2 concentration:

$$[N_2O_5] = ([NO_2]_{ii} - [NO_2]_i)/3 \quad \text{(E2-10)}$$

where $[NO_2]_{ii}$ is the NO_2 concentration measured by the cavity with a heated inlet, and $[NO_2]_i$ is the NO_2 concentration measured by the other cavity without the heater inlet.

During an experiment, the gas flow was first switched through the blank filter and the initial NO_2 and N_2O_5 concentration were measured; then it was switched through the sample path, and the NO_2 and N_2O_5 concentration after the reaction with dust particles loaded on the filter were measured. During the experiment, the flow was regularly switched back to the blank path to check whether initial NO_2 and N_2O_5 concentrations were both stable over time. From the change of NO_2 and N_2O_5 concentrations due to the reaction with Saharan dust, the production yield of NO_2 was determined.

2.4.2 Particulate nitrate detection

After exposure to N_2O_5, the dust-loaded filter was transferred into 10.00 mL deionized water, extracted for 30 min in an ultrasonic bath, filtered using 0.45 μm micro-porous membranes, and then analyzed by ion chromatography(IC, Dionex ICS-1100) to measure the nitrate content in the dust particles. Dr. Xiguang Chi is acknowledged for performing the IC analysis for me.

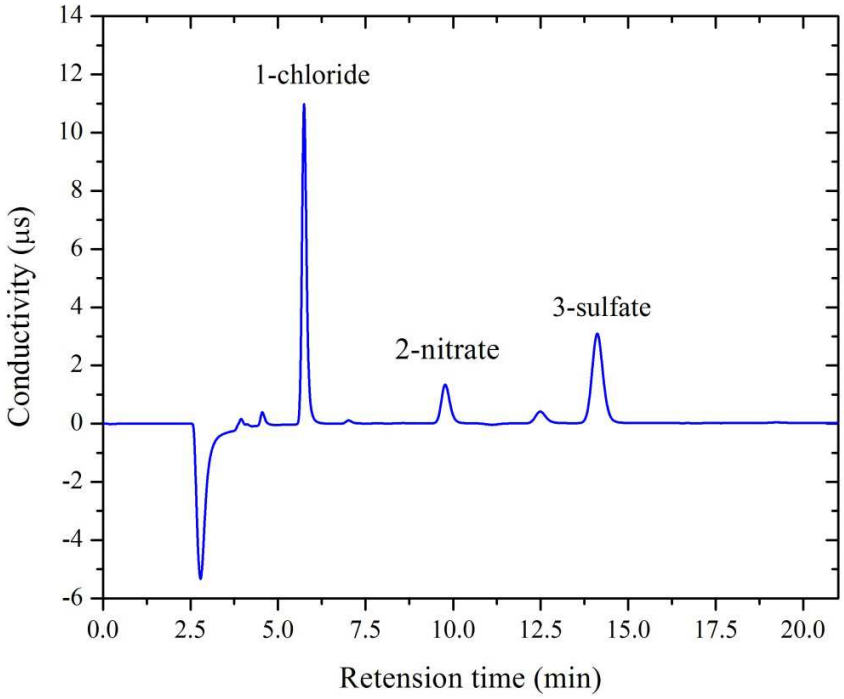

Figure 2-14. A typical chromatogram of the solution analyzed by the ion chromatography method used in this study. Please note that Cl^-, SO_4^{2-}, and also NO_3^- are present in the fresh Saharan dust particles.

The Dionex ICS-1100 system is a basic integrated IC instrument, consisted of a dual piston pump, a vacuum Degas Assembly, a six-port injection valve, and a DS6 heated conductivity detector. In this study, a Dionex Ionpac AG22 4-mm guard column, a Dionex Ionpac AS22 4-mm separation column, and a Dionex ASRS300 4-mm self-regenerating suppressor were used. The eluent, consisting of 4.5 mmol L^{-1} Na_2CO_3 and 1.4 mmol L^{-1} $NaHCO_3$, was maintained at a flow rate of 1.0 mL/min for a total analysis time of 21 min. Under this condition, the retention time for NO_3^- was about 9.7 min, as shown in Figure 2-14.

3 Heterogeneous uptake of NO_3 and N_2O_5: a relative rate study

3.1 Introduction

In this study a novel relative rate method was developed and used to investigate the heterogeneous interaction of NO_3 and N_2O_5 with Saharan dust, ambient aerosol and soot at different relative humidities. The use of Cavity Ring-Down spectroscopy to simultaneously detect both trace gases enabled the measurements to be performed at low mixing ratios (< 500 pptv or 1×10^{10} molecules cm^{-3}). The uptake coefficient ratio, $\gamma(NO_3)/\gamma(N_2O_5)$, was determined for Saharan dust, soot, and ambient urban aerosols.

3.2 Data analysis

In the experimental determination of absolute uptake coefficients for a heterogeneous process, the number of collisions of the trace gas with the surface is usually calculated (based on gas kinetic theory) and the net rate of change in concentration of the trace gas is monitored during exposure to the surface of interest. The experimental uptake coefficient, γ, is the fraction of collisions that lead to removal of the trace gas from the gas-phase and is related to the experimental observables:

$$\frac{d[X]}{dt} = \frac{\gamma \cdot \bar{c}}{4} \cdot \frac{a}{V} \cdot [X] \qquad \text{(E3-1)}$$

where [X] is the gas-phase concentration of species X (molecules cm^{-3}), a/V is the surface area (a, cm^2) per volume (V, cm^3), and $\bar{c}$ is the mean molecular speed of the trace gas (cm s^{-1}). By measuring fractional changes in concentration it becomes:

$$\frac{d[X]}{[X]dt} = k_{exp} = \frac{\gamma \cdot \bar{c}}{4} \cdot \frac{a}{V} \qquad \text{(E3-2)}$$

implying that measurement of the experimental uptake coefficients requires accurate knowledge of the available surface area (a). However, for bulk samples used in the studies of heterogeneous reactions, this is non-trivial and almost always the major source of uncertainty in heterogeneous kinetics. Different treatments such as use of geometric area, BET surface area, or application of pore-diffusion corrections can lead to uptake coefficients that deviate by orders of magnitude for the same reaction [*Goodman et al.*, 2000; *Hanisch and Crowley*, 2001a; *Underwood et al.*, 2001].

For two well-mixed trace gases, in this case NO_3 and N_2O_5, interacting simultaneously with the same particles sample, we have

$$k_{exp}(NO_3) = \frac{\gamma(NO_3)\cdot\bar{c}(NO_3)}{4}\cdot\frac{a}{V} \quad \text{(E3-3)}$$

$$k_{exp}(N_2O_5) = \frac{\gamma(N_2O_5)\cdot\bar{c}(N_2O_5)}{4}\cdot\frac{a}{V} \quad \text{(E3-4)}$$

$$\text{where } -k_{exp}(X) = \frac{(ln[X]_0 - ln[X]_t)}{t} \quad \text{(E3-5)}$$

and $[X]_0$ and $[X]_t$ are the concentration of the trace gas X measured via the blank path and the sample path, respectively. In the relative rate method, the parameters, *a*, *V*, and *t*, are unchanged for both NO_3 and N_2O_5. By rearranging (E3-3), (E3-4), and (E3-5), we derive:

$$\frac{\gamma(NO_3)}{\gamma(N_2O_5)} = \frac{ln[NO_3]_0 - ln[NO_3]_t}{n[N_2O_5]_0 - ln[N_2O_5]_t}\cdot\frac{\bar{c}(N_2O_5)}{\bar{c}(NO_3)} \quad \text{(E3-6)}$$

The ratio of molecular speeds, the last term on the right-hand side of (E3-6), calculated from the ratio of the square root of the molecular masses of N_2O_5 and NO_3 according to (E3-7), is 0.758:

$$\frac{\bar{c}(N_2O_5)}{\bar{c}(NO_3)} = \sqrt{\frac{8RT}{\pi M(N_2O_5)}} \Big/ \sqrt{\frac{8RT}{\pi M(NO_3)}} = \sqrt{M(N_2O_5)/M(NO_3)} \quad \text{(E3-7)}$$

where *R* is the gas constant, *T* is the temperature in Kelvin, and $M(N_2O_5)$ and $M(NO_3)$ are the molar mass of N_2O_5 and NO_3, respectively.

In the present set-up, the relative change in $[NO_3]$ and $[N_2O_5]$ was measured as the trace gases passed through filters loaded with reactive samples. As described in Section 2.1, two filters/filter-holders were used: one was used as blank and the other one contained the sample. Control experiments, in which both filter-holders contained clean filters, were conducted routinely. The result of passing a flow containing ~180 pptv NO_3 and ~160 pptv N_2O_5 through the blank path or the sample path without aerosols on the filter is shown in upper panel of Figure 3-1. Some losses (less than 5% and quite stable) of both NO_3 and N_2O_5 were observed, showing that the tubing/filter-holder in the sample path is slightly more reactive than these in the blank path. Values of $[NO_3]_t$ and $[N_2O_5]_t$ obtained in the presence of a sample were always corrected for this effect. It was estimated that, due to the loss of NO_3 and N_2O_5 in the absence of a sample, ~10% change

of concentrations of NO_3 and N_2O_5 attributed to reaction with the sample could be accurately measured.

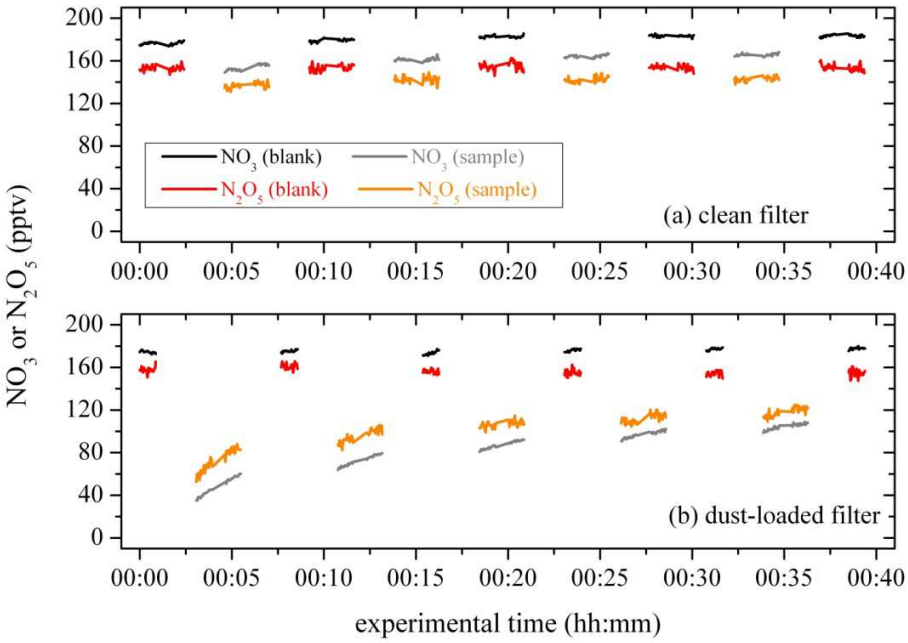

Figure 3-1. Measured NO_3 and N_2O_5 mixing ratios when the gas passed through the blank path and the sample path. Upper panel: a clean (control) filter was used in the sample path; lower panel: a filter loaded with 1.15 mg Saharan dust was used in the sample path.

In a relative uptake experiment (i.e. with a particle-loaded filter in the sample path), the gas mixture was first switched through the blank filter, and $[NO_3]_0$ and $[N_2O_5]_0$ were measured by the CRD; the flow was then switched to the sample path, in order to monitor $[NO_3]_t$ and $[N_2O_5]_t$. During the experiment, the flow was regularly switched back to the blank path (e.g. at 8, 16, 24, 32, and 39 min in the lower panel of Figure 3-1) to determine whether $[NO_3]_0$ and $[N_2O_5]_0$ were both stable over time. Only the datasets in which $[NO_3]_0$ and $[N_2O_5]_0$ fulfilled this requirement were used.

3.3 Results and discussion

3.3.1 Saharan dust

The uptake of NO_3 and N_2O_5 on Saharan dust was the main focus of this work and experiments were carried out with different dust loadings and at four different relative

humidities (RH). In order to observe a measurable change in the NO_3/N_2O_5 mixing ratios, dust samples in excess of ~0.5 mg were required.

The uptake of NO_3 and N_2O_5 on 1.15 mg Saharan dust at RH=0% is displayed in the lower panel of Figure 3-1. The NO_3 and N_2O_5 mixing ratios decreased rapidly when the gas flow passed through the dust-loaded filter, indicating substantial heterogeneous interaction of both trace gases with dust. Both NO_3 and N_2O_5 concentrations did however increase again during the exposure of ~40 min, presumably due to a reduction in the rates of uptake as the number of reactive surface sites depleted as reactions processed.

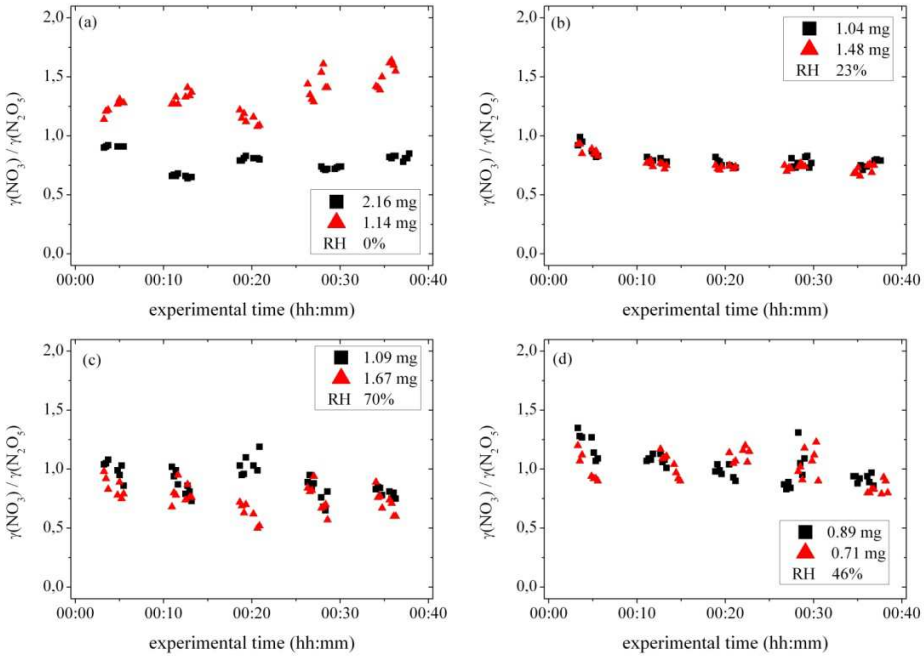

Figure 3-2. Uptake coefficient ratios for NO_3 and N_2O_5 uptake to Saharan dust at four different relative humidities. The sample masses used in each experiment were also indicated.

Using a BET surface area of 39.6 m^2 g^{-1} for the Saharan dust sample [*Wagner et al.*, 2008], the total sample surface area was calculated to be ~450 cm^2, corresponding to about 1×10^{17} surface sites (assuming each site for NO_3 and N_2O_5 is about 5×10^{-15} cm^2 in area). Over the exposure of ~40 min, the sum of NO_3 and N_2O_5 molecules which passed through the filter was about 3×10^{15}. Contrary to observation, the number of NO_3 and N_2O_5 molecules was thus calculated to be insufficient to deactivate a significant fraction of all the adsorption/reaction sites in this Saharan dust sample. However, the simple

calculation assumes that the entire BET surface area was available for NO_3 and N_2O_5 uptake. As the filters were loaded with aerosols at relatively slow flow rates (0.8 SLM) the area of the filter containing dust was larger than that through which the NO_3/N_2O_5 gas flow (10 SLM) passed during an uptake experiment. Visual inspection of aerosol deposited at high flow rates suggested that the flow dynamics led to only a small area (~1 cm^2) if the total filter being used. This implies that the dust area (and thus the mass) available for the reactions is actually smaller than that given for each sample, though the exact factor remains unknown. Indeed, the rate of deactivation of the dust surface was found to be independent of the sample mass, confirming that only a small fraction of the mass (presumably that fraction located on the filter directly under the 1/4'' inlet) is available for the reactions.

Time-dependent uptake coefficients(decreasing with exposure time), indicating consumption of reactive sites on bulk dust samples (see Figure 1-3), have been reported previously for the reaction with N_2O_5 [*Karagulian et al.*, 2006; *Seisel et al.*, 2005; *Wagner et al.*, 2008] and also with NO_3 [*Karagulian and Rossi*, 2005]. The Knudsen-cell reactor studies [*Karagulian and Rossi*, 2005; *Karagulian et al.*, 2006; *Seisel et al.*, 2005] used orders of magnitude larger NO_3 and N_2O_5 concentrations, but generally also much larger dust masses in the 100-1000 mg range. Those studies were also carried out using very dry samples, with relative humidity close to 0%, and thus were not able to investigate the role of H_2O in the reactivation of the dust sample due to surface reorganization of (soluble) nitrate containing sites. The phenomenon of reactivation is anticipated to take place in the atmosphere as evidenced by measurements of a substantial nitrate mass fraction (and loss of carbonate) in chemically aged mineral dust particles, implying that (on sufficiently long time scales) reaction with acidic traces gases is not confined to the initially available surface following dust mobilization [*Carmichael et al.*, 1996]. This has been also confirmed qualitatively in laboratory experiments on $CaCO_3$ [*Krueger et al.*, 2003]. In this study, surface saturation/deactivation also occurred at RH up to 70% and at approximately the same rate as that at RH=0%. A deactivation rate which is independent of RH may indicate that the rate limiting step in surface reorganization (e.g. nitrate dissolution and re-crystallization) takes place over longer time scale than the 40 min duration of the experiment.

Table 3-1 Uptake coefficient ratios and corresponding experimental conditions.

Particle type	RH (%)	NO_3 (pptv)	N_2O_5 (pptv)	Particle mass (mg)	$\gamma(NO_3) / \gamma(N_2O_5)$[a]
Saharan dust	0	200	160	0.43	c
	0	630	340	0.53	c
	0	175	155	1.15	1.33 ± 0.15
	0	560	320	2.15	0.78 ± 0.09
	23	335	440	1.04	0.80 ± 0.07
	23	360	430	1.48	0.77 ± 0.07
	46	220	320	0.71	1.01 ± 0.13
	46	320	410	0.89	1.04 ± 0.14
	70	365	200	1.09	0.91 ± 0.14
	70	360	165	1.67	0.73 ± 0.13
Soot	0	295	190	b	1.2 – 1.8[d]
	0	510	370	b	2.31 ± 0.26
Ambient aerosols	0	450	310	0.36	>15
	0	450	360	0.55	>15
	0	450	390	0.80	>15

[a] The errors (1σ) are statistical only and do not necessarily reflect the total uncertainty in the measured uptake coefficients ratios. [b] The masses of soot particles were not measured due to the experimental difficulties (see the text for details) [c] Uptake coefficient ratios were not reported due to the relative small change in $[NO_3]$ and $[N_2O_5]$ (see the test for details). [d] Time dependent, see text for details.

Although the rate of uptake of NO_3 and N_2O_5 decreased with exposure time, the uptake coefficient ratio, $\gamma(NO_3)/\gamma(N_2O_5)$, changed only slightly or insignificantly during the experiments, as shown in Figure 3-2, which summarizes results for Saharan dust at different RH and different masses of dust samples. A slight decrease in the $\gamma(NO_3)/\gamma(N_2O_5)$ ratio was observed for most samples (generally less than 15%) though it was close to the minimum discernable change in $\gamma(NO_3)/\gamma(N_2O_5)$ above the experimental uncertainties. For this reason, average (exposure-time-independent) values of $\gamma(NO_3)/\gamma(N_2O_5)$ were listed in Table 3-1.

Also apparent from Figure 3-2 is the fact that the value of $\gamma(NO_3)/\gamma(N_2O_5)$ does not change systematically with RH between 0% and 70%. Initially, this result may appear unexpected, as heterogeneous reaction of N_2O_5 are generally believed to be driven by hydrolysis [*Mentel et al.*, 1999; *Thornton et al.*, 2003], whereas the reaction of NO_3 should not depend on available surface-adsorbed H_2O but on the number of oxidisible sites. On the other hand, this result substantiated the previous report in our group that the uptake coefficient of N_2O_5 with the same Saharan dust sample is independent of RH (up to 58%) and close to 1×10^{-2} [*Wagner et al.*, 2008], which is similar to the value of N_2O_5 on the aqueous surface. It was also found that no significant change in $\gamma(NO_3)/\gamma(N_2O_5)$ upon varying the absolute mixing ratios of NO_3 or N_2O_5 within the range indicated in Table 3-1. The results were generally consistent from experiment to experiment (using slightly different aerosol mass), the exception being the dataset displayed in panel (a) of Figure 3-2, where ratios of 0.75 and 1.3 were obtained for two samples. Taking this as an indication of the maximum variability, for all the dataset an average uptake coefficient ratio of $\gamma(NO_3)/\gamma(N_2O_5)=0.9\pm0.4$ was derived, independent of $[NO_3]$, $[N_2O_5]$, or RH. This result is the first measurement of a relative uptake coefficient for NO_3 and N_2O_5 to any surface but can be compared to separately determined values for $\gamma(NO_3)$ and $\gamma(N_2O_5)$ obtained by using similar samples. $\gamma(NO_3)$ and $\gamma(N_2O_5)$ on Saharan dust were measured by the same group using the same Knudsen-cell method [*Karagulian and Rossi*, 2005; *Karagulian et al.*, 2006]. From the reported absolute uptake coefficients (both initial and steady-state), we calculate $\gamma(NO_3)/\gamma(N_2O_5)\approx1.8$ for the initial uptake and a steady-state value of ~1.1, when $[NO_3]=4\times10^{12}$ molecules cm^{-3} and $[N_2O_5]= 3.8\times10^{12}$ molecules cm^{-3}. Experiments with $[NO_3]=7\times10^{11}$ molecules cm^{-3} and $[N_2O_5]= 4\times10^{11}$ molecules cm^{-3}, resulted in values of $\gamma(NO_3)/\gamma(N_2O_5)\approx0.8$ (initial uptake) and $\gamma(NO_3)/\gamma(N_2O_5)\approx0.6$ (steady-state uptake). Considering the large uncertainties in measuring uptake coefficients of heterogeneous reactions, the ratios directly measured in our study agreed well with the values calculated from previous absolute studies [*Karagulian and Rossi*, 2005; *Karagulian et al.*, 2006].

Combing our relative measurement results with the absolute value of $\gamma(N_2O_5)= 1\times10^{-2}$ for RH up to ~60% [*Wagner et al.*, 2008], which is also the currently preferred value by

the IUPAC panel [*IUPAC*, 2009], a value of $\gamma(NO_3)=9\times10^{-3}$ was derived, with an uncertainty that stems mainly from the uncertainties of a factor of about two in $\gamma(N_2O_5)$ [*Wagner et al.*, 2008]. This uptake coefficient is a factor of ~10 lower than the value of 0.1-0.2 measured by using bulk samples of Saharan dust [*Karagulian and Rossi*, 2005].

3.3.2 Ambient Urban aerosols

The underlying intention behind conducting experiments using ambient aerosols was to establish the operational range of the relative rate method, so that a sample with a relative reactivity far from unity was sought. The uptake of N_2O_5 to the surface of ambient aerosols can be important for the night-time NOx budget, whereas NO_3 is generally thought to be lost less rapidly when compared with the gas-phase reactions with organic species. Carrying out relative uptake experiments on real ambient aerosol samples could thus provide a way to characterize the aerosol "reactivity", with a low value of $\gamma(NO_3)/\gamma(N_2O_5)$ expected for aqueous, inorganic particles, and a larger value if the particles were coated with organics or nitrates, which tend to reduce the uptake coefficient for N_2O_5 [*Cosman et al.*, 2008; *Folkers et al.*, 2003; *Griffiths et al.*, 2009; *Hallquist et al.*, 2000; *Mentel et al.*, 1999; *Thornton et al.*, 2003].

The interaction of NO_3 and N_2O_5 with ambient aerosols was investigated at RH=0% only. Raw data from the uptake of NO_3 and N_2O_5 to three ambient aerosol samples are displayed in Figure 3-3. The behavior was quite different from that of Saharan dust, with a significantly smaller uptake of N_2O_5 compared with NO_3. In the left panel of Figure 3-3, the N_2O_5 mixing ratio initially decreased slightly from ~380 pptv to 360 pptv upon exposure, whereas the NO_3 mixing ratio plummeted from 450 pptv to about 50 pptv. The small change in the mixing ratio of N_2O_5 was close to that detectable with our apparatus so that only a lower limit of $\gamma(NO_3)/\gamma(N_2O_5)>15$ was reported. Laboratory experiments have shown that orders of magnitude larger efficiency of uptake of NO_3 to large and unsaturated organic species (e.g., oleic acid) compared with N_2O_5 [*Gross et al.*, 2009], and it is expected that a significant organic fraction was responsible for the large NO_3 uptake observed here. During a field campaign [*Crowley et al.*, 2010a] using the same filters (but only exposed to ambient air for only 1 h), occasional loss of NO_3 (but never loss of N_2O_5) on the filter was observed and it was concluded that the aerosol at the rural

measurement site was largely organic or coated with organic compounds. As mentioned before, the dark color of the urban aerosols sampled outside the main building of the institute indicated a significant mass fraction of elemental carbon, though during the formation and through the aging processes the aerosol had become coated with organics.

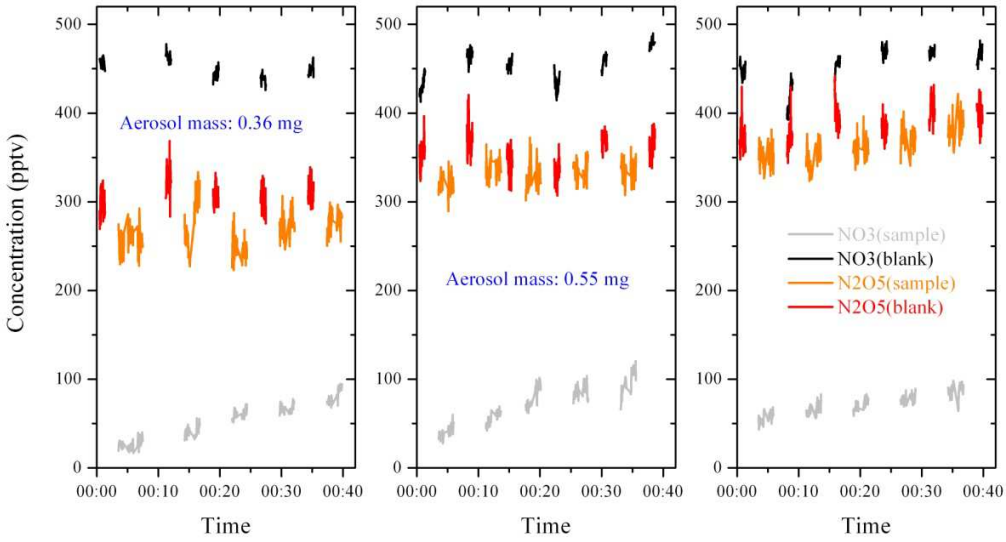

Figure 3-3. Uptake of NO_3 and N_2O_5 to three samples (with different masses) of ambient aerosols at RH=0%.

A further difference between the uptake of NO_3 and N_2O_5 to ambient aerosols, when compared with Saharan dust, was the relatively slow deactivation of the NO_3 uptake despite the use of high NO_3 mixing ratios (given in Table 2-1). The high reactivity and large capacity is further evidence for an important role of unsaturated organic components, which are very reactive to NO_3 [*Gross and Bertram*, 2009; *Moise and Rudich*, 2002].

3.3.3 Soot

As stated above, the ambient aerosols sampled outside the main building of the institute contained an elemental carbon fraction. Two experiments were therefore carried out to examine the interaction of NO_3 and N_2O_5 with soot particles at RH=0%. The generation of soot particles is described in Section 2.1.

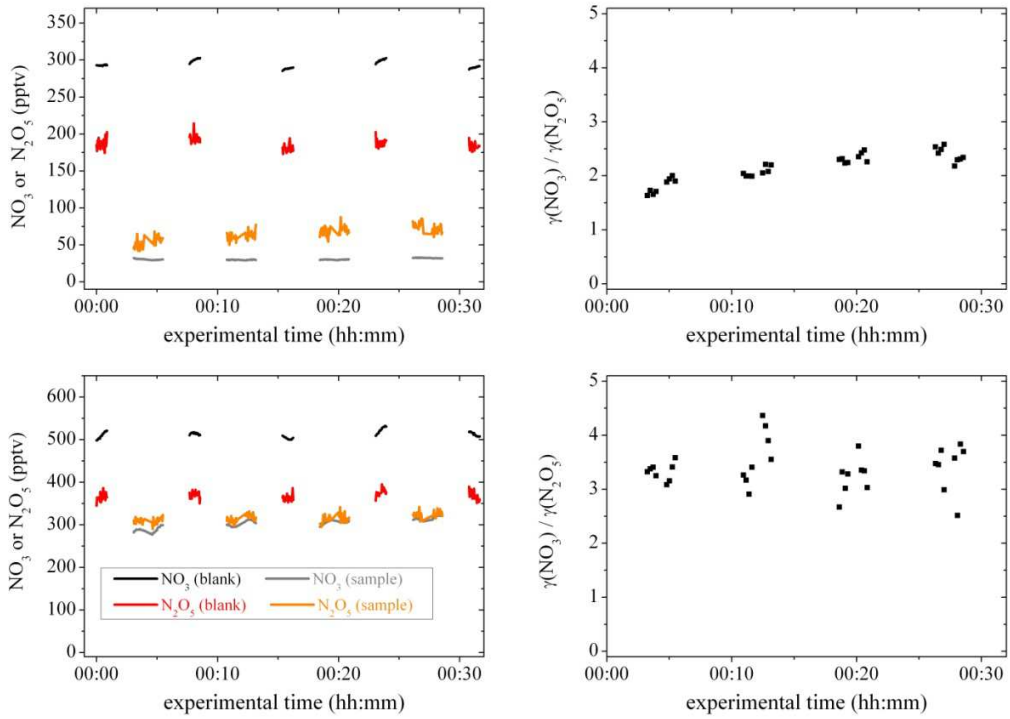

Figure 3-4. Raw data (left-side panels) and uptake coefficient ratios (right-side panels) for NO_3 and N_2O_5 uptake to candle-generated soot particles.

The result displayed in the top-left panel of Figure 3-4 indicated that the soot particles were reactive to both NO_3 (decreasing from ~300 pptv initially to 30 pptv after exposure) and N_2O_5 (decreasing from ~180 pptv to 50 pptv). In this sample there was evidence for a more rapid rate of surface deactivation for N_2O_5 than NO_3, with the ratio $\gamma(NO_3)/\gamma(N_2O_5)$ increasing from ~1.5 to 2.5 over the 30 min exposure, as shown in the top-right panel of Figure 3-4. This contrasted the behavior observed for Saharan dust. A change in the relative uptake coefficient with exposure time indicated different modes of reactivity of NO_3 and N_2O_5, since NO_3 probably reacted with unsaturated organics while N_2O_5 may have undergone hydrolysis. The second sample (bottom-left panel) showed somewhat different behavior, with no apparent saturation of NO_3 and N_2O_5 loss during the exposure of 30 min. The ratio of uptake coefficients was large (~2-4), favoring NO_3 uptake.

The sampling of soot particles from the flame of a burning candle is a haphazard process and the different reactivity of the two soot samples is attributed to chaotic sampling from steady-burning and flickering flames, which led to very different chemical

characteristics of the soot and different organic/inorganic contents [*Pagels et al.*, 2009]. A lack of characterization of our soot samples means that no real quantitative comparison could be made with results from other studies. The uptake of NO_3 and N_2O_5 was studied by the same group using the Knudsen-cell reactor [*Karagulian and Rossi*, 2007; *Saathoff et al.*, 2001]. When NO_3 and N_2O_5 concentrations were both around 2×10^{12} molecules cm^{-3}, the steady-state uptake coefficients on gray soot were determined to be $(7.2\pm1.5)\times10^{-2}$ for NO_3 and $(2.0\pm0.3)\times10^{-2}$ for N_2O_5, yielding a ratio of uptake coefficients, $\gamma(NO_3)/\gamma(N_2O_5)$, of about 3-4, and the steady-state uptake coefficients on gray soot were determined to be $(4.8\pm1.0)\times10^{-2}$ for NO_3 and $(2.0\pm0.5)\times10^{-2}$ for N_2O_5, yielding a ratio of uptake coefficients, $\gamma(NO_3)/\gamma(N_2O_5)$, of about 2-3. The uptake coefficient ratios, $\gamma(NO_3)/\gamma(N_2O_5)$, calculated from the separately measured uptake coefficients, agree quite well with the directly measured values in this study, though the composition of the soot samples might vary a lot.

3.4 Summary

The relative rates of uptake of NO_3 and N_2O_5 to Saharan dust at different relative humidities have been investigated, and some exploratory experiments on the relative uptake to ambient aerosols sampled from the outside of our institute and soot particle generated from a burning candle have been carried out. The uptake coefficient ratio, $\gamma(NO_3)/\gamma(N_2O_5)$, was determined to be 0.9±0.4 (1 σ) for Saharan dust particles, indicating similar reactivity for NO_3 and N_2O_5 and resulting in an uptake coefficient of $\gamma(NO_3)= 9\times10^{-3}$, with an associated uncertainty of at least a factor of two.

The limited set of experiments with poorly characterized soot particles and ambient aerosols allows no comparison to be made with previous work or quantitative conclusions to be made regarding their role in the atmosphere. Of interest however is the relatively large uptake of NO_3 compared with N_2O_5 to the urban aerosols sampled at our institute and this should be explored in future studies. The experiments on soot particles and ambient aerosols also illustrate the range of relative uptake coefficients that can be measured by using this method, and suggest that samples with a maximum factor of ~10 differences in reactivity for uptake of NO_3 and N_2O_5 can be examined. The maximum (or

minimum) measurable change in concentrations could be improved by increasing the stability of the NO_3/N_2O_5 source and reducing the noise in the $NO_3+N_2O_5$ channel.

4 Kinetics of heterogeneous uptake of N_2O_5 on mineral dusts: aerosol flow tube studies

4.1 Introduction

Uptake coefficients of N_2O_5 on Saharan dust particles were determined using two aerosol flow tubes (AFT) at different relative humidities and different initial N_2O_5 concentrations ranging from 5×10^{11} to 3×10^{13} molecules cm^{-3}. The influence of NO_2 and O_3 on the uptake of N_2O_5 was investigated. In addition, the uptake coefficients of N_2O_5 on illite and Arizona Test Dust (ATD) were also measured at different relative humidities.

4.2 Data analysis

The loss of N_2O_5 in the AFT under pseudo-first-order conditions (number of reactive sites on the dust surface does not change significantly during the reaction time), can be described by

$$ln\frac{[N_2O_5]_t}{[N_2O_5]_0} = -(k_w + k_d)\cdot t \quad \text{（E4-1）}$$

$$k_d = \frac{\gamma\cdot\bar{c}\cdot N\cdot A}{4} \quad \text{(E4-2)}$$

where k_w is the pseudo-first-order loss rate of N_2O_5 to the wall of the AFT (s^{-1}, limited by gas-phase diffusion and thus constant in this study), k_d is the pseudo-first-order loss rate of N_2O_5 to the dust surface (s^{-1}), N (cm^{-3}) is the number concentration of dust particles with an average surface area of A (cm^2), γ is the effective uptake coefficient, defined as the probability of removing N_2O_5 on a per collision basis, and $\bar{c}$ is the average molecular speed of N_2O_5 (24096 cm s^{-1} at 296 K), calculated from gas kinetics theory:

$$\bar{c} = \sqrt{8RT/(\pi M)} \quad \text{(E4-3)}$$

where R is the gas constant, T is the temperature in K, and M is the molar mass of the molecule (in this case, N_2O_5).

In a typical aerosol flow tube, dispersed aerosols with constant concentration are generated by atomization or homogeneous nucleation, and the difference of the decay rates of a trace gas (in this case, N_2O_5) is measured in the absence and presence of aerosol

to determine the effective uptake coefficients [*Hallquist et al.*, 2003; *Thornton et al.*, 2003]. In this work, despite efforts to provide a stable supply of dust particle into the flow tube, the measured aerosol number concentration showed large variation during an experiment and therefore the experiments were conducted by using short burst (typically about 5-10 min) of dust particles at each injector position. (E4-1) and (E4-2) suggest that, at any fixed contact time (*t*), the relative N_2O_5 concentration should show an exponential dependence on the aerosol number concentration, *N*, i.e.

$$k'(t) = \frac{1}{N} ln \frac{[N_2O_5]_{(0)}}{[N_2O_5]_{(N)}} = \frac{\gamma \cdot \bar{c} \cdot A \cdot t}{4} \qquad \text{(E4-3)}$$

where *k'(t)* is the slope of the exponential fit of the N_2O_5 concentration to the dust number concentration at the contact time, *t*, and $[N_2O_5]_{(N=0)}$ and $[N_2O_5]_{(N=N)}$ are the N_2O_5 concentrations when the aerosol number concentrations are 0 and *N*, respectively. Each injector position corresponds to a different reaction time, *t*, and thus has different values of *k'(t)*. There should be a linear relationship between *k'(t)* and *t*, as indicated by (E4-3), with a slope equal to

$$k^* = \frac{\gamma \cdot \bar{c} \cdot A}{4} \qquad \text{(E4-4)}$$

In every experiment, *k'(t)* and *k** are experimentally determined, *A* is derived from the aerosol size distribution measured by the APS, so the effective uptake coefficient, γ, can be determined. In this work the N_2O_5 concentration measured by the CRD was used to derive the kinetics information because the uptake is a pseudo-first order process and thus the uptake coefficient only depends on the relative change of N_2O_5 concentration; in the other cases, the N_2O_5 concentration in the AFT is always used.

Operating the AFT with dust "bursts" has the disadvantage that the axial N_2O_5 diffusion correction [*Brown*, 1978] is not easy to apply; however, a previous study [*Wagner et al.*, 2008] has shown that under almost the same flow conditions as that used in present work, the axial diffusion correction is only ~10%, which is negligible when compared to the variability of the experimentally-determined uptake coefficients (see later). This operation mode can also result in axial gradient in dust number concentration, the severity of which depends on the relationship between the burst's duration time and the residence time in the AFT. The effects of axial dust concentration gradients are not

considered in the simple steady-state analysis and thus may lead to systematic errors. However, as shown in Section 4.3, there is no significant and systematic deviation from the expected exponential dependence of the measured N_2O_5 concentration on dust number density even in experiments with numerous dust features of variable duration. Although some of the experimental scatter in these datasets may be due to partial break down of the steady state analysis, this is not the major source of error in these experiments. It might lead to a slight underestimation of the uptake coefficient.

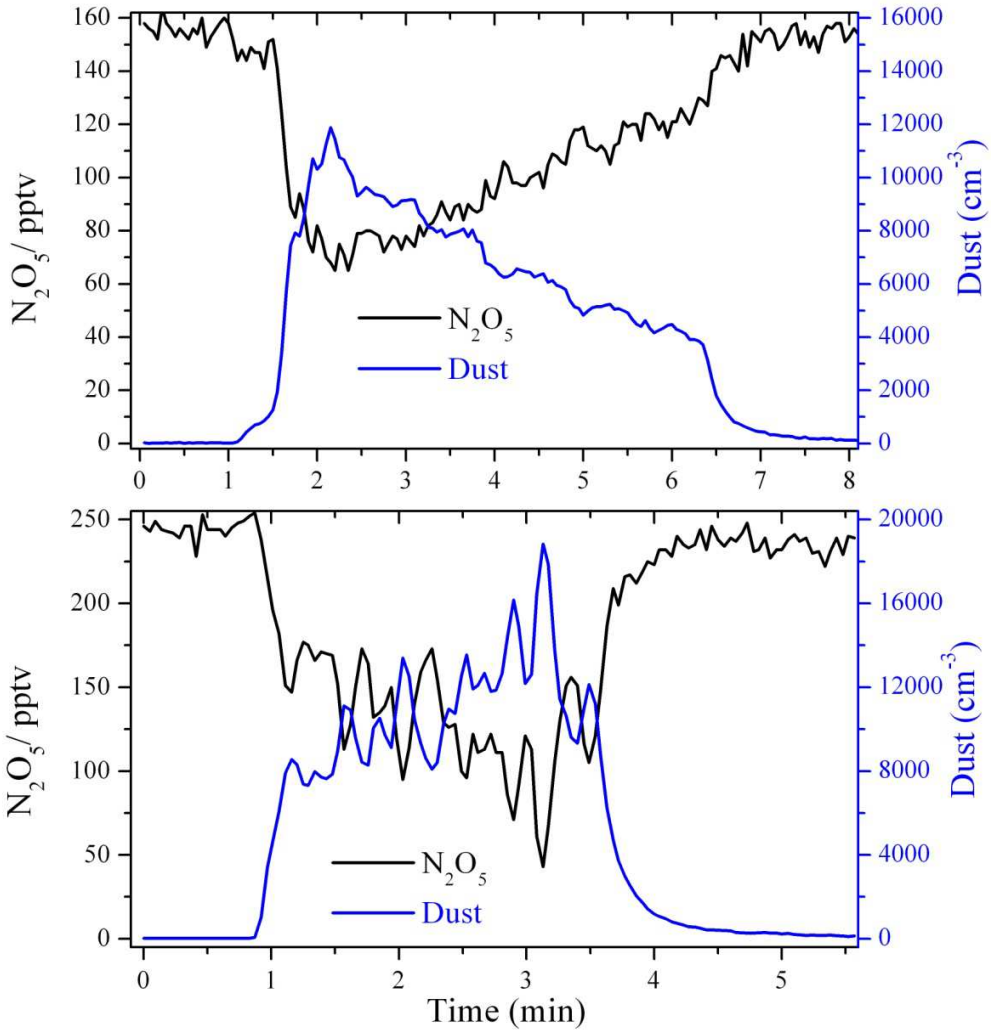

Figure 4-1. Response of the measured N_2O_5 concentration (black line, left y-axis) to the introduction of a Saharan dust pulse (blue line, right y-axis) into the AFT. The time between acquisition of neighboring data points is about 3 s. Upper panel: The mixing volume was used to smooth the spikes in the dust pulse, and RH=0%. Lower panel: The mixing volume was not used, and RH=33%.

Two typical datasets on the response of the measured N_2O_5 mixing ratios to introduction of Saharan dust aerosols are displayed in Figure 4-1. Evident from the upper panel is that, using the mixing volume (its volume is ~5 L, giving a residence time of ~6 min when the aerosol flow is 800 sccm) prevented sharp changes of dust concentration during an uptake experiment, when compared with the lower panel in which the mixing volume was not used. The anti-correlation between the measured N_2O_5 mixing ratio and the aerosol number concentration shows that N_2O_5 was substantially taken up to the dust surface. In this figure, the aerosol number concentration is derived from the analogue output of the APS, measured with the same time step (integration time) as the N_2O_5 mixing ratio.

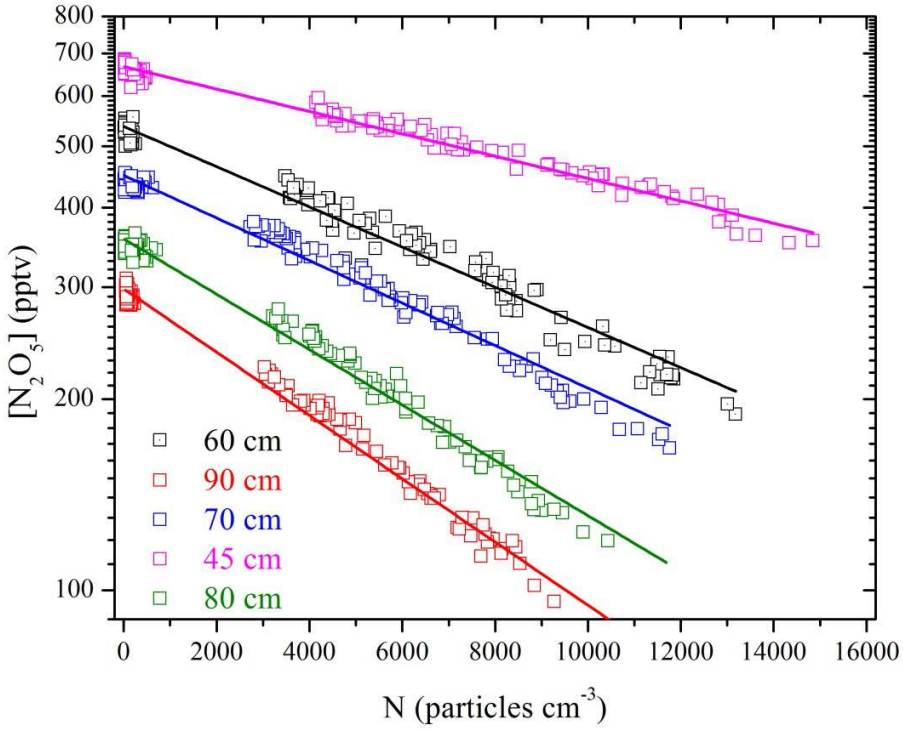

Figure 4-2. Dependence of the measured N_2O_5 mixing ratios on the dust number concentration (*N*) at five different injector positions. The statistical errors on each single data points are with the symbol size. There are no data points around 2000 particles cm^{-3} because the mixing volume was bypassed when *N* was smaller than ~3000 particles cm^{-3}; otherwise it took too long for *N* to reach 0 again after introduction of a dust pulse. The slope at each injector position is equal to k'(t), as given in (E4-3). In this figure, k'(t) were determined to be$(4.050\pm0.006)\times10^{-3}$, $(7.280\pm0.014)\times10^{-3}$, $(7.710\pm0.012)\times10^{-3}$, $(10.040\pm0.013)\times10^{-3}$, and $(11.460\pm0.014)\times10^{-3}$ (cm^3, 1 σ) when the injector was at 45, 60, 70, 80, and 90 cm, respectively.

The exponential dependence of the measured N_2O_5 mixing ratio on dust number concentration at five different injector positions is displayed in Figure 4-2. As defined in (E4-1) and (E4-2), the slopes are equal to *k'(t)*, which is given in (E4-3). The plot of *k'(t)* versus contact time is shown in Figure 4-3, and the slope of the linear fit is equal to *k** which can be used to derive γ_{expt}, as expected from (E4-4). The mixing length and the mixing time are calculated in Chapter 2 to be ~42 cm and ~10 s, respectively. The fact that the linear fit in Figure 4-3 does not go through zero (an x-axis intercept of ~ 7 s in this case) is expected and is related to the offset in the contact time due to the mixing effect.

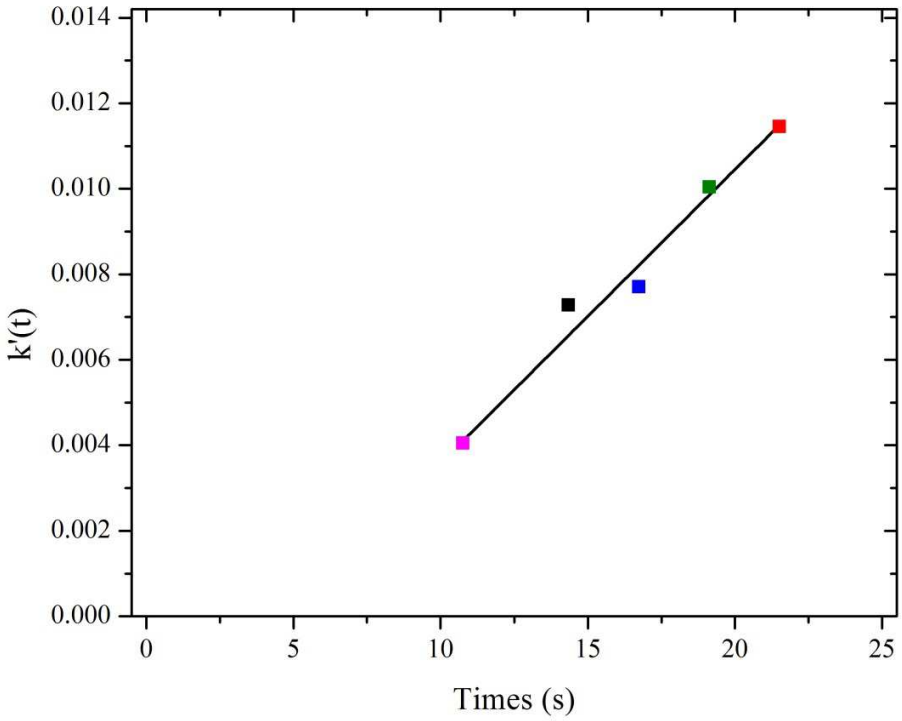

Figure 4-3. The slopes of the exponential fits to data as shown in Figure 4-2, as a function of the contact time of N_2O_5 with dust particles in the AFT. The statistical errors on each single data points are with the symbol size. The colors of the points in this Figure correspond to these in Figure 4-2. The slope of this linear fitting, k^*, was (6.87±0.47))×10^{-4} (1 σ).

Typical size distributions of dust samples measured by the APS are displayed in Figure 4-4, showing maxima of aerodynamic diameters (*Da*) at 2.129 μm for Saharan dust, 1.486 μm for illite, 0.965 μm for quartz, and 1.596 μm for ATD with a second

maximum at 7.774 μm. No significant change in size distribution was observed over the course of each experiment.

The rate of uptake of a trace gas to the airborne particles can be reduced by the concentration gradient close to the particle surface, leading to an underestimation of the true uptake coefficient, γ_{true}. This effect can be corrected [*Fuchs and Sutugin*, 1970] using

$$\frac{1}{\gamma_{true}} = \frac{1}{\gamma_{expt}} - \frac{0.75+0.283Kn}{Kn(1+Kn)} \quad \text{(E4-5)}$$

where γ_{expt} is the experimentally-measured uptake coefficient, and Kn is the Knudsen number, given by

$$Kn = \frac{3D}{\bar{c} \times r} \quad \text{(E4-6)}$$

where D is the gas-phase diffusion coefficient (0.085 $cm^2\ s^{-1}$ at atmospheric pressure and 296 K for N_2O_5, [*Wagner et al.*, 2008]), and r is the radius of the particle (cm).

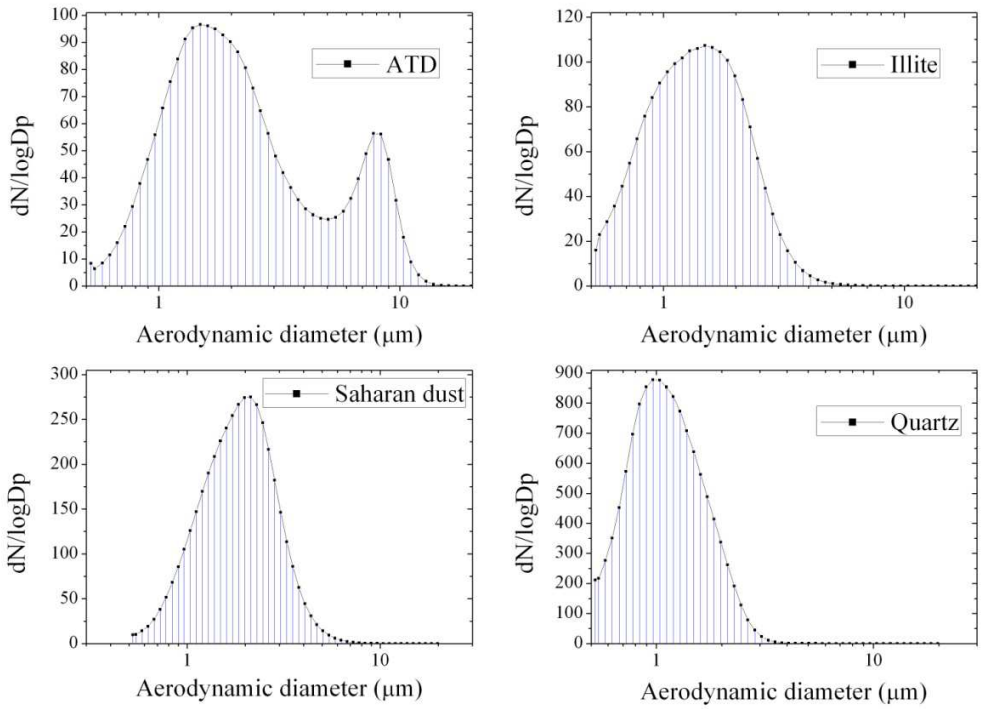

Figure 4-4. Size distributions (aerodynamic diameter) of ATD, illite, Saharan dust and quartz, as measured by the APS. Note that no particles were observed out of 17 μm, the end of the measurement range.

The reported uptake coefficients in this work are based on the surface area calculated from the Stokes diameter, *Ds*, i.e. after correcting the aerodynamic diameter for particle's

density (Section 2.2.4). As mentioned in Section 2.2.4, the surface area of Saharan dust particles is corrected by a factor of 1.6 to correct the effects of non-sphericity of the particles; for the other types of dust particles, the possible shape effects are ignored. In this work mineral dust particles are initially assumed to be nonporous, i.e. the geometrical area of a single dust particle is assumed to be equal to its BET area. The implications of this assumption are considered later.

The most exact method to derive γ_{true} is to apply the diffusion correction individually to each bin of the measured aerosol size distribution, but this method (denoted as Method A) requires a first guess of the γ_{true} value and iteration until the k_d calculated from γ_{true} is close enough to the experimentally determined k_d, making it more difficult to use. Method A gives a γ_{true} of 2.29×10^{-2} and a correction factor of 14.5% when γ_{expt} is 2.0×10^{-2} for N_2O_5 on Saharan dust particles. In the previous work the radius of the particle at the maximum of the surface area weighted size distribution, r_{sw}, was used in (E4-6) to determine *Kn* [*Wagner et al.*, 2009; *Wagner et al.*, 2008]. However, it is difficult to apply this method (denoted as Method B) to non-single-peak aerosol size distribution (such as ATD in this work). Method B gives a γ_{true} of 2.39×10^{-2} and a correction factor of 19.5% when γ_{expt} is 2.0×10^{-2} on Saharan dust particles.

Table 4-1 Characteristic properties of typical dust samples used in this work.

	Density [A]	*Da* [B]	*Ds* [C]	Surface area [D]	*Kn* [E]
Saharan dust	2.7	2.129	1.296	7.79	0.124
ATD	2.7	1.596 [F]	0.971	21.1	0.099
Illite	2.7	1.486	0.904	3.56	0.141
Quartz	2.6	1.037	0.643	2.13	0.174

[A]: g cm^{-30}. The density was provided by [*Wagner et al.*, 2008] for Saharan dust, by [*Wagner et al.*, 2009] for ATD and quartz. The density of illite is unknown and it is assumed to have the same density as Saharan dust. [B]: Equivalent aerodynamic diameter in µm. [C]: Equivalent Stokes diameter in µm. [D]: Surface area of per particle in μm^2, calculated by using the Stokes diameter and assuming spherical particles (For Saharan dust, the surface area was corrected using a factor of 1.6). In this study it is assumed that the dust particles are nonporous, i.e. the geometrical area of dust particles is equal to the BET area. [E]: The Knudsen number is calculated by (E4-7), using a diffusion coefficient of 0.085 cm^2 s^{-1} at atmospheric pressure and 296 K,

and the mean molecular speed of 24094 cm s^{-1} for N_2O_5. [F]: The equivalent aerodynamic diameter at the more intense mode, with a second maximum at 7.774 μm; see the text for details.

In the present study, *Kn* is calculated for each bin of the size distribution and then an effective *Kn* can be calculated by

$$Kn = \frac{\sum N_i \cdot Kn(i)}{\sum N_i} = \frac{3D}{\bar{c}} \cdot \frac{\sum N_i / r_i}{\sum N_i} \quad \text{(E4-7)}$$

where *Ni* and *Kn(i)* are the aerosol number concentration and the Knudsen number in the *i*th size bin with the radius of r_i, respectively. This method (denoted as Method C) gives a γ_{true} of 2.24×10^{-2} and a correction factor of 12.0% when γ_{expt} is 2.0×10^{-2} on Saharan dust particles. The value of γ_{true} calculated by using Method C is only about 2% different from the value calculated by using Method A (the most accurate method), and it requires much less calculation. Therefore, in present study only Method C is used to calculate γ_{true}. Typical aerodynamic and Stokes diameters of dust particles used in this study are listed in Table 4-1 together with other important parameters (e.g. surface area per particle and the Knudsen number).

4.3 Uptake of N_2O_5 on Saharan dust

In this work, the effects of RH, initial N_2O_5 concentrations, and the presence of NO_2 and O_3 on $\gamma(N_2O_5)$ on Saharan dust were investigated. The uptake coefficients of N_2O_5 on Saharan dust particles were measured at five different RH (up to 67%), using the old aerosol flow tube. Totally 23 experiments without the mixing volume and 18 experiments with the mixing volume were carried out, and the initial concentrations of N_2O_5 ranged from 3×10^{12} to 2.7×10^{13} molecules cm^{-3} (varied by almost a factor of 10). The results are summarized in Table 4-2, and the average diffusion correction is about 10%. The uptake coefficients determined by using the mixing volume agree with the corresponding values without the mixing volume within the experimental errors.

Some experiments with a total flow of 2 SLM in the AFT confirmed that there is no difference in measured uptake coefficients from those when the total flow was 3 SLM.

Table 4-2. Uptake coefficients and experimental conditions in the old AFT: Saharan dust

RH (%)	N_2O_5 [a]	γ_{true} [b]	RH(%)	N_2O_5 [a]	γ_{true} [b]
0	26.5	0.018±0.001	33	10.1	0.016±0.002
0	27.3	0.023±0.001	33	9.4	0.016±0.001
0	17.9	0.021±0.002	33	21.8	0.013±0.002
0	16.4	0.023±0.001	33	23.4	0.014±0.001
0	12.5	0.018±0.002	33	23.4	0.014±0.002
0	5.5	0.027±0.001	33	3.9	0.044±0.001
0	5.9	0.013±0.001	33	14.0	0.023±0.001
0	6.6	0.013±0.001	33	20.7	0.018±0.001
0	11.7	0.013±0.001	50	14.4	0.028±0.001
0	11.7	0.013±0.001	50	14.4	0.020±0.001
0	17.6	0.021±0.002	50	14.8	0.031±0.001
0	25.4	0.015±0.002	50	5.1	0.026±0.001
17	11.7	0.011±0.002	50	19.5	0.016±0.002
17	21.1	0.026±0.002	67	19.5	0.012±0.002
17	13.7	0.023±0.002	67	19.5	0.012±0.002
17	17.9	0.022±0.003	67	18.3	0.013±0.001
17	17.2	0.024±0.002	67	10.9	0.021±0.001
17	4.3	0.033±0.001	67	11.7	0.021±0.001
17	12.5	0.026±0.002	67	3.1	0.032±0.001
17	20.3	0.022±0.002	67	10.1	0.016±0.001
			67	15.6	0.014±0.001

$\gamma(N_2O_5)$ determined when the mixing volume was not used are in black, and in red when the mixing volume was used. [a] Initial N_2O_5 concentration in the units of 10^{12} molecules cm^{-3}. [b] The values of γ_{true} have been corrected for diffusion limit to the uptake. The errors (1 σ) are statistical only.

4.3.1 Influence of relative humidity

As shown in Figure 4-4, the uptake coefficient does not depend on the RH (0-67%) within the experimental uncertainties, with a weighted average value of 0.016±0.002 (1 σ), when the mixing volume was used. This is equal to the result obtained without the

mixing volume (a weighted average γ_{true} of 0.022±0.003 (1 σ) was determined when RH ranged from 0% to 67%). Taking all the data into account, $\gamma(N_2O_5)$ was determined to be 0.020±0.002 (1 σ). The statistical error for each determined uptake coefficient was much smaller than the deviation of uptake coefficients, as shown in Table 4-2 and Figure 4-5, suggesting that the systematical error in determining an uptake coefficient is larger than the statistical error associated with the uptake coefficient.

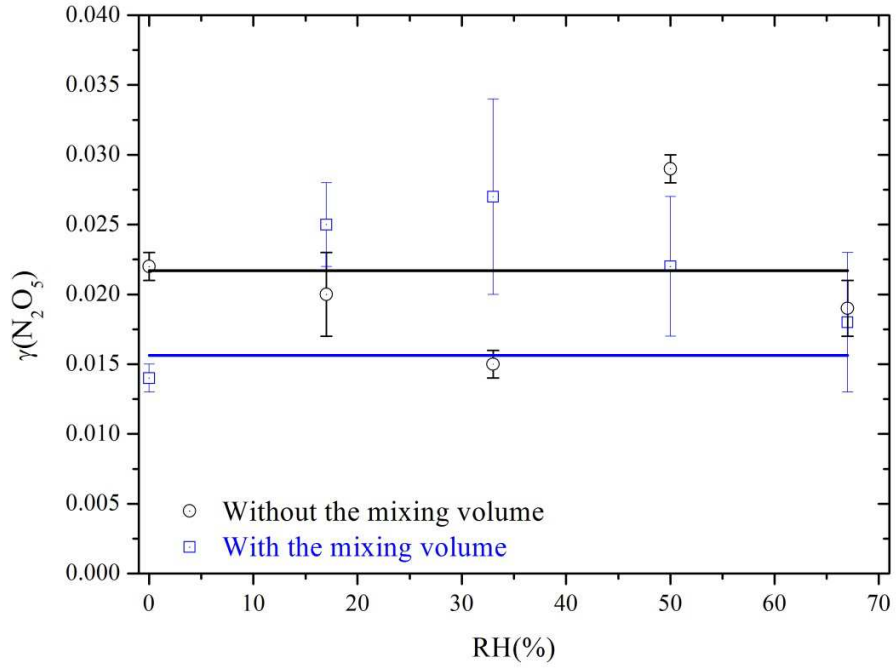

Figure 4-5. Uptake coefficients of N_2O_5 on Saharan dust particles at different relative humidities. The two horizontal lines are the corresponding trend-lines.

4.3.2 Influence of initial N_2O_5 concentration

The effect of the trace gas concentrations on the uptake coefficients may provide clues on the mechanism of the heterogeneous reaction [*Ammann et al.*, 2003]. The uptake coefficients of HNO_3 [*Vlasenko et al.*, 2009], O_3 [*Hanisch and Crowley*, 2003], and HCHO [*Sassine et al.*, 2010] on mineral dust particles were all found to decrease when initial concentrations of the corresponding trace gases increased, implying that the Langmuir-Hinshelwood mechanism was operative for the uptake of HNO_3, O_3, and HCHO on dust surface.

In order to investigate the effects of initial N_2O_5 concentrations, uptake coefficients of N_2O_5 on Saharan dust were also determined by using the new aerosol flow tube, which enabled the experiments to be performed at lower initial N_2O_5 concentrations. The uptake coefficients at RH=0% at different initial N_2O_5 concentrations, obtained by using the two aerosol flow tube, are displayed in Figure 4-6. It shows clearly that, within the experimental uncertainties, the uptake coefficient does not change with initial N_2O_5 concentrations, which were varied by almost two orders of magnitude (5×10^{11}-3×10^{13} molecules cm^{-3}, corresponding to ~20 ppbv to ~1 ppmv at atmospheric pressure). The systematical error in determining an uptake coefficient is larger than the statistical error associated with the uptake coefficient, leading to that the deviation of uptake coefficients measured in different experiments are much larger than the statistical error associated with each uptake coefficient, as shown in Figure 4-6.

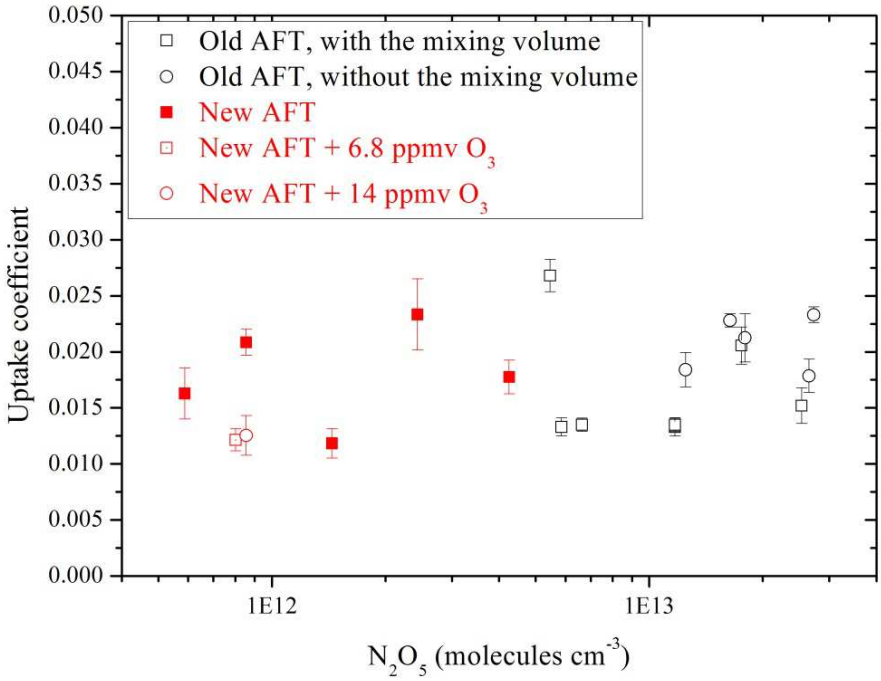

Figure 4-6. Uptake coefficients of N_2O_5 on Saharan dust particles at different initial N_2O_5 concentration when RH=0%.

4.3.3 Influence of O_3 and NO_2

Other reactive traces gases in the flow tube (or in the atmosphere) can affect the uptake of N_2O_5 by either reactivating or deactivating surface sites. In these experiments,

the presence of NO_2 and O_3 with N_2O_5 in the AFT can compete for the reactive surface sites with N_2O_5 (thus suppresses the uptake of N_2O_5) or they may reactivate the surface, accelerating the uptake of N_2O_5. In order to investigate the effects of O_3, in two experiments carried out using the new AFT, 20 sccm O_3 was combined into the N_2O_5 flow, leading to several ppmv O_3 in the AFT. As shown in Figure 4-6, the presence of O_3 (6.8 ppmv and 14 ppmv) has no influence on the uptake coefficients of N_2O_5 on Saharan dust particles. Note that such O_3 mixing ratios are about two orders of magnitude higher than that typically found in the troposphere.

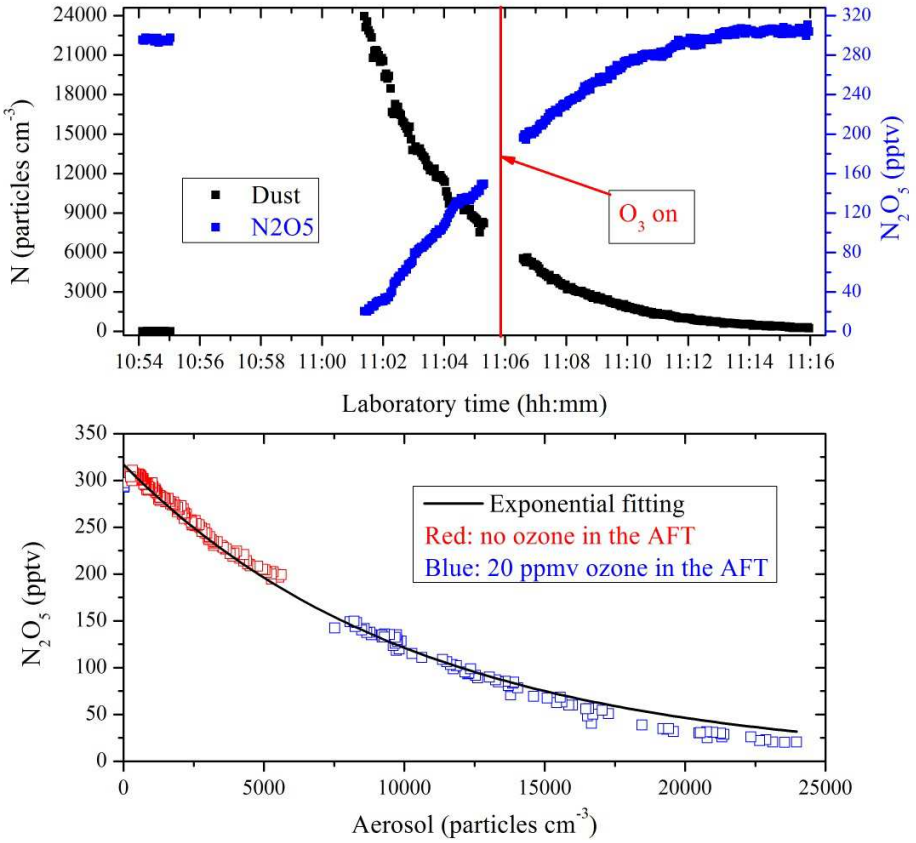

Figure 4-7. Influence of O_3 on the measured N_2O_5 mixing ratio during one dust pulse. The injector was at 60 cm.

In a further experiment, gaseous N_2O_5 was generated from N_2O_5 crystals, and 20 sccm of O_3 or O_2 was introduced into the flow tube from the injector by switching the O_2 flow through a low pressure Hg lamp. As shown in Figure 4-7, when O_3 was introduced into the flow tube (~ 20 ppmv O_3 in the AFT), there was no significant change in N_2O_5

concentration, and the dependence of the measured N_2O_5 mixing ratio on dust number concentration can be fitted by the same exponential function. It further confirms that the presence of O_3 does not influence the uptake of N_2O_5 on Saharan dust particles.

In a series of experiments carried out using the new AFT, gaseous N_2O_5 was also generated by reacting NO_2 with O_3 in the FEP-coated glass reactor, and then transported into the flow tube through the 1/8'' PFA tube in the injector. These experiments were performed to investigate the effects of the coexistence of NO_2 and O_3 on the N_2O_5 uptake. No significant difference in uptake coefficients was found when the different gaseous N_2O_5 sources were used, i.e. the presence of NO_2 together with O_3 did not influence the uptake coefficient of N_2O_5 on Saharan dust.

4.3.4 Possible interference in measuring uptake coefficients

Gaseous N_2O_5 (generated from N_2O_5 crystalline) introduced into the AFT was not a pure substance but in dynamic equilibrium with NO_3 and NO_2. Any process that removes N_2O_5 or NO_3 will adjust the equilibrium between N_2O_5, NO_3, and NO_2, leading to additional loss or reformation of N_2O_5. The heterogeneous losses of N_2O_5 on the wall and the dust surface will adjust the equilibrium concentrations of NO_3 and NO_2 and lead to the reformation of N_2O_5 (R4-1), and these processes lead to underestimation of the uptake coefficient of N_2O_5. On the other hand, the heterogeneous removal (by the wall and the dust surface) and photolysis of NO_3 will lead to further decomposition of N_2O_5 (R4-1), and these processes would result in overestimation of the uptake coefficient of N_2O_5. The heterogeneous uptake of NO_2 on the wall and the dust surface will also lead to the overestimation of the N_2O_5 uptake; but this effect must be negligible due to the smaller uptake coefficient of NO_2 (less than 1×10^{-6}, [*IUPAC*, 2009]). Here the effects of reformation of N_2O_5 and the heterogeneous removal of NO_3 were investigated by simulating the chemical reactions in the aerosol flow tube, using FACSIMILE, and the code of the corresponding program is given in Appendices A4.2.

$$NO_3 + NO_2 + M \leftrightarrow N_2O_5 + M \qquad \text{(R4-1)}$$

A previous study [*Wagner et al.*, 2008] showed that the reformation of N_2O_5 due to the recombination of NO_3 and NO_2 and the additional indirect loss of N_2O_5 due to the uptake of NO_3 on the dust (assuming γ=0.1) do not have any significant effects on the

analysis of N_2O_5 uptake kinetics. Here another potential error, the indirect loss of N_2O_5 due to the loss of NO_3 on the wall of the AFT (limited by gas-phase diffusion, with the NO_3 diffusion coefficient of 80±15 Torr cm^2 s^{-1} in N_2 reported by [*Rudich et al.*, 1996b]), is also considered. In the simulations, a dust number concentration of 10,000 particles cm^{-3}, the average diameter of 1.12 μm, $\gamma(N_2O_5)$ of 0.02, and $k_w(N_2O_5)$ of 0.05 s^{-1} are used. In Chapter 3, $\gamma(N_2O_5)/\ \gamma(NO_3)$ was determined to be 0.9±0.4 (1 σ) on Saharan dust, leading to $\gamma(NO_3)$=0.018. An uptake coefficient of 0.1 for NO_3 on dust surface was used in the simulations, so the effect of heterogeneous uptake of NO_3 on dust surface should be smaller than that simulated here. The kinetics data for the gas-phase reactions are taken from the JPL evaluation [*Sander et al.*, 2006]. The initial N_2O_5 concentration was 5.0×10^{12} molecules cm^{-3}, and the initial NO_2 and NO_3 concentrations were both set to 2.7×10^{11} molecules cm^{-3}, in equilibrium with N_2O_5.

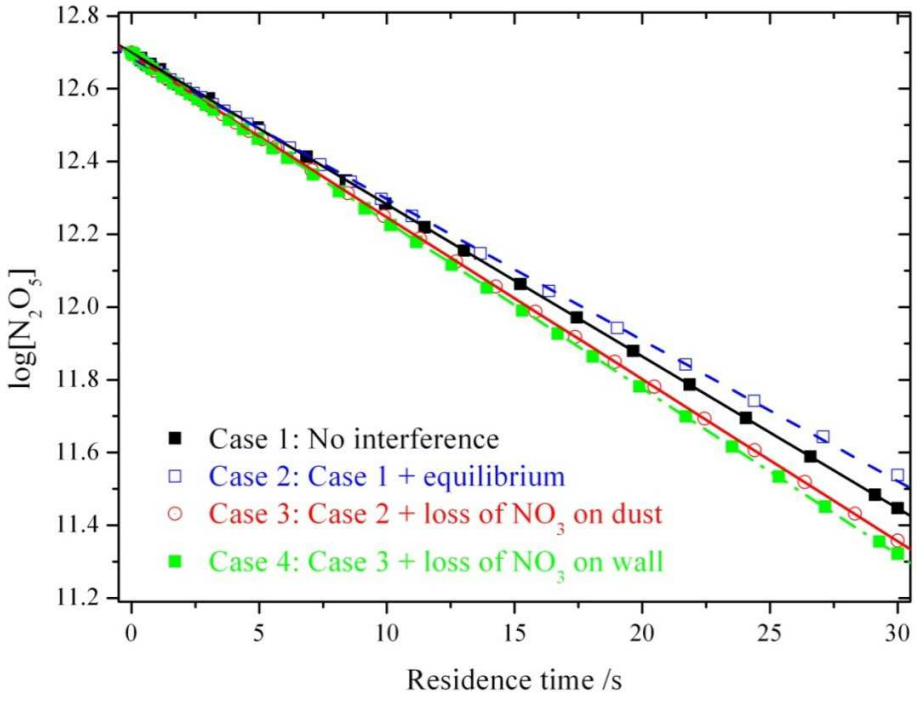

Figure 4-8. Simulated N_2O_5 profiles when different conditions are considered (see text for details).

As shown in Figure 4-8, the N_2O_5 decay profile remains exponential even when all the potential interference are considered, and these interferences together lead to an overestimation of the measured N_2O_5 decay rates (the slope of the exponential fitting) by ~9.5% if the NO_3 uptake is as efficient as modeled, i.e. the measured uptake coefficient

would be overestimated by ~9.5%. This effect would be larger at higher temperatures because the equilibrium constant of (R4-1) decreases quickly when temperature increases [*Sander et al.*, 2006], and thus the heterogeneous loss of NO_3 will contribute more significantly to the measured decay of N_2O_5 in the aerosol flow tube.

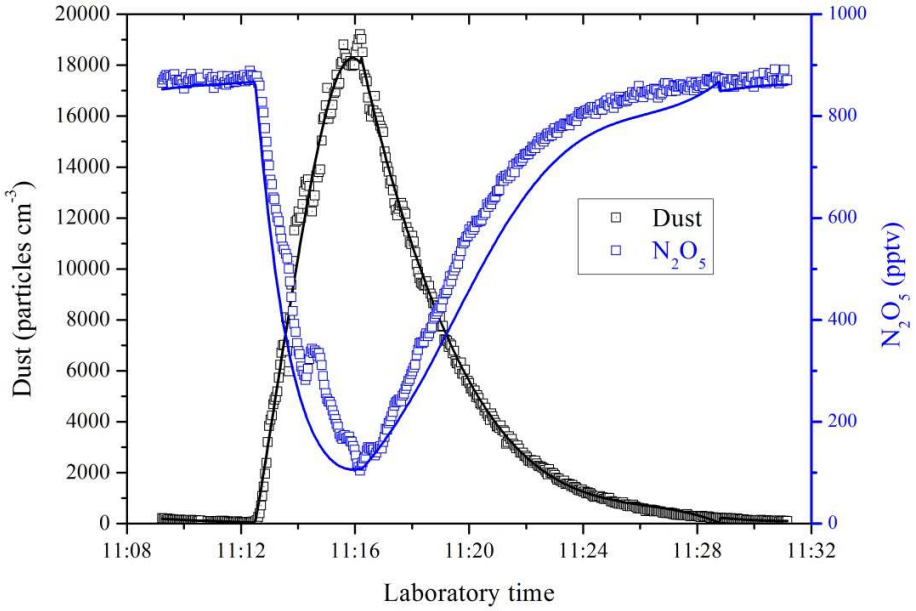

Figure 4-9. Measured (blue square) and simulated (blue line) response of N_2O_5 to the introduction of Saharan dust aerosols into the new aerosol flow tube (see text for details).

The same processes considered in the simulation shown in Figure 4-8 were used to simulate the response of N_2O_5 to the introduction of dust aerosols into the new aerosol flow tube when the injector is at 60 cm. The code of this FACSIMILE program is listed in Appendices A4.3. The same kinetics parameters were used in this simulation, expect that a more realistic value of 0.018 for $\gamma(NO_3)$ instead of 0.1 was adopted. The measured time-dependent dust aerosol density (black square in Figure 4-9) was fitted by a continuous function (black line in Figure 4-9), which was used as the input parameters in the simulation. The initial N_2O_5 concentration in the AFT was calculated from the CRD-measured N_2O_5 mixing ratio when there was no dust present in the AFT, the known dilution factor, and the wall loss rate. Steady state is assumed in the simulation, e.g. at every data point the N_2O_5 concentration only depends on the dust aerosol density and not influenced by the N_2O_5 concentrations in the previous or later data points. Steady-state is also assumed in (E4-1) and (E4-2), which are the basis for analyzing the data in this study.

The simulated N_2O_5 profile (blue line), consisting of the results from more than 400 simulations at different dust number concentrations, is displayed in Figure 4-9 to compare with the measured N_2O_5 profile (blue square) during a dust pulse. The good agreement between the measured and simulated N_2O_5 profiles suggests that the steady-state assumption and thus the method used to analyze the data in this study are valid.

NO_3 is very photo-labile and the normal illumination in the laboratory could potentially lead to additional loss of NO_3 (and thus N_2O_5) in the flow tube due to the photolysis of NO_3. The effect of laboratory illumination was investigated by measuring the NO_3 and N_2O_5 concentrations at different injector positions without the presence of dust particle in the flow tube when the lab was normally bright or totally dark. No significant change of NO_3 or N_2O_5 concentration was found when the laboratory was totally dark, compared with that when it was normally bright. To conclude, the effect of laboratory illumination of NO_3 and N_2O_5 concentrations in the flow tube is negligible.

4.4 Uptake of N_2O_5 on other dust particles

4.4.1 Uptake of N_2O_5 on ATD

The heterogeneous interaction of N_2O_5 with ATD was studied by using the old AFT, the bulk samples were dispersed by a self-made generator, and the mixing volume for the dust particles was not used. The results from 20 experiments are summarized in Table 4-3 (the average diffusion correction is less than 10%). As shown in Figure 4-10, $\gamma(N_2O_5)$ does not depend on relative humidity. The reactivity of ATD towards N_2O_5 is significantly smaller than that of both Saharan dust and illite, maybe due to the high fraction of quartz in ATD. The systematical error in determining an uptake coefficient is larger than the statistical error associated with the uptake coefficient, leading to that the deviation of uptake coefficients measured in different experiments are much larger than the statistical error associated with each uptake coefficient, as shown in Table 4-3 and Table 4-4.

The uptake coefficient of N_2O_5, $\gamma(N_2O_5)$, is smaller on ATD than that on Saharan dust particles. It might be due to that ATD contained a large fraction of quartz (~70% by mass), which has low reactivity towards N_2O_5.

Table 4-3. Uptake coefficients of N_2O_5 on ATD and experimental conditions

RH (%)	N_2O_5 [a]	γ_{true} [b]	RH (%)	N_2O_5 [a]	γ_{true} [b]
0	24	0.008±0.001	33	9	0.011±0.001
0	24	0.009±0.001	33	18	0.009±0.001
0	17	0.011±0.001	33	18	0.010±0.001
0	9	0.013±0.001	50	12	0.004±0.001
0	9	0.011±0.001	50	16	0.007±0.001
17	9	0.007±0.001	50	11	0.005±0.001
17	10	0.008±0.001	50	11	0.009±0.001
17	20	0.005±0.001	67	18	0.006±0.001
17	13	0.005±0.001	67	16	0.007±0.001
33	8	0.012±0.001	67	9	0.006±0.001

[a] Initial N_2O_5 concentration in the units of 10^{12} molecules cm^{-3}. [b] The values of γ_{true} have been corrected for diffusion limit to the uptake. The errors (1 σ) are statistical only.

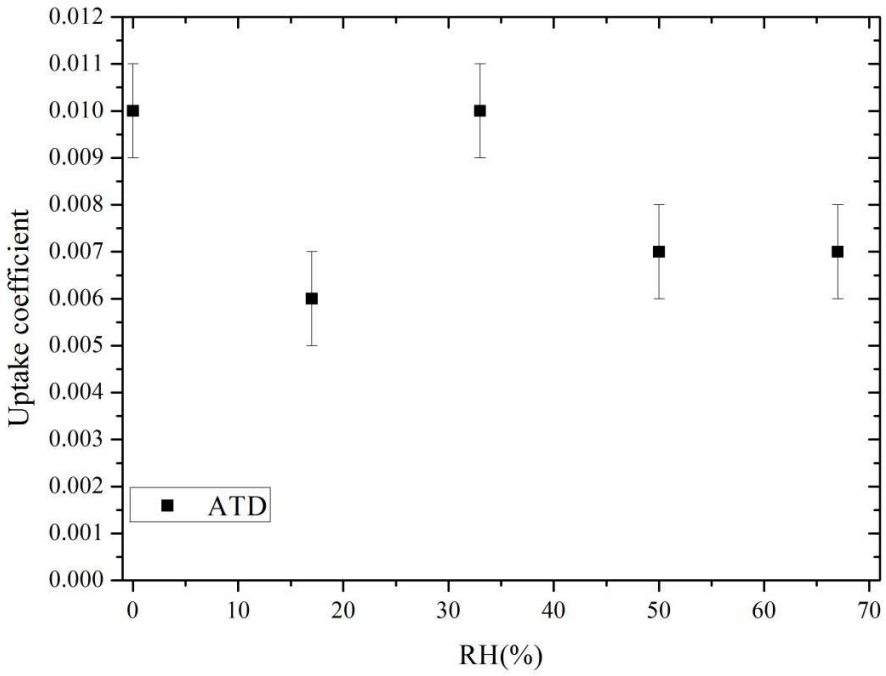

Figure 4-10 Uptake coefficients of N_2O_5 on ATD particles, as a function of RH.

4.4.2 Uptake of N_2O_5 on Illite

The experiments on the reaction of illite particles with N_2O_5 were conducted in the old AFT, using the mixing volume. 15 uptake experiments were carried out at five different relative humidities (RH), and the results are listed in Table 4-4. The diffusion correction is up to 40-50% at low RH (due to the large reactivity) and about 20% at high RH (due to relatively small reactivity). Figure 4-11 shows that the uptake coefficient of N_2O_5 to illite might have a negative dependence on RH.

Table 4-4. Uptake coefficients of N_2O_5 on Illite particles and experimental conditions

RH (%)	N_2O_5 [a]	γ_{true} [b]	RH (%)	N_2O_5 [a]	γ_{true} [b]
0	11.6	0.068±0.002	33	17.4	0.055±0.004
0	15.1	0.096±0.005	50	15.1	0.041±0.002
0	16.3	0.137±0.055	50	16.8	0.051±0.002
17	20.5	0.093±0.004	50	14.0	0.045±0.003
17	17.1	0.079±0.004	67	13.2	0.033±0.005
17	18.8	0.075±0.002	67	12.3	0.027±0.003
33	13.4	0.078±0.001	67	16.8	0.049±0.002
33	12.8	0.047±0.006			

[a] Initial N_2O_5 concentration in the units of 10^{12} molecules cm^{-3}. [b] The values of γ_{true} have been corrected for diffusion limit to the uptake. The errors (1 σ) are statistical only.

The uptake coefficient of N_2O_5, $\gamma(N_2O_5)$, is larger on Illite than that on Saharan dust, probably suggesting that Illite has higher reactivity towards N_2O_5. Further studies on the uptake of N_2O_5 on other minerals (e.g. kaolinite, calcite, et al.) will be helpful to understand the reactivity of N_2O_5 towards dust.

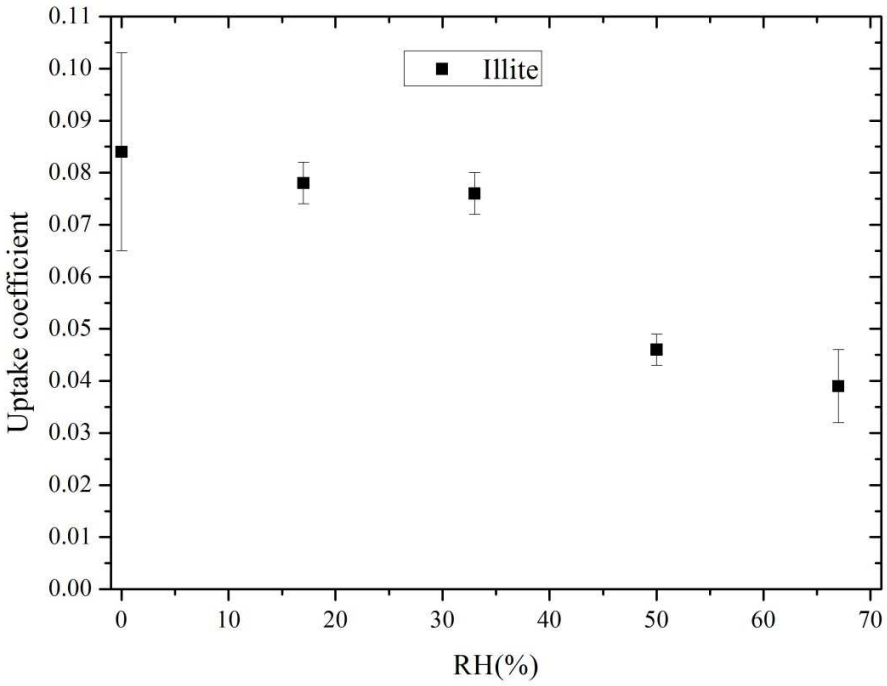

Figure 4-11 Uptake coefficients of N_2O_5 on Illite particles, as a function of RH.

4.5 Comparison with previous results

4.5.1 Uptake onto bulk dust samples

There have been several studies on the uptake of N_2O_5 on mineral dust particles at room temperature. In the first study [*Seisel et al.*, 2005], bulk Saharan dust samples were prepared spreading an aqueous suspension on sample holders prior to being dried under vacuum before each experiments. The uptake coefficients were measured in a Knudsen cell which was operated in both pulsed and steady-state modes, with N_2O_5 (3×10^{10} - 1×10^{12} molecules cm^{-3}) monitored by a quadrupole mass spectrometer. The Knudsen cell study gave a time-dependent uptake coefficient of N_2O_5:

$$\gamma = (1.7 \pm 0.3) \times 10^{-2} + (6.2 \pm 0.5) \times 10^{-2} \times e^{-[(1.8\pm0.5)\times10^{-3}\times t]} \quad \text{(E4-8)}$$

where t is the reaction time in s. This reaction was also studied by using diffuse reflectance FTIR to measure the nitrate formed on the surface, and it gave a lower reactive uptake coefficient of $(9.1\pm0.7)\times10^{-3}$, when the N_2O_5 concentrations were varied between 4×10^{11} and 5×10^{12} molecules cm^{-3}.

A further Knudsen reactor study also investigated the uptake of N_2O_5 on bulk samples of mineral dust particles [*Karagulian et al.*, 2006]. The uptake coefficients were also found to be time-dependent, and thus both initial and steady-state uptake coefficients (γ_0 and γ_{ss}, respectively) were reported. γ_0 and γ_{ss} were determined to be $(9.0\pm2.6)\times10^{-2}$ and $(5.9\pm1.6)\times10^{-2}$ on Saharan dust, and $(6.4\pm1.9)\times10^{-2}$ and $(1.6\pm0.4)\times10^{-2}$ on ATD, respectively, when the N_2O_5 concentration was $(3.8\pm0.5)\times10^{12}$ molecules cm^{-3}. When N_2O_5 concentration was $(4.0\pm1.0)\times10^{11}$ molecules cm^{-3}, γ_0 and γ_{ss} were determined to be 0.3±0.08 and 0.2±0.05 on Saharan dust, and 0.2±0.06 and 0.11±0.03 on ATD, respectively.

The uptake of N_2O_5 on bulk dust samples was also investigated using a Knudsen cell by the third study [*Wagner et al.*, 2008]. In this case, the uptake coefficients were found to be time-independent, e.g. γ_0 was equal to γ_{ss}, in contrast with the two previous studies in which similar apparatus were used. In this study, N_2O_5 concentration was in the range of $(2\text{-}20)\times10^9$ molecules cm^{-3}, and the uptake coefficients of N_2O_5 were reported to be $(3.7\pm1.2)\times10^{-2}$ on Saharan dust, and $(2.2\pm0.8)\times10^{-2}$ on ATD, respectively.

There are several important drawbacks for the Knudsen cell studies. First of all, the Knudsen cell has to be operated at the molecular flow regime (usually P<1 mTorr, e.g. [*Hanisch and Crowley*, 2001b]) so that the average mean free path is larger than the dimension of the reactor and the intermolecular collision frequency is negligible when compared with the gas-surface collision frequency. Therefore, it is not possible to vary the relative humidity over a broad range. In addition, the measurement of uptake coefficients requires accurate knowledge of the surface area available for the reactions, and it is non-trivial and often the major source of uncertainty in heterogeneous kinetics. Different bulk samples preparation and different treatments such as geometric area of the sample holder, BET surface area of the particles, or application of pore-diffusion corrections can lead to uptake coefficients which deviate by orders of magnitude for the same reaction [*Goodman et al.*, 2000; *Hanisch and Crowley*, 2001a; *Underwood et al.*, 2000]. For the uptake of N_2O_5 on mineral dust, the three Knudsen cell studies [*Karagulian et al.*, 2006; *Seisel et al.*, 2005; *Wagner et al.*, 2008] reported different uptake coefficients which vary by a factor of ~10, when geometric surface areas of the bulk samples were used in all the studies to calculate the uptake coefficients.

4.5.2 Uptake onto dispersed dust particles

The first study of the uptake of N_2O_5 on dispersed mineral dust particles [*Mogili et al.*, 2006] was performed in an environmental aerosol chamber, into which a known amount of particles was introduced. N_2O_5 was generated inside the chamber by reacting NO_2 with ozone, and monitored by transmission FTIR. The decay of N_2O_5 after introduction of aerosols into the chamber was used to determine the uptake coefficient, and the aerosol surface area was calculated from the mass of dust introduced into the chamber and its BET area (in m^2 g^{-1}). The measured $\gamma(N_2O_5)$ on mineral dust particles were in the range of 10^{-5} – 10^{-4}, and a $\gamma(N_2O_5)$ of 0.03-0.15 was recommended, after scaled up by a factor of ~160. The physical basis for this correction factor is not clear. Furthermore, the production yield of gaseous HNO_3 was reported to be approximately two, which is the expected stoichiometry of the hydrolysis reaction. However, gaseous HNO_3 also undergoes efficient heterogeneous reactions with mineral dust particles [*IUPAC*, 2009]. In fact, the same group reported substantial uptake of HNO_3(g) onto dust surface, using the same aerosol chamber [*Prince et al.*, 2007]. Therefore, the measured yield of HNO_3(g) should be significantly smaller than two, even assuming that N_2O_5 undergoes heterogeneous hydrolysis on dust surface.

The uptake coefficients of N_2O_5 on mineral dust particles measured by two previous aerosol flow tube studies [*Wagner et al.*, 2009; *Wagner et al.*, 2008] are currently recommended by the IUPAC Subcommittee for Gas Kinetic Data Evaluation [*IUPAC*, 2009]. The uptake coefficients reported by these two studies are listed in Table 4-5 to compare with the values determined in this work. Considering the experimental uncertainties, $\gamma(N_2O_5)$ on Saharan dust measured in present study agrees reasonably with the work of [*Wagner et al.*, 2008], though no dependence of uptake coefficients on RH is observed in this work and they show a slightly negative dependence. $\gamma(N_2O_5)$ on ATD determined in this study agrees very well with the values previously reported [*Wagner et al.*, 2009].

The flow conditions in the aerosol flow tubes used in previous work [*Wagner et al.*, 2009; *Wagner et al.*, 2008] and this study were almost the same, and dust particles were generated by the same methods, measured the same APS, and have very similar size

distributions. This work has several advantages compared to the previous studies [*Wagner et al.*, 2009; *Wagner et al.*, 2008], which are listed below:

Table 4-5 Comparison of AFT studies of N_2O_5 uptake to mineral dust samples at room temperature

Dust	RH (%)	γ_{true} [a]	Reference
SDCV [b]	0	0.026±0.004	Wagner et al., 2008
	29	0.016±0.004	
	58	0.010±0.004	
	0	0.014±0.001	This work
	17	0.025±0.003	
	33	0.027±0.007	
	50	0.022±0.005	
	67	0.018±0.005	
ATD	0	0.010±0.001	Wagner et al., 2009
	29	0.007±0.001	
	0	0.010±0.001	This work
	17	0.007±0.001	
	33	0.010±0.001	
	50	0.007±0.001	
	67	0.007±0.001	

[a] Errors(1 σ) listed are all statistical only. [b] Surface area of Saharan dust particles has been corrected by a factor of 1.6 in both studies.

1) In the experiments of Wagner et al., [2008, 2009], N_2O_5 failed to reach the initial concentrations when the dust aerosol density recovered to 0 particles cm^{-3} in the flow tube after the introduction of dust pulses, probably due to loss of N_2O_5 on dust particles deposited in the gas sampling inlet when the dust aerosol density in the flow tube was high. The effect had to be corrected and introduced additional uncertainty in the uptake coefficients measurement. In this work the aerosol-free sampling strategies prevented this problem.

2) In this work the decay of N_2O_5 was monitored by Cavity Ring-Down spectroscopy, which provides quasi-direct measurement with high accuracy and high sensitivity towards N_2O_5. In the two previous studies, N_2O_5 was decomposed (R4-2) and titrated by NO (R4-3) at 363 K:

$$N_2O_5 + M \rightarrow NO_3 + NO_2 + M \quad \text{(R4-2)}$$

$$NO_3 + NO \rightarrow NO_2 + NO_2 \quad \text{(R4-3)}$$

and N_2O_5 was monitored as the change of NO concentration, as measured by a modified chemiluminescence detector (CLD). It is rather an indirect method and substantial measurement errors could come from the determination of small change in NO concentration, especially when N_2O_5 concentration was quite low.

3) The N_2O_5 measurement by the CRD is not influenced by water vapor, whereas the CLD was found to become less sensitive at higher relative humidities.

4) The statistical errors in each single uptake coefficient are quite large in the two previous studies (usually around 20% but up to ~50% in a few experiments), and in this work they seldom exceed 10%, as shown in Table 4-2, 4-3, and 4-4.

4.6 Summary

The heterogeneous reactions of N_2O_5 on airborne mineral dust particles have been investigated via using two aerosol flow tube at different initial N_2O_5 concentrations and different relatively humidities. $\gamma(N_2O_5)$ on Saharan dust was found to be 0.020±0.002 (1 σ), independent of relative humidity and initial N_2O_5 concentration. $\gamma(N_2O_5)$ at RH=0% 0.100±0.035 (1 σ) for illite and 0.010±0.002 (1 σ) for ATD, respectively. No dependence of $\gamma(N_2O_5)$ on RH is observed for Saharan dust or ATD particles, while there is a negative dependence on RH of $\gamma(N_2O_5)$ on illite.

5 Mechanisms of heterogeneous reaction of N_2O_5 and NO_3 radicals with mineral dust particles

5.1 Introduction

The heterogeneous uptake of N_2O_5 on aqueous particles has been extensively studied, and the reaction mechanism is relatively well understood. In contrast, the uptake of N_2O_5 on mineral dust particles has not received much attention, and the reaction mechanism is largely unknown. Therefore, the present database on the heterogeneous uptake of N_2O_5 (and also NO_3) on aqueous particles is briefly reviewed before the mechanisms of heterogeneous uptake of N_2O_5 and NO_3 on mineral dust particles are discussed.

5.1.1 Reactions of N_2O_5 and NO_3 with aqueous particles

The mechanism of the heterogeneous reaction of N_2O_5 with aqueous aerosol particles (e.g. NH_4HSO_4, NaCl) is believed to be heterogeneous hydrolysis (Figure 5-1) [*Bertram and Thornton*, 2009; *Thornton et al.*, 2003]. The reaction starts with the accommodation of N_2O_5 into the aqueous surface layer (R5-1), forming aqueous phase N_2O_5 which undergoes reversible hydrolysis (R5-2) to form one NO_3^- ion and one protonated nitric acid intermediate ($H_2ONO_2^+$).

$$N_2O_5(g) \leftrightarrow N_2O_5(aq) \quad \text{(R5-1)}$$

$$N_2O_5(aq) + H_2O(l) \leftrightarrow NO_3^-(aq) + H_2ONO_2^+(aq) \quad \text{(R5-2)}$$

$H_2ONO_2^+$ will react with liquid water to form NO_3^- ion (R5-3) or react with X^- (where X=Cl, Br, or I) to form nitryl halides (R5-4), which will be released into gas phase due to their limited solubility.

$$H_2ONO_2^+(aq) + 2H_2O(l) \leftrightarrow 2H_3O^+(aq) + NO_3^-(aq) \quad \text{(R5-3)}$$

$$H_2ONO_2^+(aq) + X^-(l) \rightarrow XNO_2 + H_2O(l) \quad \text{(R5-4)}$$

Though the intermediate $H_2ONO_2^+$ or solvated N_2O_5 ($N_2O_5(aq)$) have not been directly observed, this mechanism does qualitatively explain the dependence of $\gamma(N_2O_5)$ on several parameters:

I) (R5-2) and R(5-3) suggests the positive dependence of $\gamma(N_2O_5)$ on liquid water content, and it has been observed that $\gamma(N_2O_5)$ increases with RH [*Badger et al.*, 2006; *Bertram and Thornton*, 2009; *Bertram et al.*, 2009b; *Griffiths et al.*, 2009; *Hallquist et al.*, 2003; *Hu and Abbatt*, 1997; *Kane et al.*, 2001; *Mozurkewich and Calvert*, 1988; *Stewart et al.*, 2004; *Thornton et al.*, 2003; *Wahner et al.*, 1998].

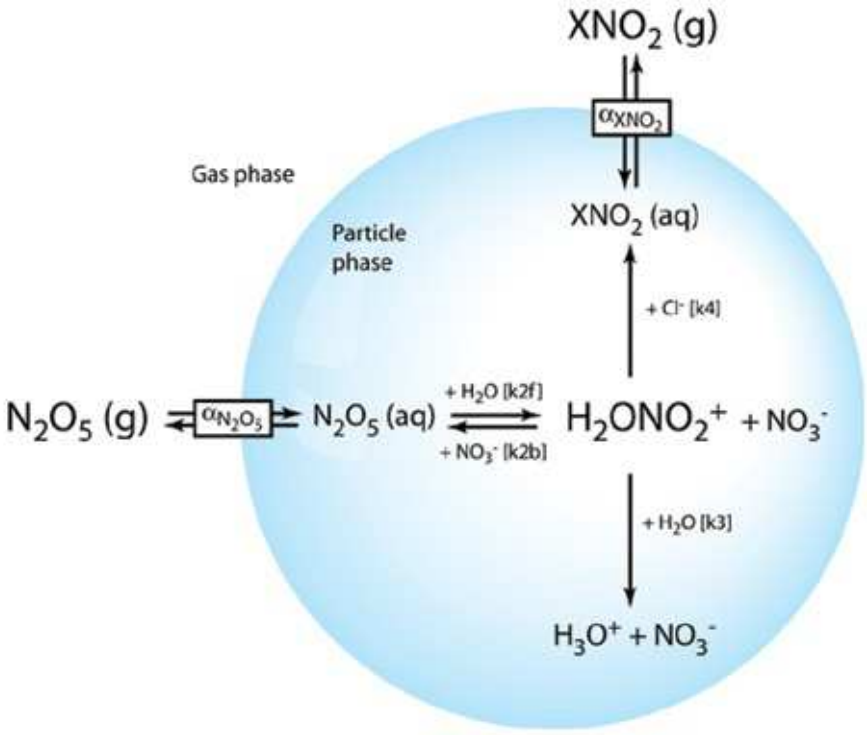

Figure 5-1. Schematic diagram of heterogeneous N_2O_5 hydrolysis, adopted from [*Bertram and Thornton*, 2009].

II) According to (R5-1), (R5-2), and (R5-3), organic coatings will either suppress the N_2O_5 accommodation or decrease the water content available on the surface, and experiments confirm that the presence of organic contents/coatings does reduce $\gamma(N_2O_5)$ [*Anttila et al.*, 2006; *Badger et al.*, 2006; *Bertram et al.*, 2009b; *Folkers et al.*, 2003; *McNeill et al.*, 2006; *Park et al.*, 2007; *Thornton et al.*, 2003].

III) (R5-3) indicates that the presence of NO_3^- in the particles will reduce $\gamma(N_2O_5)$, and it has also been validated by several studies [*Bertram and Thornton*, 2009; *Griffiths et al.*, 2009; *Mentel et al.*, 1999; *Wahner et al.*, 1998].

IV) As predicted by (R5-4), $ClNO_2$ and $BrNO_2$ have been observed in the reaction of N_2O_5 with particles with the presence of Cl^- and Br^-, respectively [*Behnke et al.*, 1997; *Roberts et al.*, 2009; *Schweitzer et al.*, 1998]. The presence of Cl^- in the particles can offset the suppression of $\gamma(N_2O_5)$ at high nitrate loadings, as (R5-4) suggests. This has been observed by Bertram and Thornton (2009) in a laboratory study.

However, increasing acidity or H_2SO_4 content in the particles has been found to promote or have no significant influence on the uptake of N_2O_5 [*Hallquist et al.*, 2000; *Hu and Abbatt*, 1997; *Kane et al.*, 2001; *Mozurkewich and Calvert*, 1988], and this is inconsistent with this mechanism, as (R5-3) predicts that $\gamma(N_2O_5)$ depends negatively on acidity in the aqueous particles. In addition, the cause of the temperature dependence of $\gamma(N_2O_5)$ [Griffiths and Cox, 2009] in some systems is not explained.

The reactive uptake of NO_3 by pure water was suggested to be caused by the reaction of NO_3(aq) with water after accommodation of NO_3 radicals into the liquid phase [*Rudich et al.*, 1996a]:

$$NO_3(g) \leftrightarrow NO_3(aq) \qquad \text{(R5-5)}$$

$$NO_3(aq) + H_2O(l) \leftrightarrow HNO_3(aq) + OH(aq) \qquad \text{(R5-6)}$$

A rise of HNO_3(g) concentration and a decrease in NO_3(g) concentration were found at elevated relative humidity, also indicating a conversion of NO_3(g) to HNO_3(g) on the moist reactor walls [*Schutze and Herrmann*, 2005]. X^- ions (X=Cl, Br, I, and NO_2) in the solution can also be oxidized by NO_3(aq) [*Rudich et al.*, 1996a; *Rudich et al.*, 1996b]:

$$X^-(aq) + NO_3(aq) \rightarrow NO_3^-(aq) + X(aq) \qquad \text{(R5-7)}$$

5.1.2 Reaction of N_2O_5 and NO_3 with mineral dust particles

There have been some qualitative studies on the mechanism of the uptake of N_2O_5/NO_3 on mineral dust particles. In one study, particulate nitrate was detected at 1350 cm^{-1} and 1452 cm^{-1} by Diffuse Reflectance FTIR Spectroscopy in the reaction of N_2O_5 with Saharan dust [*Seisel et al.*, 2005]. Based on the products measurement and the time-dependent uptake coefficient, the heterogeneous reaction of N_2O_5 with Saharan dust was proposed to proceed simultaneously via reaction with surface OH-groups (γ_{reac}) and

hydrolysis (γ_{hydr}). γ_{hydr} was found to be time-independent while γ_{reac} decreased with time due to the consumption of surface OH-groups [*Seisel et al.*, 2005].

In a Knudsen-cell study, HNO_3(g) was observed as a gas-phase product with a low yield of 4-6% by mass spectrometry in the reaction of N_2O_5 with Saharan dust [*Karagulian et al.*, 2006], and the heterogeneous hydrolysis mechanism was adopted to explain the result.

In contrast, an environmental chamber study found that the ratio of the produced HNO_3(g) to the N_2O_5 reacted with dust aerosols was approximately 2 for all cases (including calcite), in good agreement with the expected stoichiometry of the hydrolysis mechanism [*Mogili et al.*, 2006]. This result is however not compatible with another study in which HNO_3(g) was found to be efficiently uptaken by calcite aerosols by the same group [*Prince et al.*, 2007]. The somehow contradictive results from the two studies of the same group shed doubts on the proposed hydrolysis mechanism of N_2O_5 on dust surface. For the other two studies [*Wagner et al.*, 2009; *Wagner et al.*, 2008], the reaction mechanism of N_2O_5 with dust particles was not discussed in detail.

Before the present work there was only one study which investigated the uptake of NO_3 radicals on dust particles, using a Knudsen cell. Mass spectrometry was used to detect NO_3, N_2O_5, and HNO_3 and resonance enhanced multiphoton ionization to specifically detect NO and NO_2 [*Karagulian and Rossi*, 2005]. In that work NO_3 was produced from the thermal decomposition of N_2O_5(g), so the NO_2 concentration in the gas phase was similar to the NO_3 concentration. The uptake of NO_3 was found to be irreversible, but there was no evidence for the formation of NO or NO_2. This conclusion was supported by the formation of some N_2O_5 and HNO_3 in the reaction and the complete saturation of the surface when small amount of dust were used. The recombination of adsorbed NO_3 with NO_2 on the surface to N_2O_5 (R5-8) and the subsequent hydrolysis (R5-9a) or desorption into the gas phase (R5-9b) of the formed N_2O_5(ad) were proposed as the mechanism:

$$NO_3(ad) + NO_2(g) \rightarrow N_2O_5(ad) \qquad \text{(R5-8)}$$

$$N_2O_5(ad) + H_2O(ad) \rightarrow 2HNO_3(g) \qquad \text{(R5-9a)}$$

$$N_2O_5(ad) \rightarrow N_2O_5(g) \qquad \text{(R5-9b)}$$

However, given the low affinity of NO_2 on dust surface, (R5-8) would be expected to be very inefficient.

5.3 Effects of particulate nitrate on the N_2O_5 uptake

5.3.1 Nitrate formed in the aerosol flow tubes

N_2O_5 is suggested to undergo heterogeneous hydrolysis on the dust surface, leading to the formation of particulate nitrate with a yield of two [*Seisel et al.*, 2005]. If this is true, in the present experiment the amount of particulate nitrate formed in the dust particles in the aerosol flow tube can be calculated as

$$[NO_3^-] = \frac{2k_d}{k_d+k_w} \cdot [N_2O_5]_0 \cdot \{1 - \exp[(k_w + k_d) \cdot t]\} \quad \text{(E5-1)}$$

$$k_d = \frac{1}{4} \cdot \gamma \cdot \bar{c} \cdot N \cdot A \quad \text{(E5-2)}$$

The uptake coefficient of N_2O_5 on Saharan dust particles, γ, was experimentally determined to be 0.020±0.002 (Chapter 4), and the dust number concentration (*N*) is assumed to be 10,000 cm^{-3}. All the parameters used in the calculation are relevant to the experimental conditions. The time required to mix dust particles with N_2O_5 and to develop the laminar flow is not considered for simplicity. Each particulate nitrate ion formed by heterogeneous uptake of N_2O_5 is assumed to occupy an area of 5×10^{-15} cm^2 on dust surface, and the surface area of one dust particle is 7.79×10^{-8} cm^2.

When the initial N_2O_5 concentration is 5×10^{11} molecules cm^{-3} which is typical for the experiments performed in the new AFT, at the exit of the AFT (100 cm, or 35 s) about 4 formal monolayers of nitrate are calculated to have been formed (upper panel in Figure 5-2). In this work the formal monolayer of nitrate is defined as the total area of the nitrate (assuming that each nitrate occupies 5×10^{-15} cm^2) divided by the geometrical area of one Saharan dust particle. The mass of one formal monolayer of nitrate is about 10^{-3} of the mass of one fresh dust particle. When the initial N_2O_5 concentration is 1×10^{13} molecules cm^{-3} which is typical for the experiments performed in the old AFT, about 80 formal monolayers of nitrate are calculated to have been formed at the exit of the AFT, i.e. after interacting with N_2O_5 for 35 s (lower panel in Figure 5-2). The maximum initial N_2O_5 concentration used in this study is 2.7×10^{13} molecules cm^{-3}, giving the formation of ~200

formal monolayers of nitrate (or a 20% increase in the mass of the fresh dust particle, assuming no volatile products are formed in this reaction).

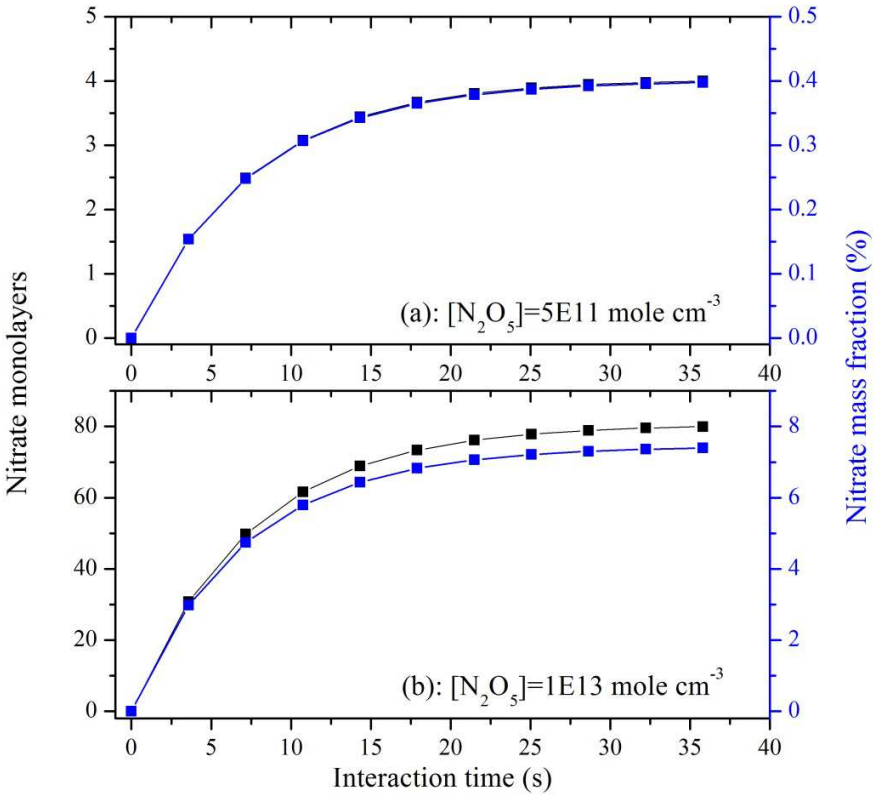

Figure 5-2. Particulate nitrate formed on the surface of dust particles due to the heterogeneous uptake of N_2O_5. Every N_2O_5 molecule which has reacted heterogeneously with dust particles is assumed to be converted to two nitrate ions on the surface (see the text for details). Upper panel: nitrate formation in the AFT, when the initial N_2O_5 concentration is 5×10^{11} molecules cm^{-3}. Lower panel: nitrate formation in the AFT, when the initial N_2O_5 concentration is 1×10^{13} molecules cm^{-3}.

It should be pointed out that the formation of 80 formal monolayers nitrate does not imply that each dust particle is evenly coated with 80 monolayers of nitrate. Though the initial concentration of N_2O_5 and thus the number of nitrate monolayers formed in the flow tube due to the heterogeneous uptake of N_2O_5 are varied by a factor of more than 20, the uptake coefficient of N_2O_5 showed no dependence on the initial N_2O_5 concentration within the experimental uncertainties (see Chapter 4 for more information). This result suggests that either the reaction does not consume surface sites or that the available surface of each particle is much larger than its geometrical area, i.e. it is highly porous.

The same parameters used in calculating the formation of nitrate monolayers, including the effective uptake coefficient of N_2O_5, the average surface area of mineral dust particle, the N_2O_5 wall loss rate, and dust number concentration, were further used to calculate the decay of N_2O_5 in the aerosol flow tube. Dust surface was assumed to be completely deactivated (i.e. no longer able to uptake any N_2O_5) after X formal monolayers of reactive sites (assuming that each particulate nitrate ion formed by heterogeneous uptake of N_2O_5 occupies an area of 5×10^{-15} cm^2 on the dust surface) were formed; while before the formation of X formal monolayers of nitrate, $\gamma(N_2O_5)$ did not change. Here the value of X can be varied in different calculations. The initial N_2O_5 concentration was set to 1×10^{13} molecules cm^{-3}.

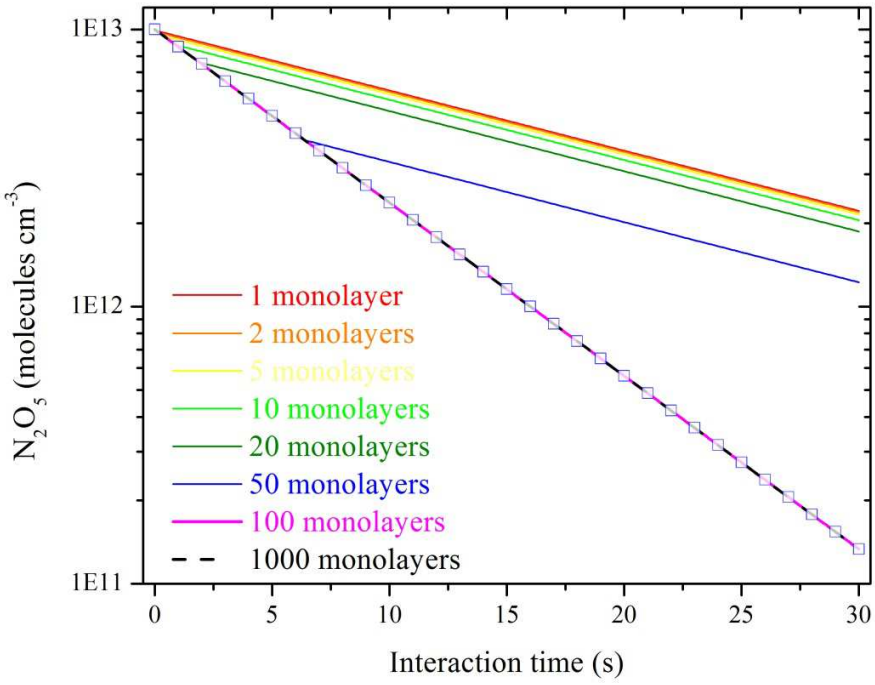

Figure 5-3. Decay of N_2O_5 concentration in the aerosol flow tube, assuming that different numbers of reactive sites (in the unit of formal monolayers) are available for the heterogeneous uptake of N_2O_5. The diamonds are the calculated N_2O_5 concentration assuming no surface deactivation, using an uptake coefficient of 0.02 determined in this work (see Chapter 4).

The results of these calculations are shown in Figure 5-3, suggesting that the N_2O_5 decay in the aerosol flow tube would be much slower than what was measured if the dust surface was deactivated by the formation of several formal monolayers of nitrate. These

simulations further confirm that the Saharan dust particles have much more capacity than one formal monolayer to uptake N_2O_5.

If the heterogeneous uptake of N_2O_5 is of Langmuir-Hinshelwood mechanism, the negative dependence of $\gamma(N_2O_5)$ on initial N_2O_5 concentration might probably be observed when the surface coverage is high (e.g. when $K_{LangC}(X)[X]_g$ is similar or larger than 1, see Section 1.5 for details). No dependence of $\gamma(N_2O_5)$ on N2O5 concentration was observed in this work. However, it does not necessarily mean that the heterogeneous uptake of N_2O_5 is of Langmuir-Hinshelwood mechanism, because it is not clear whether the surface coverage was high under the experimental conditions in this study. Further experiments at higher N2O5 concentration might help to understand the reaction mechanism.

5.3.2 Effects of nitrate coating on the N_2O_5 uptake

As stated in the previous section, the uptake coefficient of N_2O_5 was experimentally determined to be ~0.018, showing no dependence on the amount of particulate nitrate in the dust particles, in contrast to the nitrate effect in the heterogeneous uptake of N_2O_5 on aqueous particles [*Bertram and Thornton*, 2009; *Mentel et al.*, 1999] and ice surface (see the compilation by [*IUPAC*, 2009]). Two possible scenarios can explain the independence of the N_2O_5 uptake coefficients on Saharan dust particles on the amount of particulate nitrate formed in the aerosol flow tube (i.e. on the initial N_2O_5 concentration): 1) heterogeneous uptake of N_2O_5 on mineral dust particles has other reaction mechanisms such as heterogeneous surface-catalyzed decomposition rather than heterogeneous hydrolysis, so that no particulate nitrate is formed on the dust particles, 2) or the particulate nitrate in the dust particles does not influence the uptake of N_2O_5, opposite to that observed for the heterogeneous hydrolysis on aqueous surfaces.

The uptake of HNO_3(g) on mineral dust particles is known to be efficient [*Hanisch and Crowley*, 2001a; *Vlasenko et al.*, 2006], and leads to the formation of particulate nitrate on the dust surface [*Goodman et al.*, 2000; *Liu et al.*, 2008]. The heterogeneous uptake of HNO_3(g) on Saharan dust was also preliminarily investigated in this work and found to be quite substantial, as shown in Appendices A1. To further investigate the effect of particulate nitrate on the uptake of N_2O_5 on dust, in some experiments Saharan

dust particles were mixed with HNO_3(g) in the 5 L mixing volume before being introduced into the aerosol flow tube to determine the uptake coefficient of N_2O_5 on the chemically modified dust particles.

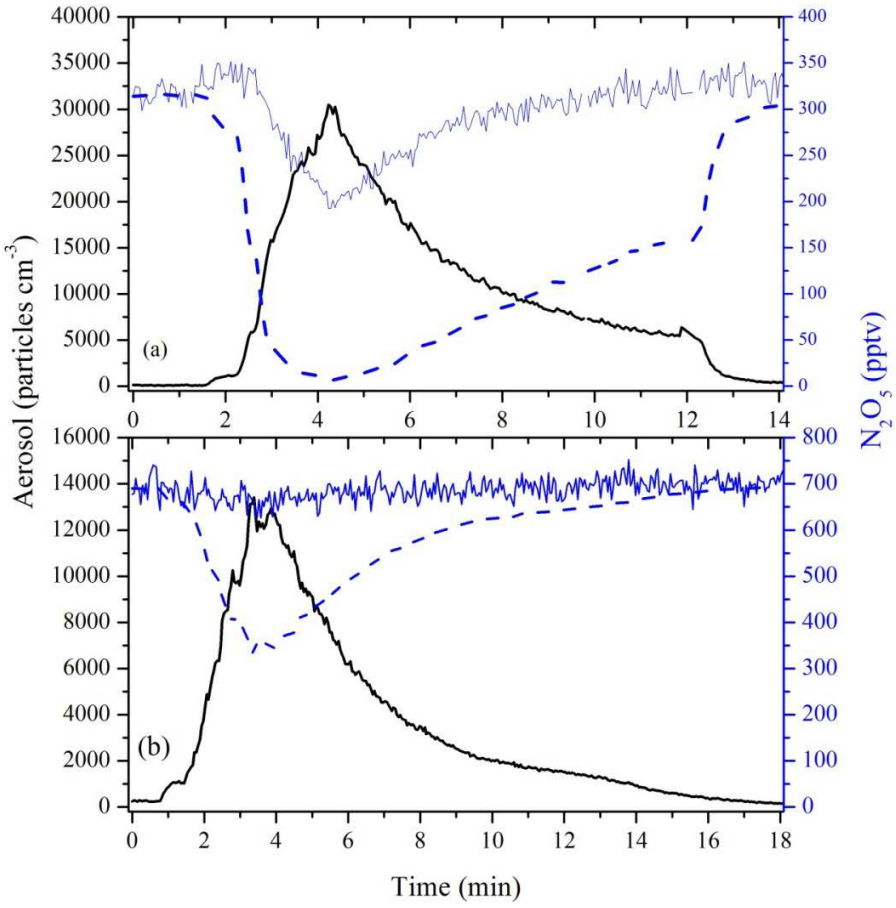

Figure 5-4. The response of N_2O_5 (solid blue line, right y-axis) to the introduction of Saharan dust particles (black line, left y-axis), which was pretreated in the mixing volume by HNO_3(g). The dash blue line is the expected response of N_2O_5 without the pretreatment by HNO_3(g). Upper panel: HNO_3(g) was produced by eluting a 65% nitric acid solution by 20 sccm N_2. Lower panel: HNO_3(g) was produced by eluting a 65% nitric acid solution by 20 sccm N_2.

HNO_3(g) was eluted from a 65% HNO_3 solution held at room temperature (with the HNO_3 vapor pressure of about 8 Torr) in 20 sccm N_2. This flow was directly transported into the mixing volume and mixed there with the Saharan dust aerosols flow (800 sccm). After exiting the mixing volume, the HNO_3(g)-pretreated Saharan dust particles were delivered into the old aerosol flow tube through the side arm and the uptake coefficients

of N_2O_5 were measured. As shown in the upper panel of Figure 5-4, the pretreatment by HNO_3(g) substantially suppressed the uptake of N_2O_5 on Saharan dust particles.

The results of these experiments in which 20 sccm N_2 was used to elute HNO_3(g), are summarized in Table 5-1. The uptake coefficients of N_2O_5 for the HNO_3(g)-pretreated Saharan dust particles are determined to be 0.0060±0.0007, 0.0043±0.0003, and 0.0027±0.0001 at RH of 0%, 25%, and 50%, showing no dependence on RH within the experimental errors. The uptake coefficient was reduced by a factor of ~5, when compared with the average value (0.016±0.002, 1 σ) for fresh Saharan dust, which was not pretreated by HNO_3(g).

Table 5-1. Uptake coefficients of N_2O_5 on chemically modified Saharan dust and experimental conditions

RH (%)	$[N_2O_5]^a$	γ_{true} [b]	Average [c]
0	24	0.0063±0.0005	0.0060±0.0007
	26	0.0039±0.0010	
	26	0.0073±0.0006	
	21	0.0037±0.0011	
25	21	0.0036±0.0007	0.0043±0.0003
	21	0.0046±0.0005	
	22	0.0045±0.0008	
50	19	0.0030±0.0006	0.0027±0.0001
	19	0.0027±0.0004	
	26	0.0025±0.0005	

In these experiments HNO_3(g) was eluted from the 65% aqueous solution by 20 sccm N2 and mixed with the 800 sccm aerosol flow in the mixing volume. [a] Initial N_2O_5 concentration in the units of 10^{12} molecules cm^{-3}. [b] The values of γ_{true} have been corrected for diffusion limit to the uptake. [c] Weighted averaged γ_{true} at the corresponding RH. The errors (1 σ) are statistical only.

In two further experiments (RH=0%), Saharan dust particles were mixed with HNO_3(g) which was eluted from a 65% nitric acid solution by 100 sccm N_2 before they were delivered into the flow tube. As shown in the lower panel of Figure 5-4, within the noise level there was no change of the measured N_2O_5 mixing ratio even when dust

aerosol reached about 14000 particles cm^{-3} in the flow tube, so only an upper limit of γ_{true} < 0.0015 is reported here. The uptake coefficient of N_2O_5 on $NaNO_3$ particle have been determined to be 0.002-0.003 at RH<60% [*Mentel et al.*, 1999; *Wahner et al.*, 1998], in accordance with the upper limit estimated in this study.

Several methods have been used to estimate the amount of nitrate formed on the dust particle by reaction with HNO_3(g) in the mixing volume, and the results are shown in Appendices A2. However, the amount of nitrate formed on the dust particles in the mixing volume is difficult to estimate for several reasons: 1) the HNO_3 concentration in the mixing volume was around 10^{15}-10^{16} molecules cm^{-3}, and in this concentration range the kinetics of the uptake of HNO_3(g) on dust particles is not readily known; 2) the loss of HNO_3(g) onto the dusty wall of the mixing volume, which might be an important non-particle sink for HNO_3(g), is difficult to take into account; 3) the estimation of the HNO_3(g) concentration in the mixing volume, based on the vapor pressure of 65% HNO_3 solution, might not be accurate enough.

5.4 Products of the heterogeneous reaction of N_2O_5 with dust particles

So far we have shown that particulate nitrate, formed by reacting HNO_3(g) with dust aerosols in the mixing volume, significantly suppresses the uptake of N_2O_5 on dust particles. However, the uptake coefficients of N_2O_5 on dust particles do not depend on initial N_2O_5 concentration or relative humidity in the flow tube. A possible explanation to this "dilemma" is that instead of hydrolysis on the dust surface, N_2O_5 undergoes heterogeneous decomposition, which does not lead to the formation of particulate nitrate and thus does not consume surface reactive sites. If N_2O_5 undergoes heterogeneous decomposition on the dust surface, NO_2 must be the final product, as shown below:

$$S + N_2O_5(g) \leftrightarrow S\text{-}N_2O_5(ad) \quad \text{(R5-10)}$$

$$S\text{-}N_2O_5(ad) \leftrightarrow NO_2(g) + S\text{-}NO_3(ad) \quad \text{(R5-11)}$$

$$S\text{-}NO_3(ad) \rightarrow NO_2(g) + S\text{-}O(ad) \quad \text{(R5-12)}$$

$$S\text{-}NO_3(ad) + S\text{-}O(ad) \rightarrow NO_2(g) + O_2(g) + S + S \quad \text{(R5-13)}$$

where S is the surface reactive site, and $S\text{-}N_2O_5$(ad), $S\text{-}NO_3$(ad), and S-O(ad) are surface adsorbed N_2O_5, NO_3, and O atom, respectively. Therefore, experiments were carried out

to measure the fraction of NO_2 produced from the heterogeneous interaction of N_2O_5 with Saharan dust.

5.4.1 Cavity Ring-Down spectroscopy detection of NO_2 and N_2O_5

As described in Section 2.4, N_2O_5 and NO_2 were simultaneously measured by Thermal dissociation Cavity Ring-Down spectroscopy (TD-CRD) after passing a filter loaded with Saharan dust particles. A control experiment was performed to check whether the two paths were identical when a fresh filter was also used in the sample path. In the absence of dust on the filter in the sample path, the measured NO_2 and N_2O_5 mixing ratios were the same as the values when the gas passed through the blank path, demonstrating that the both paths have the same reactivity towards NO_2 and N_2O_5.

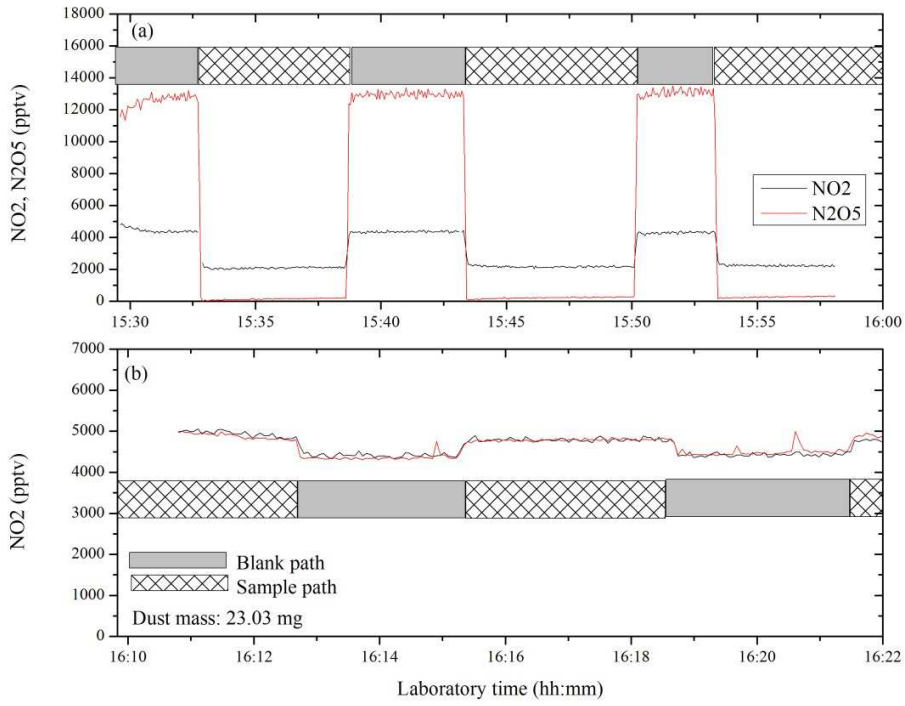

Figure 5-5. NO_2 and N_2O_5 concentration observed when the gas passed through the blank path and the sample path with a filter loaded with 23.03 mg Saharan dust particles at RH=0%. Upper panel: N_2O_5 passed through the paths. Lower panel: NO_2 passed through the paths; in this case both channels of the TD-CRD only measured NO_2 concentration.

The result of an experiment in which N_2O_5 was passed through a filter loaded with 23.03 mg Saharan dust particle (RH=0%) is shown in the upper panel of Figure 5-5. When the 4 SLM gas passed through the blank path, about 13 ppbv N_2O_5 was measured

together with about 5 ppbv NO_2, which came from the decomposition of N_2O_5 before and after the filter. When the gas was switched through the dust-loaded filter, the mixing ratio of N_2O_5 dropped almost to 0 due to the interaction with relatively large amount of dust particles loaded on the filter, and there was no significant deactivation of dust surface after ~30 min exposure. Meanwhile the mixing ratio of NO_2 decreased from ~5 ppbv to ~ 2ppbv. An increase in the measured NO_2 mixing ratio should have been observed if N_2O_5 underwent heterogeneous decomposition on the dust surface, assuming that the direct loss of NO_2 onto the dust surface is not significant.

Further experiments were conducted to examine whether the heterogeneous loss of NO_2 was negligible. 5 ppbv NO_2 was passed through the same sample path, and the result is shown in the lower panel of Figure 5-5. The NO_2 mixing ratio was only reduced by less than 10%, qualitatively agreeing with that $\gamma(NO_2)$ is a factor of 1000 smaller than $\gamma(N_2O_5)$ on Saharan dust [*IUPAC*, 2009]. Therefore, the significant decrease of the measured NO_2 mixing ratio (more than 50%) when N_2O_5 passed through the sample path could not result from the uptake of NO_2 on Saharan dust.

N_2O_5 decomposed before and after the filters. When the gas passed through the blank path, NO_2 came from the N_2O_5 decomposition before and after the clean filter. When the gas passed through the sample path and the measured N_2O_5 mixing ratio dropped to almost 0 after the interaction with Saharan dust (upper panel of Figure 5-5), NO_2 could only originate from the decomposition of N_2O_5 before the filter. Therefore, the measured NO_2 mixing ratio also decreased significantly when the gas passed through the sample path.

From the upper panel of Figure 5-5, ~16.7% of N_2O_5 (2.2 ppbv NO_2 in 13.2 ppbv N_2O_5) was estimated to decompose to NO_2 before the filter and totally 32.1% of N_2O_5 (4.2 ppbv NO_2 in 13.2 ppbv N_2O_5) decomposed in the system, i.e. 15.4% of N_2O_5 decomposed after the filter. The measured decomposition fraction (15.4%) of N_2O_5 agrees well with the calculated value of 15.5% in the cavity (2000 sccm flow in the cavity of 168 cm^3 at 298K), assuming that NO_3 radicals formed from the decomposition react with the wall and the recombination of NO_3 and NO_2 is negligible. The

decomposition fractions of N_2O_5 before and after the filter were also used to correct other data, which are shown in Figure 5-6.

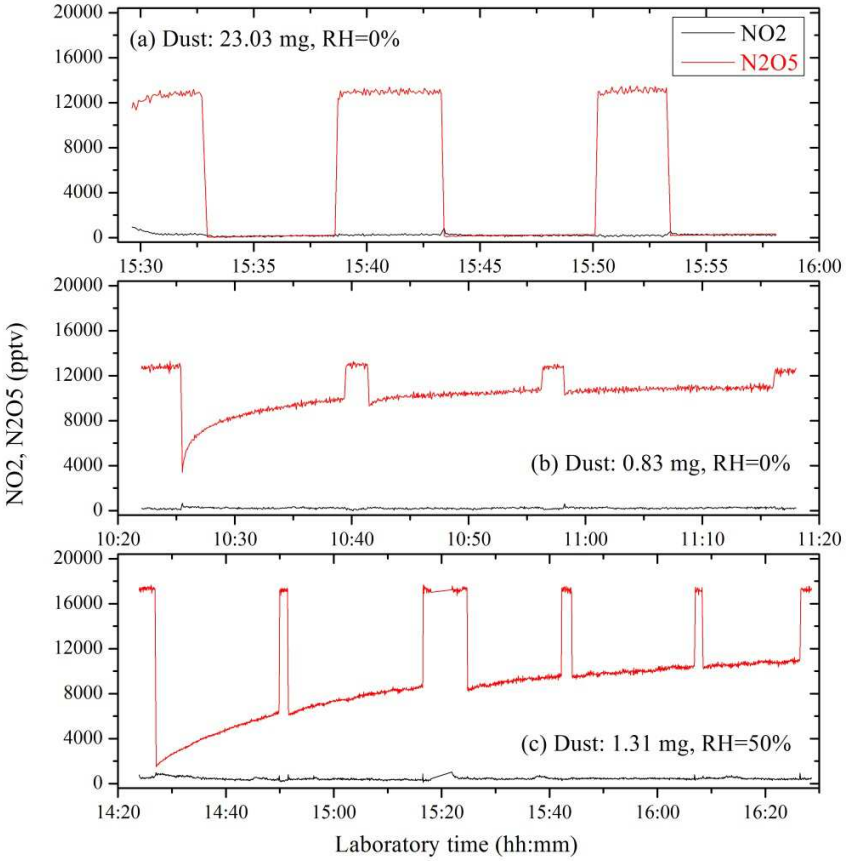

Figure 5-6. The measured NO_2 and N_2O_5 mixing ratios when the gas passed through the blank and the sample paths. Upper panel: 23.03 mg dust, and RH=0%; Middle panel: 0.83 mg dust, and RH=0%; Lower panel: 1.31 mg dust, and RH=50%. During the experiments the gas flow was switched to the blank path to check if the initial N_2O_5 mixing ratio was stable.

Three experiments in which different amounts of Saharan dust were loaded on the filter, were performed at different relative humidities (RH) to investigate the influence of dust mass, reaction time (thus deactivation of dust surface), and RH on the production yield of NO_2. The results are displayed in Figure 5-6, in which the mixing ratios of NO_2 and N_2O_5 were both corrected for the N_2O_5 decomposition. All the N_2O_5 reacted with dust in the first experiment (upper panel), in the second experiment N_2O_5 almost recovered to the initial level (close to 95%) at the end of exposure (middle panel), and in the third one the dust surface started to be deactivated but was still far from being totally

saturated (lower panel). In all the three cases (and also two different RH), no NO_2 was observed to be formed in the reaction of N_2O_5 with Saharan dust. Due to the small loss of NO_2 onto the dust particles (<10%, shown in the lower panel of Figure 5-5), an upper limit of 10% for the NO_2 production yield was estimated.

5.4.2 Ion chromatography analysis of particulate nitrate

After exposure to N_2O_5, the three dust samples were extracted in 10.00 mL deionized water in an ultrasonic bath for 30 min, and the solutions were analyzed by ion chromatography to measure the nitrate contents (see Section 2.4). Another three fresh dust samples were also analyzed by the same method to measure the nitrate present in the fresh dust. After subtracting the amount of nitrate present in the fresh dust particles, the nitrate production yield from the reaction of Saharan dust with N_2O_5 was determined to be 1.75±0.83 (1 σ), reasonably agreeing with the theoretical value of 2, assuming that every N_2O_5 molecule which has reacted with dust is converted to two nitrate ions on the particles. The large uncertainty of the measured nitrate production yield stems from the variation of the nitrate mass fraction in the fresh dust samples (0.247±0.085 μg nitrate in 1 mg Saharan dust), because the nitrate mass in the fresh dust samples were of the similar magnitude of the mass of the nitrate formed in the heterogeneous reaction of N_2O_5.

The measurements of the gas phase (no NO_2 produced) and the condensed phase (nitrate) products both suggest that N_2O_5 indeed undergoes heterogeneous hydrolysis on the dust surface, forming particulate nitrate with a production yield of about two within the experimental uncertainties. It remains to be understood why $\gamma(N_2O_5)$ is independent of relative humidity or N_2O_5 concentration, as shown in Chapter 4.

5.5 Mechanism

It is shown in Section 5.4 that undoubtedly N_2O_5 undergoes heterogeneous hydrolysis on the Saharan dust surface to form particulate nitrate with a production yield of about 2. Why do the uptake coefficients of N_2O_5 show no dependence on relative humidity, as shown in Section 4.3.1? Each N_2O_5 molecule which undergoes heterogeneous hydrolysis consumes one H_2O molecule and forms two nitrate ions, i.e.

$$m(H_2O) = \frac{m(NO_3^-)}{2} \cdot \frac{M(H_2O)}{M(NO_3^-)} \quad \text{(E5-3)}$$

where $m(H_2O)$ is the mass of H_2O consumed and $m(NO_3^-)$ is the mass of formed nitrate formed due to the heterogeneous hydrolysis of N_2O_5, and $M(H_2O)$ and $M(NO_3^-)$ are the molar mass of H_2O and NO_3^-, respectively. As stated in Section 5.3.1, the maximum initial N_2O_5 concentration used in this study was 2.7×10^{13} molecules cm^{-3}, leading to the formation of nitrate whose mass is ~20% of the fresh dust particle (corresponding to an increase of ~6% in diameter, assuming that the dust density did not change), and therefore required H_2O whose mass is about 3% of the fresh dust particle to react with N_2O_5, according to (E5-3). Water contained in clay minerals includes adsorbed water and internal water, which consists of interlayer water and lattice OH water. The internal water can contribute to more than 10% of the total mass, and it can only be removed after being heated to more than 800 °C [*Grim*, 1953]. The independence of uptake coefficients of N_2O_5 on RH may thus suggest that Saharan dust particles always contain a large amount of internal water which is available for the hydrolysis, and that the heterogeneous uptake of N_2O_5 is not purely a surface process. The uptake coefficient of N_2O_5 on water surface at room temperature is in the range of 0.01-0.02 [*IUPAC*, 2009], approximately equal to the uptake coefficient on Saharan dust particles.

The uptake coefficient of N_2O_5 on Saharan dust particles does not vary with initial N_2O_5 concentration in the flow tube, even when nitrate of more than 100 monolayers is formed. This phenomenon again suggests that the uptake of N_2O_5 on Saharan dust is not purely a surface process and a large fraction of the internal surface of dust particles is also available for the uptake. The geometric area of the airborne Saharan dust particles is 3.03 $m^2\ g^{-1}$ (7.79 μm^2 per particle), and the BET area of bulk Saharan dust is 39.6 $m^2\ g^{-1}$, which is about a factor of 10 times of the geometrical area. It should also be noticed that the BET area of the airborne dust particles can even be much larger than 39.6 $m^2\ g^{-1}$ (the BET area of bulk dust particles), because during the dispersion of bulk samples and transport of dust aerosols into the flow tube, bigger particles have larger probability to be removed from the gas flow due to deposition and impaction. The large difference in the geometric area and the BET area of a single particle can explain why the uptake coefficient of N_2O_5 shows no dependence on N_2O_5 concentration (5×10^{11} - 3×10^{13} molecules cm^{-3}).

The mechanism of the heterogeneous reaction of N_2O_5 with dust particles is proposed to be the hydrolysis of N_2O_5 (R5-12, R5-13) after being adsorbed on the dust surface (R5-11):

$$N_2O_5(g) \leftrightarrow N_2O_5(ad) \quad \text{(R5-11)}$$

$$N_2O_5(ad) \leftrightarrow NO_2^+(ad) + NO_3^-(ad) \quad \text{(R5-12)}$$

$$NO_2^+(ad) + H_2O(ad) \leftrightarrow HNO_3(ad) + H^+(ad) \quad \text{(R5-13)}$$

where $H_2O(ad)$ is the water content contained in the dust particles. This mechanism is the analogue to the heterogeneous hydrolysis of N_2O_5 on aqueous surface, and it explains why pretreatment of Saharan dust particles with $HNO_3(g)$ can suppress the N_2O_5 uptake. It has been shown in Chapter 3 that $\gamma(NO_3)/\gamma(N_2O_5)$ was close to unity, and the surface deactivation processes were similar for both species, suggesting that the mechanism of the uptake of NO_3 on dust particles is similar to that of uptake of N_2O_5. The uptake of NO_3 radicals on dust particles is thus proposed to proceed via adsorption of NO_3 radicals on the dust surface (R5-14) followed by the reaction of adsorbed NO_3 with water contained in the particles (R5-15):

$$NO_3(g) \leftrightarrow NO_3(ad) \quad \text{(R5-14)}$$

$$NO_3(ad) + H_2O(ad) \leftrightarrow HNO_3(ad) + OH(ad) \quad \text{(R5-15)}$$

(R5-15) suggests that particulate nitrate also suppresses the uptake of NO_3 on dust surface, and it explains why the measured NO_3 and N_2O_5 mixing ratios had similar time profiles when the gas passed the same bulk dust sample, as shown in Section 3.3.1.

5.6 Summary

Particulate nitrate has been identified as the product of the heterogeneous reaction of N_2O_5 with mineral dust particles with a yield of ~2 within the experimental uncertainties, and no NO_2 is formed in this reaction, suggesting that N_2O_5 undergoes heterogeneous hydrolysis on the dust surface. The uptake coefficient of N_2O_5 on Saharan dust particles, $\gamma(N_2O_5)$, does not change even when up to about 200 formal monolayers of nitrate are formed, indicating that the uptake of N_2O_5 on dust particles is not purely a surface process but the internal surface is also available for the reaction. The independence of $\gamma(N_2O_5)$ on relative humidity can be explained by the availability of internal water

contained by the dust particles. Exposure of Saharan dust particles to HNO_3(g) of high concentration (around 10^{15}-10^{16} molecules cm^{-3}) can largely suppress the uptake of N_2O_5, and the extent depends on the concentration of HNO_3(g) used to pretreat dust particle. Presumably the effect of nitrate is to consume crystalline water in the dust particles and thus prevent the uptake of N_2O_5, though no quantitative relation between $\gamma(N_2O_5)$ and the nitrate content can be derived from this work.

6 Atmospheric implication and outlook

6.1 Summary

In this work the heterogeneous reactions of mineral dust particles with N_2O_5 and NO_3 radicals have been studied. The major findings include:

1) Using two aerosol flow tubes, the uptake coefficient of N_2O_5, $\gamma(N_2O_5)$, was determined to be 0.020±0.002 (1 σ) on airborne Saharan dust particles, independent of relative humidity in the range of 0-67%. It also shows no dependence on N_2O_5 concentration in the range of 5×10^{11}-3×10^{13} molecules cm^{-3}. In addition, the uptake coefficients of N_2O_5 on Arizona Test Dust and Illite have also been measured at different relative humidities up to 67%. At RH=0%, $\gamma(N_2O_5)$ were 0.084±0.019 (1 σ) for illite and 0.010±0.001 (1 σ) for Arizona Test dust.

2) The quantitative analysis of the gas phase and particulate products suggests that N_2O_5 undergoes hydrolysis on the dust surface to form particulate nitrate with a yield of about 2. The independence of the uptake coefficient of N_2O_5 on relative humidity is due to the large amount of internal water (up to more than 10% of the dust mass) available for the reaction.

3) The heterogeneous reaction of N_2O_5 with Saharan dust particles is not a purely surface process. The internal surface, whose area is much larger than the geometric area, is also available for the heterogeneous hydrolysis of N_2O_5, explaining why there is no dependence of the uptake coefficients on N_2O_5 concentration. Nevertheless, the dust particles could be deactivated if the particulate nitrate reached high levels after the dust particles were exposed to HNO_3(g) of about 10^{15}-10^{16} molecules cm^{-3}, and presumably would be deactivated if exposed to N_2O_5 with sufficiently high concentration.

4) Using a relative rate method, the uptake coefficient ratio of NO_3 to N_2O_5, $\gamma(NO_3)/\gamma(N_2O_5)$, was measured to be 0.9±0.4 (1 σ) for Saharan dust particles, independent of relative humidity (0-70%), NO_3 and N_2O_5 concentrations, and reaction time, though surface deactivation was observed during the experiments for both species. The heterogeneous reaction of NO_3 radicals with mineral dust particles is proposed to

proceed via the reaction of adsorbed NO_3 with surface-adsorbed and internal water, in which particulate nitrate is formed.

5) At RH=0%, the uptake coefficient ratio of NO_3 to N_2O_5, $\gamma(NO_3)/\gamma(N_2O_5)$, was measured to be larger than 15 for ambient urban particles, and in the range of ~1.5-3 for candle-generated soot particles.

6.2 Atmospheric implications

Neglecting diffusive limitation to mass transport, the lifetime (τ, in s) of a trace gas, X, with respect to uptake on the surface of atmospheric particles, can be calculated using the following equation:

$$\tau_X = \frac{4}{\gamma_X \cdot \bar{c} \cdot A} \qquad \text{(E6-1)}$$

where γ_X is the uptake coefficient, $\bar{c}$ is the average molecular speed in cm s^{-1}, and A is the surface area concentration of atmospheric particles in cm^2 cm^{-3}. If assuming that the average diameter of mineral dust particles is 1 μm and the density of dust particles is 2.7 g cm^{-3}, (E6-1) then becomes [*Wagner et al.*, 2008]:

$$\tau = \frac{1.8}{\gamma_X \cdot \bar{c} \cdot L} \times 10^8 \qquad \text{(E6-2)}$$

where L is the atmospheric dust particles loading in μg cm^{-3}. In this calculation, $\gamma(N_2O_5)$ of 0.020 and $\gamma(NO_3)$ of 0.018 determined in this work are used, and the average molecule speed at 23 °C is 24100 cm s^{-1} for N_2O_5 and 31800 cm s^{-1} for NO_3, respectively.

The dependence of the N_2O_5 and NO_3 lifetimes on the mineral dust loading is displayed in Figure 6-1. With a dust loading of 10-100 μg m^{-3}, which is typical in dust-impacted regions [*Chun et al.*, 2001; *Ginoux et al.*, 2001; *Prospero*, 1979; 1999; *Zhao et al.*, 2010], the lifetime of N_2O_5 with respect to the uptake on dust particles is 1.2-12 h. The steady-state lifetime of N_2O_5 determined by field measurements typically varies between 5 min and several hours [*Aldener et al.*, 2006; *Crowley et al.*, 2010a; *Heintz et al.*, 1996; *Martinez et al.*, 2000; *Wood et al.*, 2005], suggesting that the uptake on dust particles can be a very important sink for N_2O_5 in dust-impacted regions. Removal of N_2O_5 (and thus NOx) impacts the levels of O_3 and OH indirectly [*Dentener and Crutzen*, 1993; *Evans and Jacob*, 2005], as shown in Figure 1-1 and 1-2. Uptake of N_2O_5, together

with the uptake of HNO_3(g), can also contribute significantly to the formation of observed particulate nitrate in mineral dust particles during long-range transportation [*Sullivan et al.*, 2007; *Tang et al.*, 2004; *Zhang et al.*, 1994], further modifying the ability of dust particles of acting as cloud condensation nuclei [*Laskin et al.*, 2005; *Liu et al.*, 2008; *Sullivan et al.*, 2009b] and ice nuclei [*Sullivan et al.*, 2010a].

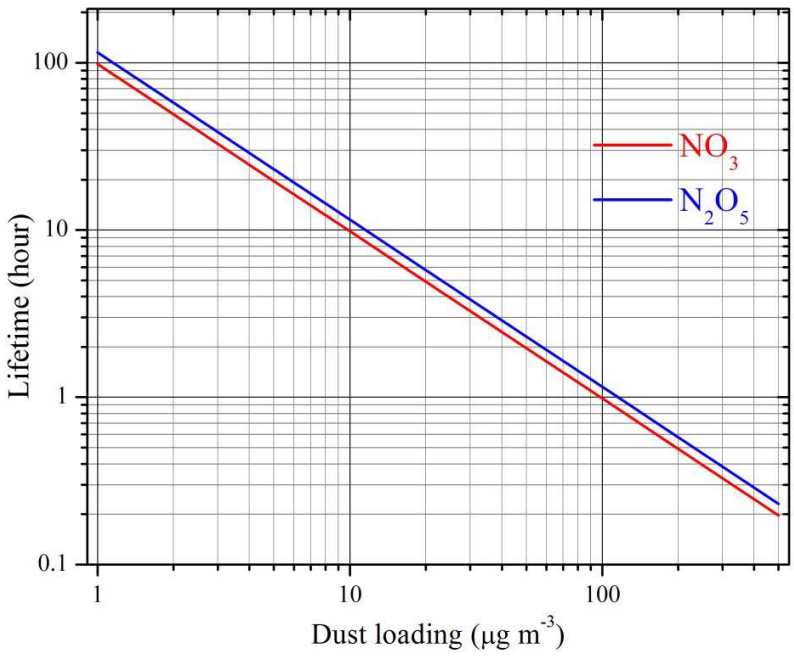

Figure 6-1. Lifetimes of N_2O_5 and NO_3 with respect to the heterogeneous uptake onto mineral dust particles, as functions of dust loading in the atmosphere.

Different $\gamma(N_2O_5)$ on mineral dust particles, which varied almost by two orders of magnitude, were used in modeling studies to investigate the effects of heterogeneous reaction of N_2O_5 with mineral dust aerosols. For example, $\gamma(N_2O_5)$ of 0.1, 0.01, 0.03, 0.01, and 0.03 were used in the modeling by Dentener et al. [1996], Bian and Zender [2003], Evans and Jacob [2005], and Zhu et al. [2010]. In addition, a value of $\gamma(N_2O_5)$ which varied between 0.003 and 0.02 with relative humidity was adopted by Bauer et al. [2004]. This work suggests that a value of 0.02 for $\gamma(N_2O_5)$, which is independent of relative humidity, should be used in modeling studies to simulate the heterogeneous reaction of N_2O_5 with mineral dust aerosols. Dust particles undergo aging processes and become enriched in nitrate during transport [*Matsuki et al., 2005; Mori et al., 2003; Sullivan et al., 2007*]. Saharan dust particles have been shown to have much higher

capacity to uptake N_2O_5 than that of the geometrical area in this work, and $\gamma(N_2O_5)$ will not change even when up to ~200 formal monolayers of nitrate is formed in dust particles.

The lifetime of NO_3 radicals in the nocturnal boundary layer is very variable but usually less than 1 h [*Aldener et al.*, 2006; *Crowley et al.*, 2010a; *Martinez et al.*, 2000], which is mainly attributed to the reactions with organic species. The presence of 20 μg $m^{-3}$of dust particles in the boundary layer gives a NO_3 lifetime of ~5 h with respect to the uptake on dust particles, which is of minor important compared with reactions with organics in the gas phase. In the free troposphere NO_3 lifetimes are significantly higher due to the reduction of concentrations of surface-emitted reactants [*Aliwell and Jones*, 1998; *Allan et al.*, 2002; *Brown et al.*, 2007b], and the uptake of NO_3 on dust particles can be an important pathway which removes NO_3 directly from the atmosphere. However, the lower temperature and also less NO_2 in the free troposphere favors N_2O_5 much more than NO_3 [*Sander et al.*, 2006]:

$$\frac{[N_2O_5]}{[NO_3]} = K_{eq}[NO_2] \quad \text{(E6-3)}$$

$$K_{eq} = 2.7 \times 10^{-27} e^{(11000/T)} \quad \text{(E6-4)}$$

where K_{eq} is the equilibrium constant in cm^3 $molecule^{-1}$, and T is the temperature in K. Mineral dust particles have almost the same reactivity towards NO_3 and N_2O_5. Therefore, in the free troposphere the heterogeneous loss of N_2O_5 must be much more important than that of NO_3 in terms of NOx removal. To conclude, the heterogeneous uptake of NO_3 on mineral dust particles is not likely to be a significant NOx removal process unless the dust loading is a few hundred μg m^{-3} (in dust plumes). Similarly, the uptake of NO_3 on dust particles is not important to the formation of particulate nitrate under typical conditions.

6.3 Future work

Ion chromatography analysis suggests that particulate nitrate is formed due to the heterogeneous uptake of N_2O_5 on dust particles, as shown in Section 5.4.2. The possibility that N_2O_5 was just adsorbed on the dust surface and then converted to nitrate after the dust particles were dissolved in the deionized water cannot be ruled out, though it is very unlikely. Analysis of the dust surface before and after the reaction with N_2O_5 by

Fourier transform infrared spectroscopy will help confirm the formation of nitrate due to the uptake of N_2O_5.

Field measurements show that the uptake coefficient of N_2O_5 on ambient particles is significantly smaller than that on aqueous sulfate particles reported by laboratory studies [*Bertram et al.*, 2009b; *Brown et al.*, 2009a], most likely due to the presence of organic species in the ambient particles. Observation-constrained modeling studies also indicate that the uptake coefficients smaller than that reported by laboratory studies have to be used in the models in order to reproduce the measured compositions of dust particles [*Fairlie et al.*, 2010; *Song et al.*, 2007]. In this work experiments with bulk and dispersed dust samples both confirm that the dust particles could be deactivated after the amount of particulate nitrate reached certain amount. The dependence of uptake coefficients of N_2O_5 on mineral dust, on the amount of particulate nitrate in the dust particles, was rather qualitatively investigated, and quantitative studies on the nitrate effect are definitely required.

A variety of organic species have been found to be associated mineral dust particles [*Falkovich et al.*, 2004; *Wang et al.*, 2009]. Laboratory studies on the effect of organic coatings on the uptake of N_2O_5 are also necessary, considering that organic contents in sulfate and NaCl aerosols can substantially suppress the uptake of N_2O_5 [*Anttila et al.*, 2006; *Cosman et al.*, 2008; *Folkers et al.*, 2003; *McNeill et al.*, 2006; *Park et al.*, 2007]. The uptake coefficient of N_2O_5 on ammonia sulfate particles shows a negative dependence on temperature in the range of 263-303 K at RH=50% [*Griffiths and Cox*, 2009]. While the effect of temperature on the uptake of N_2O_5 on mineral dust particles, which might be important in the troposphere, has not been considered yet and needs further investigation.

The original plan of the PhD study was to investigate the heterogeneous reactions of mineral dust aerosols with NO_3 and N_2O_5, by combining laboratory studies with field measurements. During the PhD study ambient NO_3 and N_2O_5 were measured by Cavity Ring-Down spectroscopy in three field campaigns. Among the motives was to determine the uptake coefficients of N_2O_5 on ambient particles. During the DOMINO campaign (Diel Oxidant Mechanisms In relation to Nitrogen Oxides) which was performed from

November 21 to December 08, 2008 on the Atlantic coast of the southern Spanish, the nocturnal loss of NOx was dominated by the reactions of NO_3 radicals with organic species [*Crowley et al.*, 2011]. In addition, particles mainly consisted of organics species, sulfate, and nitrate, with no contribution by mineral dust [*Diesch et al.*, 2011]. In the second campaign, HUMPPA-COPEC 2010 (Hyytiälä United Measurement of Photochemistry and Particles- Comprehensive Organic Particle and Environmental Chemistry) [*Williams et al.*, 2011], the lifetimes of NO_3 and N_2O_5 were very short and exclusively controlled by the reactions of NO_3 with biogenic hydrocarbons emitted by the plants in the boreal forest. The third field campaign took place from August 08 to September 09, 2011 at the Taunus Observatory, located at the summit of the Kleiner Feldberg Mountain in South-western Germany. Previous measurement in May 2008 suggests that the nocturnal loss of NOx at this site was dominated by the reactions of NO_3 with volatile organic carbons and the loss of N_2O_5 was only of secondary importance [*Crowley et al.*, 2010a].

To better investigate the uptake of N_2O_5 on ambient dust particles, field measurements in future should be carried out at the periods when dust storms frequently occur and sites which are heavily impacted by dust storms. The Global Atmospheric Watch station Izana on Tenerife, where aerosol mass concentration could exceed 500 μg m^{-3} and substantially reduced the levels of several traces gases including NOx and O_3 [*de Reus et al.*, 2005], would be an ideal field site to study the heterogeneous interaction of ambient fresh Saharan dust particles with N_2O_5. Field measurement of NO_3 and N_2O_5 should also be performed during the break out of Asian dust storms at sites along the dust transport routes, where dust particles undergo aging during transport [*Arimoto et al.*, 2004; *Mori et al.*, 2003]. An alternative way is to develop an experimental technique which can be used to directly measure the N_2O_5 reactivity on ambient particles [*Bertram et al.*, 2009a] and deploy it in field to measure the reactivity of N_2O_5 on ambient dust particles which have been aged to different extents.

7 References

Aldener, M., et al. (2006), Reactivity and loss mechanisms of NO_3 and N_2O_5 in a polluted marine environment: Results from in situ measurements during New England Air Quality Study 2002, *J. Geophys. Res.-Atmos.*, *111*(D23).

Aliwell, S. R., and R. L. Jones (1998), Measurements of tropospheric NO3 at midlatitude, *J. Geophys. Res.-Atmos.*, *103*(D5), 5719-5727.

Allan, B. J., J. M. C. Plane, H. Coe, and J. Shillito (2002), Observations of NO_3 concentration profiles in the troposphere, *J. Geophys. Res.-Atmos.*, *107*(D21).

Ammann, M., U. Poschl, and Y. Rudich (2003), Effects of reversible adsorption and Langmuir-Hinshelwood surface reactions on gas uptake by atmospheric particles, *Physical Chemistry Chemical Physics*, *5*(2), 351-356.

Ansmann, A., et al. (2003), Long-range transport of Saharan dust to northern Europe: The 11-16 October 2001 outbreak observed with EARLINET, *J. Geophys. Res.-Atmos.*, *108*(D24).

Anttila, T., A. Kiendler-Scharr, R. Tillmann, and T. F. Mentel (2006), On the reactive uptake of gaseous compounds by organic-coated aqueous aerosols: Theoretical analysis and application to the heterogeneous hydrolysis of N_2O_5, *J. Phys. Chem. A*, *110*(35), 10435-10443.

Archuleta, C. M., P. J. DeMott, and S. M. Kreidenweis (2005), Ice nucleation by surrogates for atmospheric mineral dust and mineral dust/sulfate particles at cirrus temperatures, *Atmos. Chem. Phys.*, *5*, 2617-2634.

Arimoto, R., X. Y. Zhang, B. J. Huebert, C. H. Kang, D. L. Savoie, J. M. Prospero, S. K. Sage, C. A. Schloesslin, H. M. Khaing, and S. N. Oh (2004), Chemical composition of atmospheric aerosols from Zhenbeitai, China, and Gosan, South Korea, during ACE-Asia, *J. Geophys. Res.-Atmos.*, *109*(D19).

Asaf, D., D. Pedersen, V. Matveev, M. Peleg, C. Kern, J. Zingler, U. Platt, and M. Luria (2009), Long-term measurement of NO_3 radicals at a semiarid urban site: 1. extreme

concentration events and their oxidation capacity, *Environ. Sci. Technol.*, *43*(24), 9117-9123.

Atkinson, R., D. L. Baulch, R. A. Cox, J. N. Crowley, R. F. Hampson, R. G. Hynes, M. E. Jenkin, M. J. Rossi, and J. Troe (2004), Evaluated kinetic and photochemical data for atmospheric chemistry: Volume I - gas phase reactions of Ox, HOx, NOx and SOx species, *Atmos. Chem. Phys.*, *4*, 1461-1738.

Atkinson, R., D. L. Baulch, R. A. Cox, J. N. Crowley, R. F. Hampson, R. G. Hynes, M. E. Jenkin, M. J. Rossi, and J. Troe (2006), Evaluated kinetic and photochemical data for atmospheric chemistry: Volume II - gas phase reactions of organic species, *Atmos. Chem. Phys.*, *6*, 3625-4055.

Avila, A., I. QueraltMitjans, and M. Alarcon (1997), Mineralogical composition of African dust delivered by red rains over northeastern Spain, *J. Geophys. Res.-Atmos.*, *102*(D18), 21977-21996.

Ayers, J. D., and W. R. Simpson (2006), Measurements of N_2O_5 near Fairbanks, Alaska, *J. Geophys. Res.-Atmos.*, *111*(D14).

Badger, C. L., P. T. Griffiths, I. George, J. P. D. Abbatt, and R. A. Cox (2006), Reactive uptake of N_2O_5 by aerosol particles containing mixtures of humic acid and ammonium sulfate, *J. Phys. Chem. A*, *110*(21), 6986-6994.

Balkanski, Y., M. Schulz, T. Claquin, and S. Guibert (2007), Reevaluation of Mineral aerosol radiative forcings suggests a better agreement with satellite and AERONET data, *Atmos. Chem. Phys.*, *7*(1), 81-95.

Bauer, S. E., Y. Balkanski, M. Schulz, D. A. Hauglustaine, and F. Dentener (2004), Global modeling of heterogeneous chemistry on mineral aerosol surfaces: Influence on tropospheric ozone chemistry and comparison to observations, J. Geophys. Res.-Atmos., 109(D2).

Behnke, W., C. George, V. Scheer, and C. Zetzsch (1997), Production and decay of $ClNO_2$, from the reaction of gaseous N_2O_5 with NaCl solution: Bulk and aerosol experiments, *J. Geophys. Res.-Atmos.*, *102*(D3), 3795-3804.

Bertram, T. H., and J. A. Thornton (2009), Toward a general parameterization of N_2O_5 reactivity on aqueous particles: the competing effects of particle liquid water, nitrate and chloride, *Atmos. Chem. Phys.*, *9*(21), 8351-8363.

Bertram, T. H., J. A. Thornton, and T. P. Riedel (2009a), An experimental technique for the direct measurement of N_2O_5 reactivity on ambient particles, *Atmos. Meas. Tech.*, *2*(1), 231-242.

Bertram, T. H., J. A. Thornton, T. P. Riedel, A. M. Middlebrook, R. Bahreini, T. S. Bates, P. K. Quinn, and D. J. Coffman (2009b), Direct observations of N_2O_5 reactivity on ambient aerosol particles, *Geophys. Res. Lett.*, *36*.

Bian, H. S., and C. S. Zender (2003), Mineral dust and global tropospheric chemistry: Relative roles of photolysis and heterogeneous uptake, J. Geophys. Res.-Atmos., 108(D21).

Bitter, M., S. M. Ball, I. M. Povey, and R. L. Jones (2005), A broadband cavity ringdown spectrometer for in-situ measurements of atmospheric trace gases, *Atmos. Chem. Phys.*, *5*(9), 2547-2560.

Bonn, B., and G. K. Moortgat (2002), New particle formation during alpha- and beta-pinene oxidation by O-3, OH and NO3, and the influence of water vapour: particle size distribution studies, *Atmos. Chem. Phys.*, *2*, 183-196.

Braman, R. S., T. J. Shelley, and W. A. McClenny (1982), Tungstic acid for pre-concentration and determination of gaseous and particulate ammonia and nitric-acid in ambient air, *Analytical Chemistry*, *54*(3), 358-364.

Brown, R. L. (1978), Tubular flow reactros with 1st-order kinetics, *Journal of Research of the National Bureau of Standards*, *83*(1), 1-8.

Brown, S. S., H. Stark, and A. R. Ravishankara (2003a), Applicability of the steady state approximation to the interpretation of atmospheric observations of NO_3 and N_2O_5, *J. Geophys. Res.-Atmos.*, *108*(D17).

Brown, S. S., H. Stark, S. J. Ciciora, R. J. McLaughlin, and A. R. Ravishankara (2002), Simultaneous in situ detection of atmospheric NO_3 and N_2O_5 via cavity ring-down spectroscopy, *Rev. Sci. Instrum.*, *73*(9), 3291-3301.

Brown, S. S., W. P. Dube, H. D. Osthoff, D. E. Wolfe, W. M. Angevine, and A. R. Ravishankara (2007a), High resolution vertical distributions of NO_3 and N_2O_5 through the nocturnal boundary layer, *Atmos. Chem. Phys.*, *7*, 139-149.

Brown, S. S., H. Stark, T. B. Ryerson, E. J. Williams, D. K. Nicks, M. Trainer, F. C. Fehsenfeld, and A. R. Ravishankara (2003b), Nitrogen oxides in the nocturnal boundary layer: Simultaneous in situ measurements of NO_3, N_2O_5, NO_2, NO, and O_3, *J. Geophys. Res.-Atmos.*, *108*(D9).

Brown, S. S., et al. (2006), Variability in nocturnal nitrogen oxide processing and its role in regional air quality, *Science*, *311*(5757), 67-70.

Brown, S. S., et al. (2009a), Reactive uptake coefficients for N_2O_5 determined from aircraft measurements during the Second Texas Air Quality Study: Comparison to current model parameterizations, *J. Geophys. Res.-Atmos.*, *114*.

Brown, S. S., et al. (2009b), Nocturnal isoprene oxidation over the Northeast United States in summer and its impact on reactive nitrogen partitioning and secondary organic aerosol, *Atmos. Chem. Phys.*, *9*(9), 3027-3042.

Brown, S. S., et al. (2007b), Vertical profiles in NO_3 and N_2O_5 measured from an aircraft: Results from the NOAA P-3 and surface platforms during the New England Air Quality Study 2004, *J. Geophys. Res.-Atmos.*, *112*(D22).

Carmichael, G. R., Y. Zhang, L. L. Chen, M. S. Hong, and H. Ueda (1996), Seasonal variation of aerosol composition at Cheju Island, Korea, *Atmos. Environ.*, *30*(13), 2407-2416.

Chernoff, D. I., and A. K. Bertram (2010), Effects of sulfate coatings on the ice nucleation properties of a biological ice nucleus and several typs of minerals, *J. Geophys. Res.-Atmos.*, *115*.

Chun, Y. S., K. O. Boo, J. Kim, S. U. Park, and M. Lee (2001), Synopsis, transport, and physical characteristics of Asian dust in Korea, *J. Geophys. Res.-Atmos.*, *106*(D16), 18461-18469.

Claquin, T., M. Schulz, and Y. J. Balkanski (1999), Modeling the mineralogy of atmospheric dust sources, *J. Geophys. Res.-Atmos.*, *104*(D18), 22243-22256.

Cosman, L. M., D. A. Knopf, and A. K. Bertram (2008), N_2O_5 reactive uptake on aqueous sulfuric acid solutions coated with branched and straight-chain insoluble organic surfactants, *J. Phys. Chem. A*, *112*(11), 2386-2396.

Crowley, J. N., G. Schuster, N. Pouvesle, U. Parchatka, H. Fischer, B. Bonn, H. Bingemer, and J. Lelieveld (2010a), Nocturnal nitrogen oxides at a rural mountain-site in south-western Germany, *Atmos. Chem. Phys.*, *10*(6), 2795-2812.

Crowley, J. N., M. Ammann, R. A. Cox, R. G. Hynes, M. E. Jenkin, A. Mellouki, M. J. Rossi, J. Troe, and T. J. Wallington (2010b), Evaluated kinetic and photochemical data for atmospheric chemistry: Volume V - heterogeneous reactions on solid substrates, *Atmos. Chem. Phys.*, *10*(18), 9059-9223.

Crowley, J. N., et al. (2011), Variable lifetimes and loss mechanisms for NO_3 and N_2O_5 during the DOMINO campaign: contrasts between marine, urban and continental air, *Atmos. Chem. Phys. Discuss.*, *11*, 17825-17877.

Curtis, A. R., and W. P. Sweetenham (1987), *Fascimile, AERE, Report R-12805*.

Cziczo, D. J., K. D. Froyd, S. J. Gallavardin, O. Moehler, S. Benz, H. Saathoff, and D. M. Murphy (2009), Deactivation of ice nuclei due to atmospherically relevant surface coatings, *Environ. Res. Lett.*, *4*(4).

Davidovits, P., J. H. Hu, D. R. Worsnop, M. S. Zahniser, and C. E. Kolb (1995), Entry of gas molecules into liquids, *Faraday Discuss.*, 65-81.

Davidovits, P., C. E. Kolb, L. R. Williams, J. T. Jayne, and D. R. Worsnop (2006), Mass accommodation and chemical reactions at gas-liquid interfaces, *Chem. Rev.*, *106*(4), 1323-1354.

Davidovits, P., J. T. Jayne, S. X. Duan, D. R. Worsnop, M. S. Zahniser, and C. E. Kolb (1991), Uptake of gas molecules by liquids-a model, *J. Phys. Chem.*, *95*(16), 6337-6340.

de Reus, M., H. Fischer, R. Sander, V. Gros, R. Kormann, G. Salisbury, R. Van Dingenen, J. Williams, M. Zollner, and J. Lelieveld (2005), Observations and model calculations of trace gas scavenging in a dense Saharan dust plume during MINATROC, *Atmos. Chem. Phys.*, *5*, 1787-1803.

DeMott, P. J., K. Sassen, M. R. Poellot, D. Baumgardner, D. C. Rogers, S. D. Brooks, A. J. Prenni, and S. M. Kreidenweis (2003), African dust aerosols as atmospheric ice nuclei, *Geophys. Res. Lett.*, *30*(14), 4.

Dentener, F. J., and P. J. Crutzen (1993), Reaction of N_2O_5 on Tropospheric Aerosols - Impact on the Global Distributions of NOx, O_3, and OH, *J. Geophys. Res.-Atmos.*, *98*(D4), 7149-7163.

Dentener, F. J., G. R. Carmichael, Y. Zhang, J. Lelieveld, and P. J. Crutzen (1996), Role of mineral aerosol as a reactive surface in the global troposphere, *J. Geophys. Res.-Atmos.*, *101*(D17), 22869-22889.

Diesch, J. M., F. Drewnick, S. L. von der Weiden-Reinmüller, M. Martinez-Harder, and S. Borrmann (2011), Variability of Aerosol, Trace Gas and Metrological Charasteristics associated with Continental, Urban, and Marine Air Masses in the Southwestern Mediterranean, edited.

Docherty, K. S., and P. J. Ziemann (2006), Reaction of oleic acid particles with NO_3 radicals: Products, mechanism, and implications for radical-initiated organic aerosol oxidation, *J. Phys. Chem. A*, *110*(10), 3567-3577.

Eastwood, M. L., S. Cremel, C. Gehrke, E. Girard, and A. K. Bertram (2008), Ice nucleation on mineral dust particles: Onset conditions, nucleation rates and contact angles, *J. Geophys. Res.-Atmos.*, *113*, 9.

Eastwood, M. L., S. Cremel, M. Wheeler, B. J. Murray, E. Girard, and A. K. Bertram (2009), Effects of sulfuric acid and ammonium sulfate coatings on the ice nucleation properties of kaolinite particles, *Geophys. Res. Lett.*, *36*.

Escorcia, E. N., S. J. Sjostedt, and J. P. D. Abbatt (1998), Kinetics of N2O5 Hydrolysis on Secondary Organic Aerosol and Mixed Ammonium Bisulfate-Secondary Organic Aerosol Particles, *J. Phys. Chem. A*, *114*(50), 13113-13121.

Escoreia, E. N., S. J. Sjostedt, and J. P. D. Abbatt (2010), Kinetics of N2O5 Hydrolysis on Secondary Organic Aerosol and Mixed Ammonium Bisulfate-Secondary Organic Aerosol Particles, *J. Phys. Chem. A*, *114*(50), 13113-13121.

Evans, M. J., and D. J. Jacob (2005), Impact of new laboratory studies of N_2O_5 hydrolysis on global model budgets of tropospheric nitrogen oxides, ozone, and OH, *Geophys. Res. Lett.*, *32*(9).

Fahey, D. W., C. S. Eubank, G. Hubler, and F. C. Fehsenfeld (1985), A Calibrated Source of N_2O_5, *Atmos. Environ.*, *19*(11), 1883-1890.

Fairlie, T. D., D. J. Jacob, and R. J. Park (2007), The impact of transpacific transport of mineral dust in the United States, *Atmos. Environ.*, *41*(6), 1251-1266.

Fairlie, T. D., D. J. Jacob, J. E. Dibb, B. Alexander, M. A. Avery, A. van Donkelaar, and L. Zhang (2010), Impact of mineral dust on nitrate, sulfate, and ozone in transpacific Asian pollution plumes, *Atmos. Chem. Phys.*, *10*(8), 3999-4012.

Falkovich, A. H., G. Schkolnik, E. Ganor, and Y. Rudich (2004), Adsorption of organic compounds pertinent to urban environments onto mineral dust particles, *J. Geophys. Res.-Atmos.*, *109*(D2).

Fenter, F. F., and M. J. Rossi (1997), Heterogeneous reaction of NO_3 with ice and sulfuric acid solutions: Upper limits for the uptake coefficients, *J. Phys. Chem. A*, *101*(22), 4110-4113.

Fenter, F. F., F. Caloz, and M. J. Rossi (1995), Experimental-Evidence for the Efficient Dry Deposition of Nitric-Acid on Calcite, *Atmos. Environ.*, *29*(22), 3365-3372.

Finlayson-Pitts, B. J. (2003), The tropospheric chemistry of sea salt: A molecular-level view of the chemistry of NaCl and NaBr, *Chem. Rev.*, *103*(12), 4801-4822.

Finlayson-Pitts, B. J., M. J. Ezell, and J. N. Pitts (1989), Formation of chemically active chlorine compounds by reactions of atmospheric NaCl particles with gaseous N_2O_5 and $ClONO_2$, *Nature*, *337*(6204), 241-244.

Folkers, M., T. F. Mentel, and A. Wahner (2003), Influence of an organic coating on the reactivity of aqueous aerosols probed by the heterogeneous hydrolysis of N2O5, *Geophys. Res. Lett.*, *30*(12).

Franze, T., M. G. Weller, R. Niessner, and U. Poschl (2005), Protein nitration by polluted air, *Environ. Sci. Technol.*, *39*(6), 1673-1678.

Frenzel, A., V. Scheer, R. Sikorski, C. George, W. Behnke, and C. Zetzsch (1998), Heterogeneous interconversion reactions of $BrNO_2$, $ClNO_2$, Br_2, and Cl_2, *J. Phys. Chem. A*, *102*(8), 1329-1337.

Fry, J. L., et al. (2011), SOA from limonene: role of NO3 in its generation and degradation, *Atmos. Chem. Phys.*, *11*(8), 3879-3894.

Fuchs, N. A., and A. G. Sutugin (1970), *Highly dispersed aerosols*, Ann Arbor Sci., Ann Arbor.

George, C., J. L. Ponche, P. Mirabel, W. Behnke, V. Scheer, and C. Zetzsch (1994), Study of the uptake of N_2O_5 by water and NaCl solutions, *J. Phys. Chem.*, *98*(35), 8780-8784.

George, I. J., and J. P. D. Abbatt (2010), Heterogeneous oxidation of atmospheric aerosol particles by gas-phase radicals, *Nat. Chem.*, *2*(9), 713-722.

Gershenzon, M. Y., S. IlIN, N. G. Fedotov, and Y. M. Gershenzon (1999), The mechenism of reative NO_3 uptake on dry NaX (X=Cl, Br), *J. Atmos. Chem.*, *34*, 119-135.

Geyer, A., B. Alicke, S. Konrad, T. Schmitz, J. Stutz, and U. Platt (2001), Chemistry and oxidation capacity of the nitrate radical in the continental boundary layer near Berlin, *J. Geophys. Res.-Atmos.*, *106*(D8), 8013-8025.

Ghosh, S. (1993), On the dissusibity of trace gases under strataspherici conditions, *J. Atmos. Chem.*, *17*(4), 391-397.

Ginoux, P., M. Chin, I. Tegen, J. M. Prospero, B. Holben, O. Dubovik, and S. J. Lin (2001), Sources and distributions of dust aerosols simulated with the GOCART model, *J. Geophys. Res.-Atmos.*, *106*(D17), 20255-20273.

Goodman, A. L., G. M. Underwood, and V. H. Grassian (2000), A laboratory study of the heterogeneous reaction of nitric acid on calcium carbonate particles, *J. Geophys. Res.-Atmos.*, *105*(D23), 29053-29064.

Griffiths, P. T., and R. A. Cox (2009), Temperature dependence of heterogeneous uptake of N_2O_5 by ammonium sulfate aerosol, *Atmos. Sci. Lett.*, *10*(3), 159-163.

Griffiths, P. T., C. L. Badger, R. A. Cox, M. Folkers, H. H. Henk, and T. F. Mentel (2009), Reactive Uptake of N_2O_5 by Aerosols Containing Dicarboxylic Acids. Effect of Particle Phase, Composition, and Nitrate Content, *J. Phys. Chem. A*, *113*(17), 5082-5090.

Grim, R. E. (1953), *Clay mineralogy*, McGraw-Hill Book Company, Inc, New York.

Gross, S., and A. K. Bertram (2008), Reactive uptake of NO_3, N_2O_5, NO_2, HNO_3, and O_3 on three types of polycyclic aromatic hydrocarbon surfaces, *J. Phys. Chem. A*, *112*(14), 3104-3113.

Gross, S., and A. K. Bertram (2009), Products and kinetics of the reactions of an alkane monolayer and a terminal alkene monolayer with NO3 radicals, *J. Geophys. Res.-Atmos.*, *114*, 14.

Gross, S., R. Iannone, S. Xiao, and A. K. Bertram (2009), Reactive uptake studies of NO_3 and N_2O_5 on alkenoic acid, alkanoate, and polyalcohol substrates to probe nighttime aerosol chemistry, *Physical Chemistry Chemical Physics*, *11*, 7792-7803.

Gustafsson, R. J., A. Orlov, C. L. Badger, P. T. Griffiths, R. A. Cox, and R. M. Lambert (2005), A comprehensive evaluation of water uptake on atmospherically relevant mineral surfaces: DRIFT spectroscopy, thermogravimetric analysis and aerosol growth measurements, *Atmos. Chem. Phys.*, *5*, 3415-3421.

Hallquist, M., D. J. Stewart, J. Baker, and R. A. Cox (2000), Hydrolysis of N_2O_5 on submicron sulfuric acid aerosols, *J. Phys. Chem. A*, *104*(17), 3984-3990.

Hallquist, M., D. J. Stewart, S. K. Stephenson, and R. A. Cox (2003), Hydrolysis of N_2O_5 on sub-micron sulfate aerosols, *Physical Chemistry Chemical Physics*, *5*(16), 3453-3463.

Hanisch, F., and J. N. Crowley (2001a), The heterogeneous reactivity of gaseous nitric acid on authentic mineral dust samples, and on individual mineral and clay mineral components, *Physical Chemistry Chemical Physics*, *3*(12), 2474-2482.

Hanisch, F., and J. N. Crowley (2001b), Heterogeneous reactivity of gaseous nitric acid on Al_2O_3, $CaCO_3$, and atmospheric dust samples: A Knudsen cell study, *J. Phys. Chem. A*, *105*(13), 3096-3106.

Hanisch, F., and J. N. Crowley (2003), Ozone decomposition on Saharan dust: an experimental investigation, *Atmos. Chem. Phys.*, *3*, 119-130.

Hanson, D. R. (1997), Surface-specific reactions on liquids, *J. Phys. Chem. B*, *101*(25), 4998-5001.

Heintz, F., U. Platt, H. Flentje, and R. Dubois (1996), Long-term observation of nitrate radicals at the tor station, Kap Arkona (Rugen), *J. Geophys. Res.-Atmos.*, *101*(D17), 22891-22910.

Hinds, W. C. (1996), *Aerosol techniques: properties, behavior, and measurement if airborne particles*, John Wiley& Sons. Inc., New York.

Hu, J. H., and J. P. D. Abbatt (1997), Reaction probabilities for N_2O_5 hydrolysis on sulfuric acid and ammonium sulfate aerosols at room temperature, *J. Phys. Chem. A*, *101*(5), 871-878.

Iannone, R., S. Xiao, and A. K. Bertram (2011), Potentially important nighttime heterogeneous chemistry: NO3 with aldehydes and N2O5 with alcohols, *Physical Chemistry Chemical Physics*, *13*(21), 10214-10223.

Imamura, T., Y. Rudich, R. K. Talukdar, R. W. Fox, and A. R. Ravishankara (1997), Uptake of NO_3 on water solutions: Rate coefficients for reactions of NO_3 with cloud water constituents, *J. Phys. Chem. A*, *101*(12), 2316-2322.

IPCC (1995), *Climate change 1994: Radiative forcing of climate change and an evaluation of the IPCC IS92 emission scenarios*, Cambridge University Press, Cambridge, UK.

IUPAC (2009), Subcommitte for gas kinetic data evaluation: (Ammann, M., Atkinson, R., Cox, R. A., Crowley, J. N., Hynes, R. G., Jenkin, M. E., Mellouki, W., Rossi, M. J., Troe, J., and Wallington, T. J.) Evaluated kinetic data: http://www.iupac-kinetic.ch.cam.ac.uk/, edited.

Jeong, G. Y. (2008), Bulk and single-particle mineralogy of Asian dust and a comparison with its source soils, *J. Geophys. Res.-Atmos.*, *113*(D2), 16.

Jickells, T. D., et al. (2005), Global iron connections between desert dust, ocean biogeochemistry, and climate, *Science*, *308*(5718), 67-71.

Johnston, H. S., H. F. Davis, and Y. T. Lee (1996), NO3 photolysis product channels: Quantum yields from observed energy thresholds, *J. Phys. Chem.*, *100*(12), 4713-4723.

Kane, S. M., F. Caloz, and M. T. Leu (2001), Heterogeneous uptake of gaseous N_2O_5 by $(NH_4)_2SO_4$, NH_4HSO_4, and H_2SO_4 aerosols, *J. Phys. Chem. A*, *105*(26), 6465-6470.

Karagulian, F., and M. J. Rossi (2005), The heterogeneous chemical kinetics of NO_3 on atmospheric mineral dust surrogates, *Physical Chemistry Chemical Physics*, *7*(17), 3150-3162.

Karagulian, F., and M. J. Rossi (2007), Heterogeneous chemistry of the NO_3 free radical and N_2O_5 on decane flame soot at ambient temperature: Reaction products and kinetics, *J. Phys. Chem. A*, *111*(10), 1914-1926.

Karagulian, F., C. Santschi, and M. J. Rossi (2006), The heterogeneous chemical kinetics of N_2O_5 on $CaCO_3$ and other atmospheric mineral dust surrogates, *Atmos. Chem. Phys.*, *6*, 1373-1388.

Kelly, J. T., C. C. Chuang, and A. S. Wexler (2007), Influence of dust composition on cloud droplet formation, *Atmos. Environ.*, *41*(14), 2904-2916.

Kercher, J. P., T. P. Riedel, and J. A. Thornton (2009), Chlorine activation by N_2O_5: simultaneous, in situ detection of $ClNO_2$ and N_2O_5 by chemical ionization mass spectrometry, *Atmos. Meas. Tech.*, *2*(1), 193-204.

Keyser, L. F. (1984), High-Pressure Flow Kinetics - a Study of the OH + HCl Reaction from 2 to 100 Torr, *J. Phys. Chem.*, *88*(20), 4750-4758.

King, M. D., E. M. Dick, and W. R. Simpson (2000), A new method for the atmospheric detection of the nitrate radical (NO_3), *Atmos. Environ.*, *34*(5), 685-688.

Klein, H., et al. (2010), Saharan dust and ice nuclei over Central Europe, *Atmos. Chem. Phys.*, *10*(21), 10211-10221.

Knipping, E. M., and D. Dabdub (2003), Impact of chlorine emissions from sea-salt aerosol on coastal urban ozone, *Environ. Sci. Technol.*, *37*(2), 275-284.

Knopf, D. A., and T. Koop (2006), Heterogeneous nucleation of ice on surrogates of mineral dust, *J. Geophys. Res.-Atmos.*, *111*(D12), 10.

Knopf, D. A., J. Mak, S. Gross, and A. K. Bertram (2006), Does atmospheric processing of saturated hydrocarbon surfaces by NO_3 lead to volatilization?, *Geophys. Res. Lett.*, *33*(17), 5.

Koehler, K. A., S. M. Kreidenweis, P. J. DeMott, M. D. Petters, A. J. Prenni, and C. M. Carrico (2009), Hygroscopicity and cloud droplet activation of mineral dust aerosol, *Geophys. Res. Lett.*, *36*, 5.

Kolb, C. E., P. Davidovits, J. T. Jayne, Q. Shi, and D. R. Worsnop (2002), Kinetics of trace gas uptake by liquid surfaces, *Prog. React. Kinet. Mech.*, *27*(1), 1-46.

Kolb, C. E., et al. (1995), Laboratory studies of atmospheric heterogeneous chemistry, in *Progress and problems in atmospheric chemistry*, edited by J. R. Barker, World Scientific, Singapore.

Krueger, B. J., V. H. Grassian, A. Laskin, and J. P. Cowin (2003), The transformation of solid atmospheric particles into liquid droplets through heterogeneous chemistry: Laboratory insights into the processing of calcium containing mineral dust aerosol in the troposphere, *Geophys. Res. Lett.*, *30*(3).

Laskin, A., M. J. Iedema, A. Ichkovich, E. R. Graber, I. Taraniuk, and Y. Rudich (2005), Direct observation of completely processed calcium carbonate dust particles, *Faraday Discuss.*, *130*, 453-468.

Li, L., Z. M. Chen, Y. H. Zhang, T. Zhu, J. L. Li, and J. Ding (2006), Kinetics and mechanism of heterogeneous oxidation of sulfur dioxide by ozone on surface of calcium carbonate, *Atmos. Chem. Phys.*, *6*, 2453-2464.

Li, X., H. Maring, D. Savoie, K. Voss, and J. M. Prospero (1996), Dominance of mineral dust in aerosol light-scattering in the North Atlantic trade winds, *Nature*, *380*(6573), 416-419.

Liu, Y., E. R. Gibson, J. P. Cain, H. Wang, V. H. Grassian, and A. Laskin (2008), Kinetics of heterogeneous reaction of $CaCO_3$ particles with gaseous HNO_3 over a wide range of humidity, *J. Phys. Chem. A*, *112*(7), 1561-1571.

Liu, Y. J., T. Zhu, D. F. Zhao, and Z. F. Zhang (2008), Investigation of the hygroscopic properties of $Ca(NO_3)_2$ and internally mixed $Ca(NO_3)_2/CaCO_3$ particles by micro-Raman spectrometry, *Atmos. Chem. Phys.*, *8*(23), 7205-7215.

Mahowald, N. M., A. R. Baker, G. Bergametti, N. Brooks, R. A. Duce, T. D. Jickells, N. Kubilay, J. M. Prospero, and I. Tegen (2005), Atmospheric global dust cycle and iron inputs to the ocean, *Glob. Biogeochem. Cycle*, *19*(4), doi:10.1029/2004GB002402.

Martin, J. H. (1990), Glacial-interglacial CO/sub 2/ change: the iron hypothesis, *Paleoceanography*, *5*(1), 1-13.

Martinez, M., D. Perner, E. M. Hackenthal, S. Kulzer, and L. Schutz (2000), NO_3 at Helgoland during the NORDEX campaign in October 1996, *J. Geophys. Res.-Atmos.*, *105*(D18), 22685-22695.

Matsuki, A., et al. (2005), Morphological and chemical modification of mineral dust: Observational insight into the heterogeneous uptake of acidic gases, Geophys. Res. Lett., 32(22).

Matsumoto, J., N. Kosugi, H. Imai, and Y. Kajii (2005), Development of a measurement system for nitrate radical and dinitrogen pentoxide using a thermal conversion/laser-induced fluorescence technique, *Rev. Sci. Instrum.*, *76*(6).

McNaughton, C. S., et al. (2009), Observations of heterogeneous reactions between Asian pollution and mineral dust over the Eastern North Pacific during INTEX-B, *Atmos. Chem. Phys.*, *9*(21), 8283-8308.

McNeill, V. F., J. Patterson, G. M. Wolfe, and J. A. Thornton (2006), The effect of varying levels of surfactant on the reactive uptake of N_2O_5 to aqueous aerosol, *Atmos. Chem. Phys.*, *6*, 1635-1644.

Mentel, T. F., M. Sohn, and A. Wahner (1999), Nitrate effect in the heterogeneous hydrolysis of dinitrogen pentoxide on aqueous aerosols, *Physical Chemistry Chemical Physics*, *1*(24), 5451-5457.

Mihelcic, D., D. Klemp, P. Musgen, H. W. Patz, and A. Volzthomas (1993), Simultaneous Measurements of Peroxy and Nitrate Radicals at Schauinsland, *J. Atmos. Chem.*, *16*(4), 313-335.

Mogili, P. K., P. D. Kleiber, M. A. Young, and V. H. Grassian (2006), N_2O_5 hydrolysis on the components of mineral dust and sea salt aerosol: Comparison study in an environmental aerosol reaction chamber, *Atmos. Environ.*, *40*(38), 7401-7408.

Moise, T., and Y. Rudich (2002), Reactive uptake of ozone by aerosol-associated unsaturated fatty acids: Kinetics, mechanism, and products, *J. Phys. Chem. A*, *106*(27), 6469-6476.

Moise, T., R. K. Talukdar, G. J. Frost, R. W. Fox, and Y. Rudich (2002), Reactive uptake of NO_3 by liquid and frozen organics, *J. Geophys. Res.-Atmos.*, *107*(D1-D2).

Mori, I., M. Nishikawa, T. Tanimura, and H. Quan (2003), Change in size distribution and chemical composition of kosa (Asian dust) aerosol during long-range transport, *Atmos. Environ.*, *37*(30), 4253-4263.

Mozurkewich, M., and J. G. Calvert (1988), Reaction Probability of N_2O_5 on Aqueous Aerosols, *J. Geophys. Res.-Atmos.*, *93*(D12), 15889-15896.

Navea, J. G., H. H. Chen, M. Huang, G. R. Carmichael, and V. H. Grassian (2010), A comparative evaluation of water uptake on several mineral dust sources, *Environ. Chem.*, *7*, 162-170.

Ndour, M., M. Nicolas, B. D'Anna, O. Ka, and C. George (2009), Photoreactivity of NO_2 on mineral dusts originating from different locations of the Sahara desert, *Physical Chemistry Chemical Physics*, *11*(9), 1312-1319.

Ndour, M., B. D'Anna, C. George, O. Ka, Y. Balkanski, J. Kleffmann, K. Stemmler, and M. Ammann (2008), Photoenhanced uptake of NO_2 on mineral dust: Laboratory experiments and model simulations, *Geophys. Res. Lett.*, *35*(5).

Ng, N. L., et al. (2008), Secondary organic aerosol (SOA) formation from reaction of isoprene with nitrate radicals (NO3), *Atmos. Chem. Phys.*, *8*(14), 4117-4140.

Niedermeier, D., et al. (2010), Heterogeneous freezing of droplets with immersed mineral dust particles – measurements and parameterization, *Atmos. Chem. Phys.*, *10*(8), 3601-3614.

Okeefe, A., and D. A. G. Deacon (1988), Cavity Ring-Down Optical Spectrometer for Absorption-Measurements Using Pulsed Laser Sources, *Rev. Sci. Instrum., 59*(12), 2544-2551.

Orlando, J. J., G. S. Tyndall, G. K. Moortgat, and J. G. Calvert (1993), QUANTUM YIELDS FOR NO3 PHOTOLYSIS BETWEEN 570 AND 635 NM, *J. Phys. Chem., 97*(42), 10996-11000.

Osthoff, H. D., et al. (2006), Measurement of atmospheric NO_2 by pulsed cavity ring-down spectroscopy, *J. Geophys. Res.-Atmos., 111*(D12).

Osthoff, H. D., et al. (2008), High levels of nitryl chloride in the polluted subtropical marine boundary layer, *Nature Geoscience*, *1*(5), 324-328.

Osthoff, H. D., et al. (2009), Regional variation of the dimethyl sulfide oxidation mechanism in the summertime marine boundary layer in the Gulf of Maine, *J. Geophys. Res.-Atmos., 114*, 13.

Pagels, J., A. Wierbicka, E. Nilsson, C. Isaxon, A. Dahl, A. Gudmundsson, E. Swietlicki, and M. Bohgard (2009), Chemical composition and mass emission factors of candle smoke particles, *J. Aerosol. Sci., 40*, 193-208.

Park, S. C., D. K. Burden, and G. M. Nathanson (2007), The inhibition of N_2O_5 hydrolysis in sulfuric acid by 1-butanol and 1-hexanol surfactant coatings, *J. Phys. Chem. A, 111*(15), 2921-2929.

Perring, A. E., A. Wisthaler, M. Graus, P. J. Wooldridge, A. L. Lockwood, L. H. Mielke, P. B. Shepson, A. Hansel, and R. C. Cohen (2009), A product study of the isoprene+NO3 reaction, *Atmos. Chem. Phys., 9*(14), 4945-4956.

Platt, U., D. Perner, A. M. Winer, G. W. Harris, and J. N. Pitts (1980), Detection of NO_3 in the Polluted Troposphere by Differential Optical-Absorption, *Geophys. Res. Lett., 7*(1), 89-92.

Poschl, U., Y. Rudich, and M. Ammann (2007), Kinetic model framework for aerosol and cloud surface chemistry and gas-phase interaction-Part 1: General equation, parameters, and terminology, *Atmos. Chem. Phys., 7*, 5989-6023.

Pradhan, M., G. Kyriakou, A. T. Archibald, A. C. Papageorgiou, M. Kalberer, and R. M. Lambert (2010a), Heterogeneous uptake of gaseous hydrogen peroxide by Gobi and Saharan dust aerosols: a potential missing sink for H2O2 in the troposphere, *Atmos. Chem. Phys.*, *10*(15), 7127-7136.

Pradhan, M., M. Kalberer, P. T. Griffiths, C. F. Braban, F. D. Pope, R. A. Cox, and R. M. Lambert (2010b), Uptake of Gaseous Hydrogen Peroxide by Submicrometer Titanium Dioxide Aerosol as a Function of Relative Humidity, *Environ. Sci. Technol.*, *44*(4), 1360-1365.

Prince, A. P., V. H. Grassian, P. Kleiber, and M. A. Young (2007), Heterogeneous conversion of calcite aerosol by nitric acid, *Physical Chemistry Chemical Physics*, *9*(5), 622-634.

Prospero, J. M. (1979), Mineral and sea salt aerosol concentrations in various ocean regions, *Journal of Geophysical Research-Oceans and Atmospheres*, *84*(NC2), 725-731.

Prospero, J. M. (1999), Long-range transport of mineral dust in the global atmosphere: Impact of African dust on the environment of the southeastern United States, *Proc. Natl. Acad. Sci. U. S. A.*, *96*(7), 3396-3403.

Prospero, J. M., and P. J. Lamb (2003), African droughts and dust transport to the Caribbean: Climate change implications, *Science*, *302*(5647), 1024-1027.

Querol, X., et al. (2009), African dust contributions to mean ambient PM10 mass-levels across the Mediterranean Basin, *Atmos. Environ.*, *43*(28), 4266-4277.

Reid, R. C., J. M. Prausnitz, and B. E. Poling (1987), *The Properties of Gases and Liquids*, McGraw-Hill, Inc. , New York.

Roberts, J. M., H. D. Osthoff, S. S. Brown, and A. R. Ravishankara (2008), N_2O_5 oxidizes chloride to Cl_2 in acidic atmospheric aerosol, *Science*, *321*(5892), 1059-1059.

Roberts, J. M., H. D. Osthoff, S. S. Brown, A. R. Ravishankara, D. Coffman, P. Quinn, and T. Bates (2009), Laboratory studies of products of N2O5 uptake on Cl- containing substrates, *Geophys. Res. Lett.*, *36*.

Rudich, Y., R. K. Talukdar, and A. R. Ravishankara (1996a), Reactive uptake of NO_3 on pure water and ionic solutions, *J. Geophys. Res.-Atmos.*, *101*(D15), 21023-21031.

Rudich, Y., R. K. Talukdar, T. Imamura, R. W. Fox, and A. R. Ravishankara (1996b), Uptake of NO_3 on KI solutions: Rate coefficient for the NO_3+I^- reaction and gas-phase diffusion coefficients for NO_3, *Chem. Phys. Lett.*, *261*(4-5), 467-473.

Saathoff, H., K. H. Naumann, N. Riemer, S. Kamm, O. Mohler, U. Schurath, H. Vogel, and B. Vogel (2001), The loss of NO_2, HNO_3, NO_3/N_2O_5, and $HO_2/HOONO_2$ on soot aerosol: A chamber and modeling study, *Geophys. Res. Lett.*, *28*(10), 1957-1960.

Salam, A., U. Lohmann, B. Crenna, G. Lesins, P. Klages, D. Rogers, R. Irani, A. MacGillivray, and M. Coffin (2006), Ice nucleation studies of mineral dust particles with a new continuous flow diffusion chamber, *Aerosol Sci. Technol.*, *40*(2), 134-143.

Sander, S. P., et al. (2006), Chemical Kinetics and Photochemical Data for Use in Atmospheric Studies. JPL Publications 06-2*Rep.*, Jet Propulsion Lab., Pasadena, CA.

Sassen, K. (2002), Indirect climate forcing over the western US from Asian dust storms, *Geophys. Res. Lett.*, *29*(10), 4.

Sassine, M., L. Burel, B. D'Anna, and C. George (2010), Kinetics of the tropospheric formaldehyde loss onto mineral dust and urban surfaces, *Atmos. Environ.*, *44*(40), 5468-5475.

Schauer, C., R. Niessner, and U. Poschl (2004), Analysis of nitrated polycyclic aromatic hydrocarbons by liquid chromatography with fluorescence and mass spectrometry detection: air particulate matter, soot, and reaction product studies, *Anal. Bioanal. Chem.*, *378*(3), 725-736.

Schuster, G., I. Labazan, and J. N. Crowley (2009), A cavity ring down/cavity enhanced absorption device for measurement of ambient NO_3 and N_2O_5, *Atmos. Meas. Tech.*, *2*(1), 1-13.

Schutze, M., and H. Herrmann (2005), Uptake of the NO_3 radical on aqueous surfaces, *J. Atmos. Chem.*, *52*(1), 1-18.

Schweitzer, F., P. Mirabel, and C. George (1998), Multiphase chemistry of N_2O_5, $ClNO_2$, and $BrNO_2$, *J. Phys. Chem. A*, *102*(22), 3942-3952.

Seinfeld, J. H., and S. N. Pandis (1997), *Atmospheric Chemistry and Physics: From air pollution to climate change*, Wiley Interscience, New York.

Seisel, S., C. Borensen, R. Vogt, and R. Zellner (2005), Kinetics and mechanism of the uptake of N_2O_5 on mineral dust at 298 K, *Atmos. Chem. Phys.*, *5*, 3423-3432.

Seisel, S., F. Caloz, F. F. Fenter, H. van den Bergh, and M. J. Rossi (1997), The heterogeneous reaction of NO_3 with NaCl and KBr: A nonphotolytic source of halogen atoms, *Geophys. Res. Lett.*, *24*(22), 2757-2760.

Shi, Q., P. Davidovits, J. T. Jayne, D. R. Worsnop, and C. E. Kolb (1999), Uptake of gas-phase ammonia. 1. Uptake by aqueous surfaces as a function of pH, *J. Phys. Chem. A*, *103*(44), 8812-8823.

Shi, Z., D. Zhang, M. Hayashi, H. Ogata, H. Ji, and W. Fujiie (2008), Influences of sulfate and nitrate on the hygroscopic behaviour of coarse dust particles, *Atmos. Environ.*, *42*(4), 822-827.

Shimizu, A., N. Sugimoto, I. Matsui, K. Arao, I. Uno, T. Murayama, N. Kagawa, K. Aoki, A. Uchiyama, and A. Yamazaki (2004), Continuous observations of Asian dust and other aerosols by polarization lidars in China and Japan during ACE-Asia, *J. Geophys. Res.-Atmos.*, *109*(D19).

Shon, Z. H., K. H. Kim, K. N. Bower, G. Lee, and J. Kim (2004), Assessment of the photochemistry of OH and NO_3 on Jeju Island during the Asian-dust-storm period in the spring of 2001, Chemosphere, 55(8), 1127-1142.

Simpson, W. R. (2003), Continuous wave cavity ring-down spectroscopy applied to in situ detection of dinitrogen pentoxide (N_2O_5), *Rev. Sci. Instrum.*, *74*(7), 3442-3452.

Slusher, D. L., L. G. Huey, D. J. Tanner, F. M. Flocke, and J. M. Roberts (2004), A thermal dissociation-chemical ionization mass spectrometry (TD-CIMS) technique for the simultaneous measurement of peroxyacyl nitrates and dinitrogen pentoxide, *J. Geophys. Res.-Atmos.*, *109*(D19).

Song, C. H., C. M. Kim, Y. J. Lee, G. R. Carmichael, B. K. Lee, and D. S. Lee (2007), An evaluation of reaction probabilities of sulfate and nitrate precursors onto East Asian dust particles, *J. Geophys. Res.-Atmos.*, *112*(D18).

Stewart, D. J., P. T. Griffiths, and R. A. Cox (2004), Reactive uptake coefficients for heterogeneous reaction of N_2O_5 with submicron aerosols of NaCl and natural sea salt, *Atmos. Chem. Phys.*, *4*, 1381-1388.

Stutz, J., B. Alicke, R. Ackermann, A. Geyer, A. White, and E. Williams (2004), Vertical profiles of NO_3, N_2O_5, O_3, and NOx in the nocturnal boundary layer: 1. Observations during the Texas Air Quality Study 2000 (vol 109, art no D12306, 2004), *J. Geophys. Res.-Atmos.*, *109*(D16).

Sullivan, R. C., S. A. Guazzotti, D. A. Sodeman, and K. A. Prather (2007), Direct observations of the atmospheric processing of Asian mineral dust, *Atmos. Chem. Phys.*, *7*, 1213-1236.

Sullivan, R. C., M. J. K. Moore, M. D. Petters, S. M. Kreidenweis, G. C. Roberts, and K. A. Prather (2009a), Effect of chemical mixing state on the hygroscopicity and cloud nucleation properties of calcium mineral dust particles, *Atmos. Chem. Phys.*, *9*(10), 3303-3316.

Sullivan, R. C., M. J. K. Moore, M. D. Petters, S. M. Kreidenweis, G. C. Roberts, and K. A. Prather (2009b), Timescale for hygroscopic conversion of calcite mineral particles through heterogeneous reaction with nitric acid, *Physical Chemistry Chemical Physics*, *11*(36), 7826-7837.

Sullivan, R. C., L. Minambres, P. J. DeMott, A. J. Prenni, C. M. Carrico, E. J. T. Levin, and S. M. Kreidenweis (2010a), Chemical processing does not always impair heterogeneous ice nucleation of mineral dust particles, *Geophys. Res. Lett.*, *37*.

Sullivan, R. C., et al. (2010b), Irreversible loss of ice nucleation active sites in mineral dust particles caused by sulphuric acid condensation, *Atmos. Chem. Phys.*, *10*(23), 11471-11487.

Tang, Y., et al. (2004), Impacts of dust on regional tropospheric chemistry during the ACE-Asia experiment: a model study with observations, *J. Geophys. Res.*, *109*(D19), 21 pp.-21 pp.

Tegen, I., and I. Fung (1994), Modeling of Mineral Dust in the Atmosphere - Sources, Transport, and Optical-Thickness, *J. Geophys. Res.-Atmos.*, *99*(D11), 22897-22914.

Textor, C., et al. (2006), Analysis and quantification of the diversities of aerosol life cycles within AeroCom, *Atmos. Chem. Phys.*, *6*(7), 1777-1813.

Thomas, K., A. Volz-Thomas, D. Mihelcic, H. G. J. Smit, and D. Kley (1998), On the exchange of NO_3 radicals with aqueous solutions: Solubility and sticking coefficient, *J. Atmos. Chem.*, *29*(1), 17-43.

Thornton, J. A., and J. P. D. Abbatt (2005), N_2O_5 reaction on submicron sea salt aerosol: Kinetics, products, and the effect of surface active organics, *J. Phys. Chem. A*, *109*(44), 10004-10012.

Thornton, J. A., C. F. Braban, and J. P. D. Abbatt (2003), N_2O_5 hydrolysis on sub-micron organic aerosols: the effect of relative humidity, particle phase, and particle size, *Physical Chemistry Chemical Physics*, *5*(20), 4593-4603.

Thornton, J. A., et al. (2010), A large atomic chlorine source inferred from mid-continental reactive nitrogen chemistry, *Nature*, *464*, 271-174.

Twohy, C. H., et al. (2009), Saharan dust particles nucleate droplets in eastern Atlantic clouds, *Geophys. Res. Lett.*, *36*, 6.

Underwood, G. M., P. Li, C. R. Usher, and V. H. Grassian (2000), Determining accurate kinetic parameters of potentially important heterogeneous atmospheric reactions on solid particle surfaces with a Knudsen cell reactor, *J. Phys. Chem. A*, *104*(4), 819-829.

Underwood, G. M., P. Li, H. Al-Abadleh, and V. H. Grassian (2001), A Knudsen cell study of the heterogeneous reactivity of nitric acid on oxide and mineral dust particles, *J. Phys. Chem. A*, *105*(27), 6609-6620.

Usher, C. R., H. Al-Hosney, S. Carlos-Cuellar, and V. H. Grassian (2002), A laboratory study of the heterogeneous uptake and oxidation of sulfur dioxide on mineral dust particles, *J. Geophys. Res.-Atmos.*, *107*(D23).

Vlasenko, A., T. Huthwelker, H. W. GÃ¤ggeler, and M. Ammann (2009), Kinetics of the heterogeneous reaction of nitric acid with mineral dust particles: an aerosol flow tube study, *Physical Chemistry Chemical Physics*, *11*, 7921-7930.

Vlasenko, A., S. Sjogren, E. Weingartner, H. W. Gaggeler, and M. Ammann (2005), Generation of submicron Arizona test dust aerosol: Chemical and hygroscopic properties, *Aerosol Sci. Technol.*, *39*(5), 452-460.

Vlasenko, A., S. Sjogren, E. Weingartner, K. Stemmler, H. W. Gaggeler, and M. Ammann (2006), Effect of humidity on nitric acid uptake to mineral dust aerosol particles, *Atmos. Chem. Phys.*, *6*, 2147-2160.

von Friedeburg, C., T. Wagner, A. Geyer, N. Kaiser, B. Vogel, H. Vogel, and U. Platt (2002), Derivation of tropospheric NO_3 profiles using off-axis differential optical absorption spectroscopy measurements during sunrise and comparison with simulations, *J. Geophys. Res.-Atmos.*, *107*(D13).

Vrekoussis, M., E. Liakakou, N. Mihalopoulos, M. Kanakidou, P. J. Crutzen, and J. Lelieveld (2006), Formation of HNO_3 and NO_3^- in the anthropogenically-influenced eastern Mediterranean marine boundary layer, *Geophys. Res. Lett.*, *33*(5).

Wagner, C., G. Schuster, and J. N. Crowley (2009), An aerosol flow tube study of the interaction of N_2O_5 with calcite, Arizona dust and quartz, *Atmos. Environ.*, *43*, 5001-5008.

Wagner, C., F. Hanisch, N. Holmes, H. de Coninck, G. Schuster, and J. N. Crowley (2008), The interaction of N_2O_5 with mineral dust: aerosol flow tube and Knudsen reactor studies, *Atmos. Chem. Phys.*, *8*(1), 91-109.

Wahner, A., T. F. Mentel, M. Sohn, and J. Stier (1998), Heterogeneous reaction of N_2O_5 on sodium nitrate aerosol, *J. Geophys. Res.-Atmos.*, *103*(D23), 31103-31112.

Wang, G. H., K. Kawamura, and M. Lee (2009), Comparison of organic compositions in dust storm and normal aerosol samples collected at Gosan, Jeju Island, during spring 2005, *Atmos. Environ.*, *43*(2), 219-227.

Warneke, C., et al. (2004), Comparison of daytime and nighttime oxidation of biogenic and anthropogenic VOCs along the New England coast in summer during New England Air Quality Study 2002, *J. Geophys. Res.-Atmos.*, *109*(D10).

Williams, J., et al. (2011), The summertime Boreal forest field measurement intensive (HUMPPA-COPEC-2010): an overview of meteorological and chemical influences, *Atmos. Chem. Phys. Discuss.*, *11*(5), 15921-15973.

Wood, E. C., T. H. Bertram, P. J. Wooldridge, and R. C. Cohen (2005), Measurements of N_2O_5, NO_2, and O_3 east of the San Francisco Bay, *Atmos. Chem. Phys.*, *5*, 483-491.

Wood, E. C., P. J. Wooldridge, J. H. Freese, T. Albrecht, and R. C. Cohen (2003), Prototype for in situ detection of atmospheric NO_3 and N_2O_5 via laser-induced fluorescence, *Environ. Sci. Technol.*, *37*(24), 5732-5738.

Yokelson, R. J., J. B. Burkholder, R. W. Fox, R. K. Talukdar, and A. R. Ravishankara (1994), Temperature-Dependence of the NO3 Absorption-Spectrum, *J. Phys. Chem.*, *98*(50), 13144-13150.

Zelenov, V. V., E. V. Aparina, S. V. Ivashin, and Y. M. Gershenson (2008), Steady-state uptake of NO_3 on NaBr/NaCl, NaI/NaCl, $MgCl_2$ 6H(2)O/NaCl, MgBr2 center dot 6H(2)O/NaCl binary salt coatings, *Russian Journal of Physical Chemistry B*, *2*(3), 408-417.

Zhang, Y., Y. Sunwoo, V. Kotamarthi, and G. R. Carmichael (1994), Photochemical Oxidant Processes in the Presence of Dust - an Evaluation of the Impact of Dust on Particulate Nitrate and Ozone Formation, *Journal of Applied Meteorology*, *33*(7), 813-824.

Zhao, Q., et al. (2010), Dust storms come to Central and Southwestern China, too: implications from a major dust event in Chongqing, *Atmos. Chem. Phys.*, *10*(6), 2615-2630.

Zhu, S., T. Butler, R. Sander, J. Ma, and M. G. Lawrence (2009), Impact of dust on tropospheric photochemistry over polluted regions: a case study of the Beijing megacity, *Atmos. Chem. Phys. Discuss.*, *9*(5), 20145-20194.

Zimmermann, F., S. Weinbruch, L. Schutz, H. Hofmann, M. Ebert, K. Kandler, and A. Worringen (2008), Ice nucleation properties of the most abundant mineral dust phases, *J. Geophys. Res.-Atmos.*, *113*, 11.

Appendices

A1. Uptake of HNO_3(g) on Saharan dust

There have been many studies on the heterogeneous uptake of HNO_3(g) on mineral dust particles, using surface detection techniques to measure the change of compositions of particles [*Goodman et al.*, 2000; *Y Liu et al.*, 2008], or measuring the decay of HNO_3(g) after being exposed to dust surface [*Fenter et al.*, 1995; *Hanisch and Crowley*, 2001a; b]. Bulk dust samples were used in most of the studies, making it difficult to estimate the surface area available to the heterogeneous uptake, and the reported uptake coefficients vary by about four orders of magnitude [*IUPAC*, 2009]. The uptake coefficients measured by using an aerosol flow tube [*Vlasenko et al.*, 2009; *Vlasenko et al.*, 2006] is currently recommended with reservations by IUPAC Subcommittee for Gas Kinetic Data Evaluation [*IUPAC*, 2009]. Clearly more studies on the uptake of HNO_3(g) on mineral dust particles are required, considering the importance of this reaction in the removal of HNO_3(g) and the formation of particulate nitrate in dust particles.

Heterogeneous reaction of gaseous HNO_3 with Saharan dust aerosols was preliminarily investigated using the new aerosol flow tube, and the decay of HNO_3 was monitored by CIMS, as described in Chapter 2. The wall loss rate of HNO_3(g) in the aerosol flow tube was determined by measuring the nitric acid concentration at different injector positions. As shown in Figure A1-1, the HNO_3 wall loss rate was experimentally measured to be -0.015 s^{-1} and the diffusion-limited wall loss rate is about -0.1 s^{-1}:

$$k_w^{diff} = \frac{3.66 \cdot D_g}{r^2} \qquad \text{(E-A1-1)}$$

where D_g is the diffusion coefficient of HNO_3 (0.12 cm^2 s^{-1},at room temperature and 1 atm, [*Braman et al.*, 1982; *Ghosh*, 1993]), and r is the radius of the flow tube (2.05 cm). The measured wall loss rate of HNO_3 was much smaller than the diffusion-limited wall loss rate, probably suggesting that the dusty wall was deactivated after exposure to gaseous HNO_3 during the experiments. The possibility that the measured wall loss was biased by the adsorption/desorption on HNO_3(g) on the tubing between the AFT and the CIMS could not be ruled out.

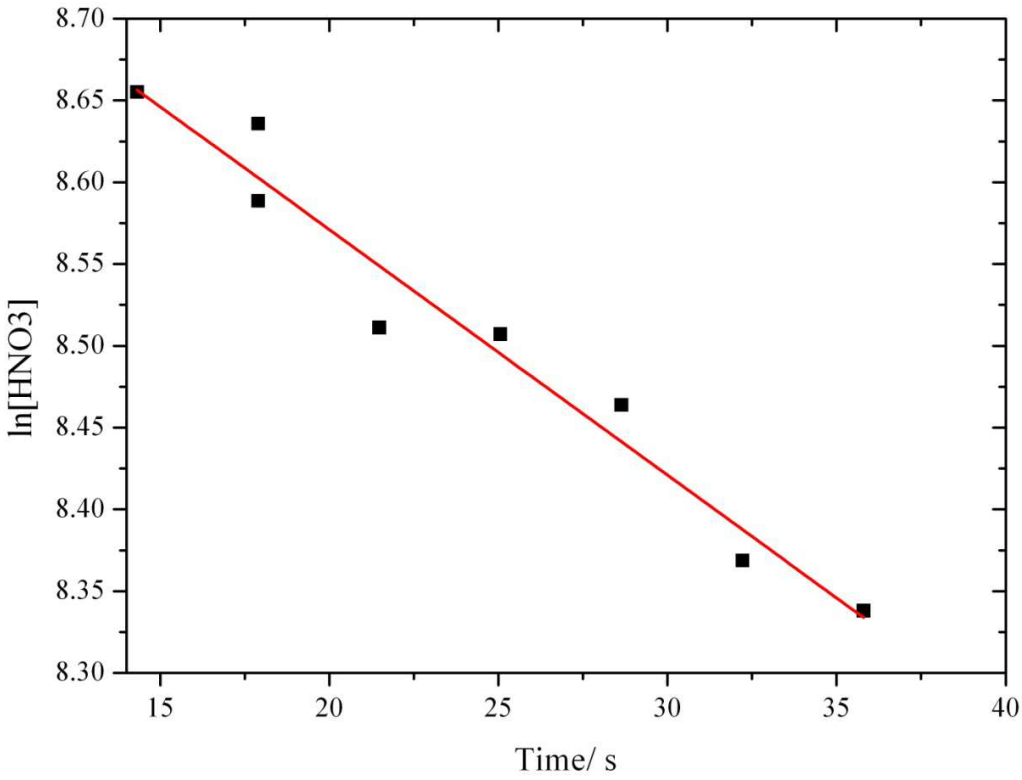

Figure A1-1. Measurement of the wall loss rate of gaseous nitric acid in the aerosol flow tube.

Dispersed Saharan dust particles were introduced into the aerosol flow tube when the injector was at 40 cm. The response of the measured HNO_3 concentration to the introduction of dust aerosol was shown in Figure A1-2. Before 13:14, the sampled flow passed through the HNO_3 scrubber and the CIMS background was determined to be about 300 cps (equal to about 300 pptv), and the instrument background was quite stable, as shown in the background measured again after 13:28. When dust particles were introduced into the flow tube (starting at around 13:15), the HNO_3 concentration started to decrease correspondingly. After the dust concentration reached 0 (around 13:27), the HNO_3 concentration returned to the initial level. During the experiment, the maximum aerosol concentration reached about 6000 particles cm^{-3} and the HNO_3 signal dropped from 2200 cps to 1000 cps. The uptake coefficient of gaseous HNO_3 on Saharan dust was preliminarily estimated to be about 0.02.

However, as shown in Figure A1-2, there was a time lag between the maximum aerosol number density and the minimum HNO_3(g) concentration. The adsorbed HNO_3

on the sampling tube would desorb into the gas phase when aerosol concentration was increasing. When aerosol concentration was decreasing, gaseous HNO_3 would partition onto the sampling tube. The dynamic adsorption-desorption equilibrium of HNO_3 on the sampling tube makes it difficult to obtain reliable kinetics data using current experimental setup.

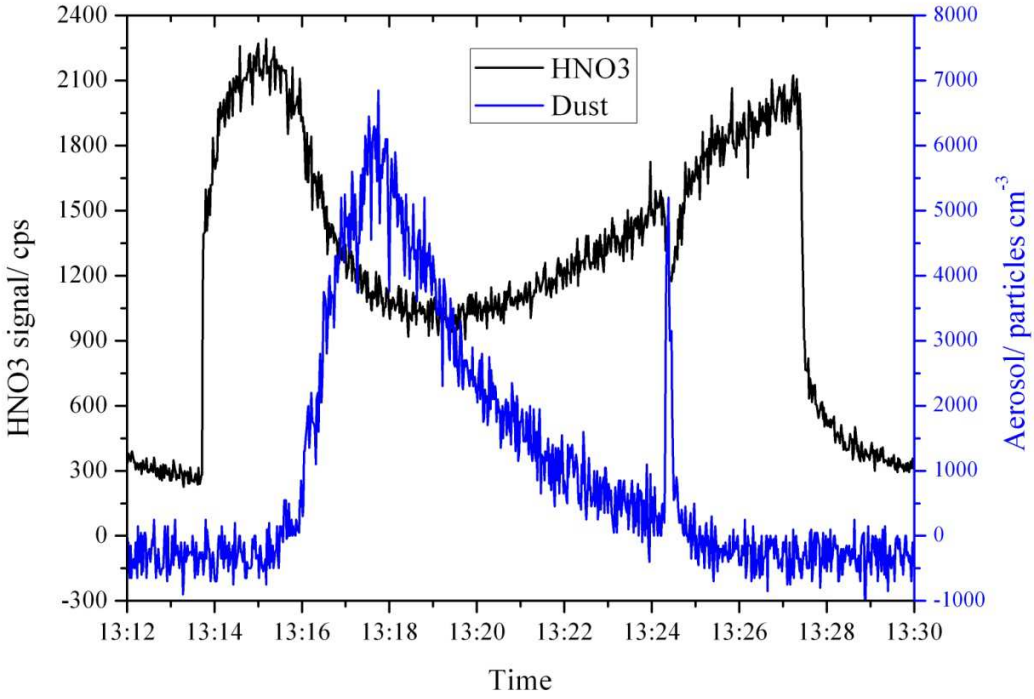

Figure A1-2. Response of gaseous nitric acid signals to the introduction of mineral dust particles. The spike between 13:24 and 13:25 resulted from the pressure change when the mixing volume was bypassed.

The preliminary result opens the possibility to study the heterogeneous uptake of HNO_3 on mineral dust particle. Future improvement is to generate dust aerosol with stable output by atomizing dust suspension [*Pradhan et al.*, 2010a; *Pradhan et al.*, 2010b]. Keeping dust aerosol concentration stable will enable HNO_3(g) to reach adsorption-desorption equilibrium at each injector positions. Therefore, the steady-state HNO_3 concentrations at different injector positions can be measured with and without the presence of dust aerosols in the flow tube to derive the uptake coefficients. In this case, the inner wall of the flow tube can be coated with inert films (e.g. FEP) to minimize the loss of HNO_3(g) on the wall.

A2. Estimation of nitrate formed in the mixing volume

The total flow in the aerosol flow tube was 3 SLM, the aerosol number concentration in the aerosol flow tube is assumed to be 10,000 particles cm^{-3}, and the surface area of each particle (after being corrected for nonsphericity) is 7.79×10^{-8} cm^2. The flow through the mixing volume consisted of the flow coming from the RBG (800 sccm) and the flow used to elute HNO_3 (20 or 100 sccm). The volume of the mixing volume is 4874 cm^3, resulting a residence time of about 5.5 min. Several methods were used to estimate the amount of nitrate formed on the dust particles due to the exposure to HNO_3(g) in the mixing volume:

Method 1:

If it is assumed that all the HNO_3(g) delivered into the mixing volume reacted with dust particles, the formed nitrate on each dust particle would be 1.81×10^{-11} g, 11.2 times of the mass of the fresh dust particle (1.61×10^{-12} g), when 20 sccm N_2 was used to elute HNO_3; when 100 sccm N_2 was used to elute HNO_3, then the mass of the formed nitrate on each dust particle would be 56.2 times of the mass of each fresh dust particle. Such a great mass increase should lead to a great change of the aerodynamic diameter. However, the APS measurement suggests no significant change of the aerodynamic diameter after the dust particles were exposed to HNO_3(g) in the mixing volume.

Method 2:

The uptake coefficient of HNO_3 on Arizona test dust can be parameterized in the following expression [*IUPAC*, 2009; *Vlasenko et al.*, 2009; *Vlasenko et al.*, 2006]:

$$\frac{1}{\gamma_{ATD}} = \frac{1}{\alpha_s} + \frac{1}{\gamma_{LH}} \quad \text{(E-A2-1)}$$

$$\gamma_{LH} = \frac{k_s[Y]_s\alpha_s\tau_{des}}{(1+K_{LangC}[HNO_3])} \quad \text{(E-A2-2)}$$

where α_s, the accommodation coefficient, is 1, $[Y]_s$ is 6.5×10^{13} at RH=0%, k_s is 4×10^{-15} cm^2 $molecule^{-1}$ s^{-1}, τ_{des} is 0.1 s, K_{LangC} is 2.25×10^{-12} cm^3 $molecule^{-1}$, and $[HNO_3]$ is the HNO_3 concentration in molecules cm^{-3}, according to the recommendation of IUPAC at 298 K [*IUPAC*, 2009]. Arizona test dust is less reactive than Saharan dust towards HNO_3; for example, the initial uptake coefficient of HNO_3 has been determined to be 0.11±0.03

on Saharan dust and 0.06±0.015 on Arizona test dust [*Hanisch and Crowley*, 2001b], showing that the reactivity of Saharan dust is about twice of that of Arizona test dust towards HNO_3. Therefore, (E5-3) and (E5-4) are used in this study to calculate the uptake coefficient of HNO3 on ATD, γ_{ATD}, which multiplied by a factor of 2 (to take into account the different reactivity) equals the uptake coefficient on Saharan dust, γ_{SD}, i.e.

$$\gamma_{SD} = 2\gamma_{ATD} = \frac{2}{31.77+6.92\times10^{-11}[HNO_3]} \quad \text{(E-A2-3)}$$

According to (E5-5), the uptake coefficient of HNO_3 on Saharan dust particles in the mixing volume was 4.5×10^{-6} when 20 sccm N_2 was used to elute HNO_3 and 9.9×10^{-7} when 100 sccm N_2 was used. Neglecting the loss of HNO_3 on the wall of the mixing volume, 408 monolayers of nitrate was formed when 20 sccm N_2 was used to elute HNO_3 and 414 monolayers of nitrate was formed when 100 sccm N_2 was used. It is very unlikely that increasing the formed nitrate from 408 to 414 monolayers (the increase is almost negligible) will lead to the decrease of $\gamma(N_2O_5)$ by a factor of larger than 3.

A3. Chemicals and materials used in this work

Chemicals			
Chemical	**Purity**	**Source**	**Comments**
Saharan dust		Cape Verde Islands	Provided by Laurent Gomes
ATD	Nominal 5-10 microns	Powder Technology Inc., MN, US	
Illite		Source Clay Minerals Repository	
Quartz	Reference material, Nr. 66	Community Bureau of Reference	
Pure NO_2	>99.5%	Sigma-Aldrich	
HNO_3 solution	65%	Carl Roth GmbH, Karlsruhe	
$CaCO_3$	10 microns powder, 98%	Sigma-Aldrich	
Palmitic acid	>99%	Sigma-Aldrich	
N_2	>99.999%	Westfalan	
Materials			
Material	**Type**	**Source**	**Comments**
Tubing	PFA AP-230	Swagelok	
Fitting	PFA-420-1-2	Swagelok	
FEP 9568	55.70% suspension in water	DuPont	
PFA 7224	59.10% suspension in water	DuPont	

A4. Codes of FACSIMILE simulations used in this work

In this study FASCIMILE [*Curtis and Sweetenham*, 1987] was used to simulate the chemical reaction in different reactors, and the codes of the programs are listed here together with brief introduction to the programs.

A4.1 Oxidation of NO_2 by O_3 in the photochemical reactor

```
*==================Photochemical reactor=====================;

* ================VAVIABLES CONSIDERED==================;

VARIABLE   NO2                          ;

VARIABLE   O3                           ;

VARIABLE   NO3                          ;

VARIABLE   N2O5                         ;

*===========TO DEFINE TEMPERATURE AND PRESSURE===========;

PARAMETER  P        750                                    ;

PARAMETER  T        298                                    ;

*=============TO CALCULATE NO2+NO3=N2O5 RATES==========;

PARAMETER  M                            ; Total molecule density

PARAMETER  kL                           ; Low-pressure-limit rate constant: NO2+NO3=N2O5

PARAMETER  kH                           ; High-pressure-limit rate constant: NO2+NO3=N2O5

PARAMETER  Keq                          ; Equilibrium constant of NO2+NO3-N2O5

PARAMETER  k1                           ; Rate constant of NO2+O3  = NO3 + O2

PARAMETER  k2                           ; Rate constant of NO2+NO3 = N2O5

PARAMETER  k3                           ; Rate constant of N2O5    = NO2+NO3

COMPILE GENERAL                         ;

k1 = 3.5e-17                            ; To set the rate constant of NO2+O3 = NO3 + O2
```

```
M  = (p/(8.314*T)) * (101300/760) * (6.022E23/1E6)      ; To convert pressure into molecules cm-3

kL = (2.0e-30) * ((T/300)@(-4.4))                ; To calculate low-pressure-limit rate constant:

kH = (1.4e-12) * ((T/300)@(-0.7))                ; To calculate high-pressure-limit rate constant:

k2 = (kL*M/(1+(kL*M/kH)))

          *0.6@((1+(LOG10(kL*M/kH))@2)@(-1))       ; To calculate the rate constant

Keq = (2.7e-27) * exp(11000/T)                   ; To calculate the equilibrium constant

k3 = K2/keq                                      ; To calculate the rate constant of N2O5=NO2+NO3

**                                               ;

*=================TO GIVE INITIAL VALUES====================;

COMPILE INITIAL                                  ;

NO2  = 2.25E13                                   ;

O3   = 2.50E15                                   ;

NO3  = 0.00E13                                   ;

N2O5 = 0.00E13                                   ;

**                                               ;

*======================TO SET CHEMISTRY=======================;

COMPILE EQUATIONS                                ;

% k1      : NO2 + O3  = NO3                       ;

% k2 % k3 : NO2 + NO3 = N2O5                      ;

**                                               ;

*==================TO OUTPUT THE RESULTS======================;

compile instant                                  ;

 open 7   "reactor.sim" new                      ;

**                                               ;
```

```
COMPILE BLOCK 3                          ;

PSTREAM 3                                ;

**                                       ;

compile header                           ;

write 1=7, ".dataset"                    ;

write 1=7, ".data" %                     ;

**                                       ;

PSTREAM 3 7 10                           ;

time NO2 O3 NO3 N2O5                     ;

**                                       ;

when

1)  time = 0 call header                 ;

2)  time = 1.0E-8 + 10*165% call block 3 ;

**                                       ;

*hmax 0.001                              ;

BEGIN                                    ;

STOP                                     ;
```

A4.2 Effects on $\gamma(N_2O_5)$ of the reformation of N_2O_5 and heterogeneous removal of NO_3 in the aerosol flow tube

```
*=============Interference on N2O5 uptake in the AFT==========;

* =================VAVIABLES CONSIDERED=============;

VARIABLE   N2O5       2.5E12              ;

VARIABLE   NO3        2.7E11              ;

VARIABLE   NO2        2.7E11              ;

*=============TO DEFIEN PARAMETERS=================;

PARAMETER  k1         1.9E-12             ; JPL

PARAMETER  k2         6.9E-2              ; JPL

PARAMETER  kwN2O5                         ;

PARAMETER  kdN2O5                         ;

PARAMETER  kwNO3                          ;

PARAMETER  kdNO3                          ;

PARAMETER  ndust      10000               ; assuming 10,000 dust particles

PARAMETER  sdust      4.8E-8              ;

PARAMETER  cN2O5      24100               ;

PARAMETER  gammaN2O5  0.02                ;

PARAMETER  DN2O5      0.085               ;

PARAMETER  cNO3       31900               ;

PARAMETER  gammaNO3   0.10                ; assuming γ(NO3)=0.1

PARAMETER  DNO3       0.105               ;

*===========TO CALCULATE RATE CONSTANTS=============;

COMPILE GENERAL                           ;
```

```
kwN2O5 = 0.05                                   ;
kdN2O5 = 0.25*ndust*sdust*cN2O5*gammaN2O5       ;
kwNO3  = 3.66*DNO3/4                            ;
kdNO3  = 0.25*ndust*sdust*cNO3*gammaNO3         ;
**                                              ;
*===============TO SET CHEMISTRY=======================;
COMPILE EQUATIONS                               ;
% k1 % k2 : NO2 + NO3 = N2O5                    ;
% kwN2O5  : N2O5 =                              ;
% kdN2O5  : N2O5 =                              ;
% kwNO3   : NO3  =                              ;
% kdNO3   : NO3  =                              ;
**                                              ;
*================TO OUTPUT THE RESULTS==================;
compile instant                                 ;
 open 7   "AFT.sim" new                         ;
**                                              ;
COMPILE BLOCK 3                                 ;
PSTREAM 3                                       ;
**                                              ;
compile header                                  ;
write 1=7, ".dataset"                           ;
write 1=7, ".data" %                            ;
**                                              ;
```

```
PSTREAM 3 7 10                          ;
time N2O5 NO3 NO2                       ;
**                                      ;
when
1)  time = 0 call header                ;
2)  time = 0.001 + 0.1*300% call block 3    ;
**                                      ;
*hmax 0.001                             ;
BEGIN                                   ;
STOP                                    ;
```

A4.3 Simulating the response of N_2O_5 to the introduction of dust aerosol

```
*=============Interference on N2O5 uptake in the AFT==========;

* =================VAVIABLES CONSIDERED=============;

VARIABLE   N2O5       2.5E12                ;

VARIABLE   NO3        2.7E11                ;

VARIABLE   NO2        2.7E11                ;

*=============TO DEFIEN PARAMETERS==================;

PARAMETER  k1         1.9E-12               ;

PARAMETER  k2         6.9E-2                ;

PARAMETER  kwN2O5                           ;

PARAMETER  kdN2O5                           ;

PARAMETER  kwNO3                            ;

PARAMETER  kdNO3                            ;

PARAMETER  ndust      10000                 ; This number can be varied by another program

PARAMETER  sdust      4.8E-8                ;

PARAMETER  cN2O5      24100                 ;

PARAMETER  gammaN2O5  0.02                  ;

PARAMETER  DN2O5      0.085                 ;

PARAMETER  cNO3       31900                 ;

PARAMETER  gammaNO3   0.018                 ; from RR study

PARAMETER  DNO3       0.105                 ;

*============TO CALCULATE RATE CONSTANTS=============;

COMPILE GENERAL                             ;

kwN2O5 = 0.05                               ;
```

```
kdN2O5 = 0.25*ndust*sdust*cN2O5*gammaN2O5              ;

kwNO3  = 3.66*DNO3/4                                   ;

kdNO3  = 0.25*ndust*sdust*cNO3*gammaNO3                ;

**                                                     ;

*===============TO SET CHEMISTRY=======================;

COMPILE EQUATIONS                                      ;

% k1 % k2 : NO2 + NO3 = N2O5                           ;

% kwN2O5  : N2O5 =                                     ;

% kdN2O5  : N2O5 =                                     ;

% kwNO3   : NO3  =                                     ;

% kdNO3   : NO3  =                                     ;

**                                                     ;

*================TO OUTPUT THE RESULTS==================;

compile instant                                        ;

 open 7   "AFT.sim" new                                ;

**                                                     ;

COMPILE BLOCK 3                                        ;

PSTREAM 3                                              ;

**                                                     ;

compile header                                         ;

write 1=7, ".dataset"                                  ;

write 1=7, ".data" %                                   ;

**                                                     ;

PSTREAM 3 7 10                                         ;
```

```
time N2O5 NO3 NO2                    ;
**                                   ;
when
1)  time = 0 call header             ;
2)  time = 0.001 + 0.1*300% call block 3   ;
**                                   ;
*hmax 0.001                          ;
BEGIN                                ;
STOP                                 ;
```

A5. Chemical formulae and structures of main minerals contained by dust particles

Most of the data presented here come from two online databases: Mineralogy database (http://www.webmineral.com/), and U. S. Geological Survey Open-File Report 01-041 (http://pubs.usgs.gov/of/2001/of01-041/). Minerals are alphabetically listed in this appendix.

Mineral	Chemical formula	Structure
Calcite	$CaCO_3$	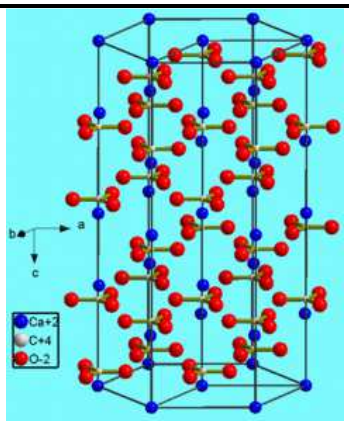
Chlorite	$(Mg,Fe)_3(Si,Al)_4O_{10}(OH)_2(Mg,Fe)_3(OH)_6$	
Dolomite	$CaMg(CO_3)_2$	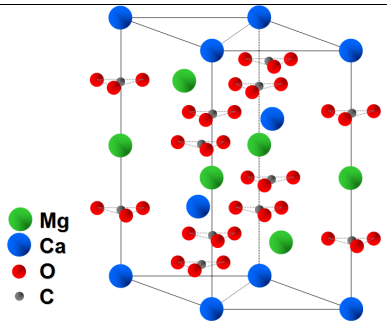
Feldspar	$KAlSi_3O_8$, $NaAlSi_3O_8$, or $CaAl_2Si_2O_8$	

Gypsum	$CaSO_4 \cdot 2H_2O$	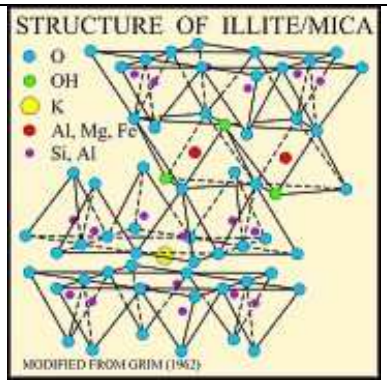
Hematite	Fe_2O_3	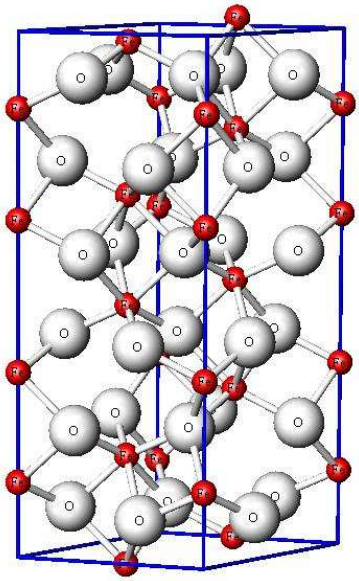
Illite	$(K,H_3O)(Al,Mg,Fe)_2(Si,Al)_4O_{10}[(OH)_2,(H_2O)]$	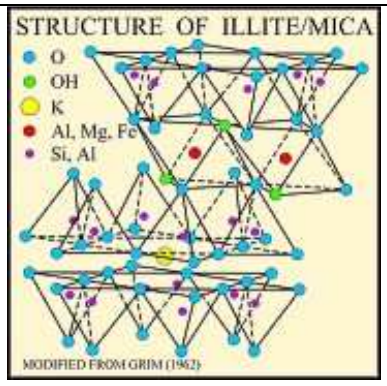

Kaolinite	$Al_2Si_2O_5(OH)_4$	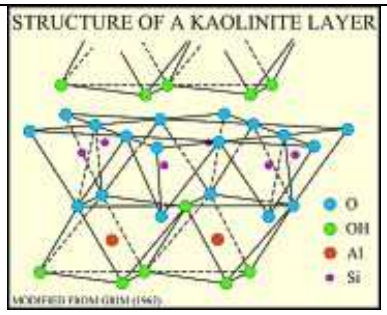
Montmorillonite	$(Na,Ca)_{0.3}(Al,Mg)_2Si_4O_{10}(OH)_2 \cdot n(H_2O)$	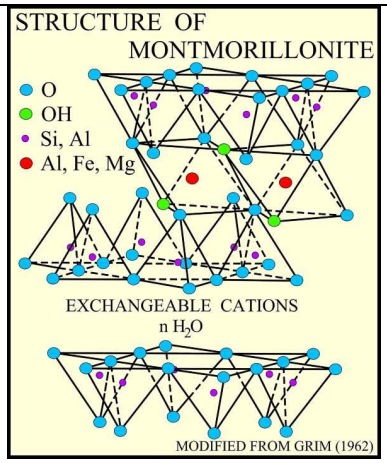
Quartz	SiO_2	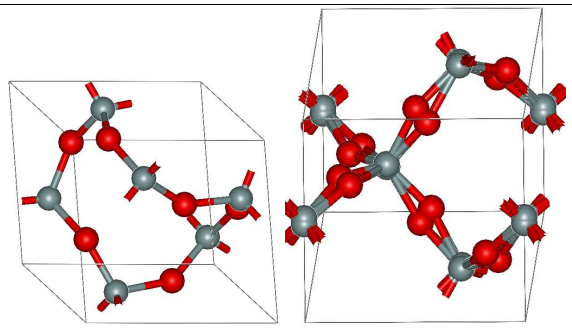

A6. Publications and projects/campaigns during the PhD study

A6.1 Publications

Laboratory studies:

[1] **Tang, M. J.**, Thieser, J., Schuster, G., and Crowley, J. N.: Uptake of NO_3 and N_2O_5 to Saharan dust, ambient urban aerosol and soot: a relative rate study, *Atmos. Chem. Phys.*, 10, 2965-2974, 2010.

[2] **Tang, M. J.**, Thieser, J., Schuster, G., and Crowley, J. N.: Kinetics and mechanism of the heterogeneous reaction of N_2O_5 with mineral dust particles, *in preparation*

Field campaigns:

[3] Williams, J., Crowley, J., Fischer, H., Harder, H., Martinez, M., Petäjä, T., Rinne, J., Bäck, J., Boy, M., Dal Maso, M., Hakala, J., Kajos, M., Keronen, P., Rantala, P., Aalto, J., Aaltonen, H., Paatero, J., Vesala, T., Hakola, H., Levula, J., Pohja, T., Herrmann, F., Auld, J., Mesarchaki, E., Song, W., Yassaa, N., Nölscher, A., Johnson, A. M., Custer, T., Sinha, V., Thieser, J., Pouvesle, N., Taraborrelli, D., **Tang, M. J.**, Bozem, H., Hosaynali-Beygi, Z., Axinte, R., Oswald, R., Novelli, A., Kubistin, D., Hens, K., Javed, U., Trawny, K., Breitenberger, C., Hidalgo, P. J., Ebben, C. J., Geiger, F. M., Corrigan, A. L., Russell, L. M., Ouwersloot, H., Vilà-Guerau de Arellano, J., Ganzeveld, L., Vogel, A., Beck, M., Bayerle, A., Kampf, C. J., Bertelmann, M., Köllner, F., Hoffmann, T., Valverde, J., González, D., Riekkola, M. L., Kulmala, M., and Lelieveld, J.: The summertime Boreal forest field measurement intensive (HUMPPA-COPEC-2010): an overview of meteorological and chemical influences, *Atmos. Chem. Phys. Discuss.*, 11, 15921-15973, 10.5194/acpd-11-15921-2011, 2011.

[4] Crowley, J. N., Thieser, J., **Tang, M. J.**, Schuster, G., Bozem, H., Hosaynali-Beygi, Z., Fischer, H., Diesch, J., Drewnick, F., Borrmann, S., Song, W., Yassaa, N., Williams, J., Poehler, D., Platt, U., and Lelieveld, J.: Variable lifetimes and loss mechanisms for NO_3 and N_2O_5 during the DOMINO campaign: contrasts between marine, urban and continental air, *Atmos. Chem. Phys. Discuss.*, 11, 17825-17877, 2011.

[5] Thieser J. et al.,: Measurement of NO_3 vertical profiles during the DOMINO campaign, *in preparation*

[6] Rinne, J., Markkanen, T., Ruuskanen, T. M., Petäjä, T., **Tang, M. J.**, Crowley, J. N., Vesala, T.: Effect of chemical degradation on fluxes of reactive compounds – a stochastic Lagrangian model study, *to be submitted*

In addition, at least three papers on the measurements carried out during the PARADE campaign will be published in future.

A6.2 Projects/campaigns

[1] CNRS-DFG bilateral project: Interaction of trace gases with mineral dust: Impact on atmospheric photochemical cycles and dust properties.

[2] DOMINO campaign: **D**iel **O**xidant **M**echanisms **I**n relation to **N**itrogen **O**xides, November 21-December 08, 2008, Spain

[3] HUMPPA campaign: **H**yytiälä **U**nited **M**easurements of **P**hotochemistry and **P**articles in **A**ir, July 12-Auguest 11, 2010, Finland

[4] PARADE campaign: **PA**rticles and **RA**dicals: **D**iel observations of the impact of urban and biogenic **E**missions, August 08-September 09, 2011, Germany

Max-Planck-Institut für Chemie

CURRICULUM VITA

Mingjin TANG

Personal information

Date of Birth: June 12, 1984 **Citizenship:** P. R. China **Gender:** Male

E-mail: mingjin.tang@mpic.de mingjintang@gmail.com

Office Phone: +49-6131-305-475

Current Address: Max Planck Institute for Chemistry, Atmospheric Chemistry Department, Joh.-Joachim-Becher-Weg 27/29, D-55128, Mainz, Germany

Educational background

2001/09-2005/07	**B.Sc., Peking University**, P. R. China, in Environmental Sciences
2005/09-2008/07	**M.Sc. Peking University**, P. R. China, in Environmental Chemistry Dissertation: Heterogeneous reactions of gaseous methanesulfonic acid with sea salt and mineral dust particles
2008/08-2011/11	**Ph.D., Max Planck Institute for Chemistry,** Germany, in Atmospheric Chemistry Dissertation: Atmospheric heterogeneous reactions of mineral dust particles with N_2O_5 and NO_3 radicals

Research interests

Heterogeneous and multiphase chemistry

Aerosol chemistry and kinetics

Nocturnal atmospheric chemistry

Surface chemistry and techniques

Online spectroscopy and mass spectrometry

Marine sulfur chemistry

Honors, awards and recognitions

2002	**Dean's Award for Academic Excellence**, awarded to students who are excellent in academic field
2003	**Dean's Award for Academic Excellence**, awarded to students who are excellent in academic field
2003-2004	**President's Undergraduate Research Fellowship of Peking University**

Professional experience

2003/04-2004/09	Undergraduate research assistant, **Peking University**, China
2004/09-2005-09	Undergraduate research assistant, **Peking University**, China
2005/09-2008/07	Graduate research assistant, **Peking University**, China
2006/09-2007/01	Teaching assistant in General Chemistry Lab, **Peking University**, China
2008/08-2011/11	graduate research assistant, **Max Planck Institute for Chemistry**, Germany
2011/11-2012/04	Postdoctoral research fellow, **Max Planck Institute for Chemistry**, Germany
2012/04-	Postdoctoral research fellow, **University of Cambridge**, UK

Publications

[9] Thieser J., **Tang, M. J.**, Schuster, G., Crowley, J. N., Lelieveld, J., Pöhler, D., Platt, U., and Ganzevelt, L.: Vertical gradients in NO_3 mixing ratios and lifetimes during DOMINO, in preparation

[8] **Tang, M. J.**, Thieser, J., Schuster, G., and Crowley, J. N.: Kinetics and mechanism of the heterogeneous reaction of N_2O_5 with mineral dust particles, to be submitted

[7] Rinne, J., Markkanen, T., Ruuskanen, T. M., Petäjä, T., **Tang, M. J.**, Crowley, J. N., Vesala, T.: Effect of chemical degradation on fluxes of reactive compounds: a stochastic Lagrangian model study, ***Atmos. Chem. Phys. Discuss.***, 11, 31819-31849, 2011

[6] Crowley, J. N., Thieser, J., **Tang, M. J.**, Schuster, G., Bozem, H., Hosaynali Beygi, Z.,

Fischer, H., Diesch, J., Drewnick, F., Borrmann, S., Song, W., Yassaa, N., Williams, J., Pöhler, D., Platt, U., and Lelieveld, J.: Variable lifetimes and loss mechanisms for NO_3 and N_2O_5 during the DOMINO campaign: contrasts between marine, urban and continental air, ***Atmos. Chem. Phys.***, 11, 10853-10870, 2011

[5] Williams, J., Crowley, J., Fischer, H., Harder, H., Martinez, M., Petäjä, T., Rinne, J., Bäck, J., Boy, M., Dal Maso, M., Hakala, J., Kajos, M., Keronen, P., Rantala, P., Aalto, J., Aaltonen, H., Paatero, J., Vesala, T., Hakola, H., Levula, J., Pohja, T., Herrmann, F., Auld, J., Mesarchaki, E., Song, W., Yassaa, N., Nölscher, A., Johnson, A. M., Custer, T., Sinha, V., Thieser, J., Pouvesle, N., Taraborrelli, D., **Tang, M. J.**, Bozem, H., Hosaynali-Beygi, Z., Axinte, R., Oswald, R., Novelli, A., Kubistin, D., Hens, K., Javed, U., Trawny, K., Breitenberger, C., Hidalgo, P. J., Ebben, C. J., Geiger, F. M., Corrigan, A. L., Russell, L. M., Ouwersloot, H., Vilà-Guerau de Arellano, J., Ganzeveld, L., Vogel, A., Beck, M., Bayerle, A., Kampf, C. J., Bertelmann, M., Köllner, F., Hoffmann, T., Valverde, J., González, D., Riekkola, M. L., Kulmala, M., and Lelieveld, J.: The summertime Boreal forest field measurement intensive (HUMPPA-COPEC-2010): an overview of meteorological and chemical influences, ***Atmos. Chem. Phys.***, 11, 10599-10618, 2011.

[4] **Tang, M.J.**, Li, M.Q., and Zhu, T.: Heterogeneous reactions of gaseous methanesulfonic acid with calcium carbonate and kaolinite particles, ***Sci. China-Chem.***, 53, 2657-2662, 2010.

[3] **Tang, M.J.**, Thieser, J., Schuster, G., and Crowley, J.N.: Uptake of NO_3 and N_2O_5 to Saharan dust, ambient urban aerosol and soot: a relative rate study, ***Atmos. Chem. Phys.***, 10, 2965-2974, 2010.

[2] **Tang, M.J.**, and Zhu, T.: Heterogeneous reactions of gaseous methanesulfonic acid with NaCl and sea salt particles, ***Sci. China Ser. B-Chem.***, 52, 93-100, 2009.

[1] **Tang, M.J.**, Xu, Z.X., Zuo, Q., Huang, M.H., Zhang, G., Tao, S.: Multimedia fate modeling of PAHs in Guangdong, Hong Kong, and Macao, ***Ecology and Environment***, 15, 670-673, 2006 (in Chinese)

Conference talks

[1] **Tang, M.J.**, Thieser, J. Schuster, G., and Crowley, J.N.: *Heterogeneous interaction of NO_3 and N_2O_5 with mineral dust: Aerosol Flow Tube and Relative Rate studies.* **21st International Symposium on Gas Kinetics**, Leuven, Belgium, July, 2010.

Conference posters

[1] **Tang, M.J.**, Thieser, J. Pouvesle, N., Schuster, G., and Crowley, J.N.: *Heterogeneous interaction of N_2O_5 with mineral dust.* **European Geosciences Union General Assembly 2011**, Vienna, Austria, April, 2011.

Current research projects

[1] Heterogeneous interaction of NO_3, N_2O_5, and HNO_3 with mineral dust aerosols

Instruments: aerosol flow tube, Cavity Ring-Down spectroscopy, Chemical Ionization Mass Spectroscopy

[2] Field measurements of NO_3 and N_2O_5 in the atmosphere

(1) DOMINO: **D**iel **O**xidant **M**echanisms **I**n relation to **N**itrogen **O**xides, November 21-December 08, 2008, Spain

(2) HUMPPA: **H**yytiäla **U**nited **M**easurements of **P**hotochemistry and **P**articles in **A**ir, July 12-Auguest 11, 2010, Finland

(3) PARADE: **PA**rticles and **RA**dicals: **D**iel observations of the impact of urban and biogenic **E**missions, August 08-September 09, 2011, Germany

[3] Development of an NO_3 reactivity measurement apparatus to measure the lifetime of NO_3 in the atmosphere